AD_____

Award Number: DAMD17-03-1-0156

TITLE: Regulated Apoptosis and Immunogene Therapy for Prostate Cancer

PRINCIPAL INVESTIGATOR: David M. Spencer, Ph.D.
Kevin M. Slawin, M.D.

CONTRACTING ORGANIZATION: Baylor College of Medicine
Houston, TX 77030

REPORT DATE: April 2006

TYPE OF REPORT: Final

PREPARED FOR: U.S. Army Medical Research and Materiel Command
Fort Detrick, Maryland 21702-5012

REPORT DOCUMENTATION PAGE

Form Approved
OMB No. 0704-0188

1. REPORT DATE	2. REPORT TYPE	3. DATES COVERED
01-04-2006	Final	1 Apr 2003 – 31 Mar 2006

4. TITLE AND SUBTITLE

Regulated Apoptosis and Immunogene Therapy for Prostate Cancer

5a. CONTRACT NUMBER

5b. GRANT NUMBER
DAMD17-03-1-0156

5c. PROGRAM ELEMENT NUMBER

6. AUTHOR(S)
David M. Spencer, Ph.D.
Kevin M. Slawin, M.D.

5d. PROJECT NUMBER

5e. TASK NUMBER

5f. WORK UNIT NUMBER

7. PERFORMING ORGANIZATION NAME(S) AND ADDRESS(ES)

Baylor College of Medicine
Houston, TX 77030

8. PERFORMING ORGANIZATION REPORT NUMBER

9. SPONSORING / MONITORING AGENCY NAME(S) AND ADDRESS(ES)
U.S. Army Medical Research and Materiel Command
Fort Detrick, Maryland 21702-5012

10. SPONSOR/MONITOR'S ACRONYM(S)

11. SPONSOR/MONITOR'S REPORT NUMBER(S)

12. DISTRIBUTION / AVAILABILITY STATEMENT
Approved for Public Release; Distribution Unlimited

13. SUPPLEMENTARY NOTES
Original contains colored plates: ALL DTIC reproductions will be in black and white.

14. ABSTRACT Purpose: The central tenet of this proposal was that methods to effectively trigger apoptosis within prostate tumors can both reduce tumor burden and elicit adaptive immunity, provided a pro-inflammatory environment can be created. Scope: We created inducible caspases (iCaspases) that were the basis of both a prophylactic vaccine and as a treatment for pre-existing subcutaneous (sc) and autochthonous (TRAMP) prostate tumors. While these studies were centered on prostate cancer, they should also be relevant to other tumor types. Major findings: The combination of iCaspases and IL-12 can completely eliminate small (≤ 40 mm3) sc tumors and largely eliminate larger (≤ 100 mm3) tumors while IL-12 alone had minimal effect and iCaspase alone had no significant effect. Anti-tumor efficacy mirrored expansion of anti-tumor cytotoxic T lymphocytes and IFN-γ-producing cells from splenocytes of vaccinated animals. Further, orthotopic injections into the prostates of tumor-bearing TRAMP mice trigger apoptosis, secondary necrosis and inflammation, and significantly extend survival. In transgenic animals, the hK2-E3/P, PSA-E2/P and ARR2PB composite promoters are highly active in prostate epithelial cells and are largely prostate specific; however, they are somewhat attenuated as tumor progression occurs, potentially reducing efficacy in tumor cells. Finally, we developed ubiquitous and tissue-specific "clinical candidate" vectors that are being tested for a potential clinical trial. Significance: This work lays the groundwork for an "off-the-shelf" injectable immunogene therapy that could treat prostate cancer as a neoadjuvant therapy or possible less mutagenic treatment for metastatic disease.

15. SUBJECT TERMS
prostate cancer, immunotherapy, apoptosis, caspases, IL-12, vaccine

16. SECURITY CLASSIFICATION OF:				18. NUMBER OF PAGES	19a. NAME OF RESPONSIBLE PERSON
					USAMRMC
a. REPORT	b. ABSTRACT	c. THIS PAGE			19b. TELEPHONE NUMBER *(include area code)*
U	U	U	UU	39	

Standard Form 298 (Rev. 8-98)
Prescribed by ANSI Std. Z39.18

Table of Contents

INTRODUCTION:

Currently, there are only palliative treatments for androgen-independent metastatic prostate cancer, and these can only provide temporary pain relief and minimal (~ 2 to 3 months) extension of survival. Among systemic therapies, including chemotherapeutic combinations (e.g. docetaxel and prednisone), novel biological targets linked to radiopharmaceuticals (e.g. PSMA/J591), and bone-targeting bisphosphonates (e.g. Zoledronic acid), all offer temporary relief at best and most demonstrate high morbidity associated with mutagenicity and off target effects. In contrast, new treatment modalities that target tumor antigens or tumor vasculature may treat disseminated disease with lower side effects. Immunotherapies that require patient-tailored cell culturing or knowledge of tumor antigens will likely remain prohibitively expensive for most patients. Therefore, we set out to develop a potentially injectable immunotherapy that could be used as a stand-alone or neoadjuvant therapy. This novel approach is based on tissue-specific expression of pharmacologically activated caspases that can kill slowly dividing prostate cancer cells in the primary (or secondary) tumor in a pro-inflammatory environment. In year one, we described the proof-of-principal of this method and initial testing of vaccination of pre-existing subcutaneous (s.c.) and orthotopic tumors and testing of various prostate-specific promoters. At the end of year two, our manuscript describing this approach appeared in Cancer Research. Over the past year, we developed several viral vectors for clinical trials that include the use of a prostate-specific promoter and secreted HSP70 protein to potentially replace IL-12. Testing of high titer viruses in vaccine settings is underway. Finally, over the past three years, we developed three distinct prostate reporter mice, based on composite prostate-specific promoters as a sensitive method to compare and appraise these tissue-specific promoters for building safer, more prostate-specific vectors.

BODY:

Following is a list of tasks along with a summary of our progress in completing (or exceeding) these goals.

Task 1: Test the hypotheses that iCaspases can trigger apoptosis in normal and malignant prostate epithelial cells *in vivo*.

We previously demonstrated that iCaspases can trigger apoptosis in syngeneic TRAMP-based tumors[1] and LNCaP xenografts[2]. To demonstrate iCaspase killing in mouse prostates, we have injected ADV/CMV-iCaspase-1[1] into the ventral prostate lobes of 20-week old TRAMP mice, which should contain primarily poorly differentiated adenocarcinoma in most animals[3]. While control virus led to no obvious increased necrosis over wild-type mice in

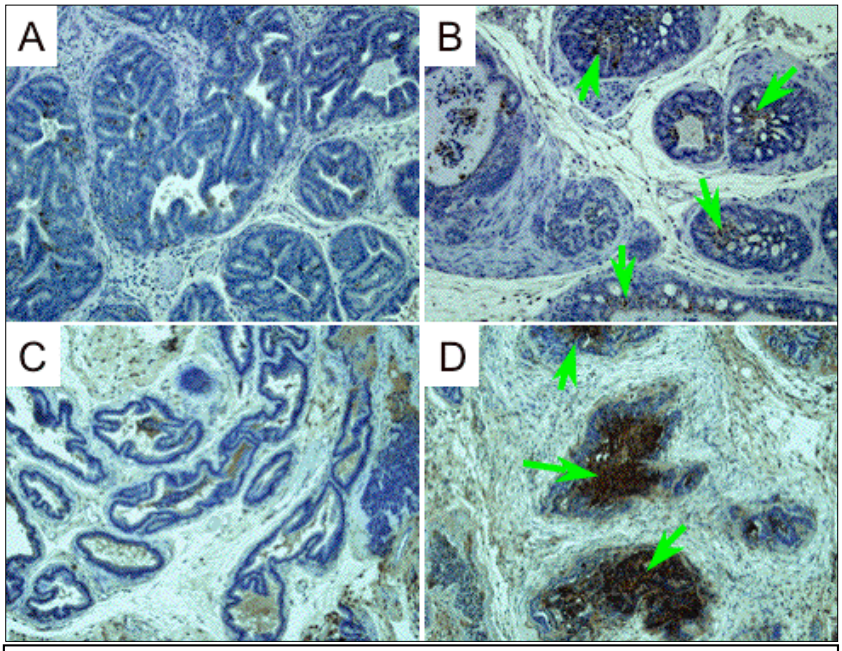

Fig. 1. Intraprostatic administration of Ad-iCasp1 followed by intraperitoneal injection of CID results in extensive cell death in prostate tissues of TRAMP mice. Ventral prostates of 20-week-old (**A**, **B**) or 32-week-old (**C**, **D**) TRAMP mice were injected once with either Ad-iCasp1 and Ad-IL-12 (**A**) or Ad-c (**C**) followed by i.p. CID carrier administration, or with either Ad-iCasp1 and Ad-IL-12 (**B**) or Ad-iCasp1 (**D**) followed by i.p. CID administration. Ventral prostate lobes were excised 20 (**A**, **B**) or 72 (**C**, **D**) hours later, and TUNEL assay was performed (counterstaining with hematoxylin). Magnification 100×. Areas with extensive cell death (brown staining) are indicated by arrows.

3/3 animals, transduction with ADV/CMV-iCaspase-1 followed by intraperitoneal CID injection 3 days later, led to widespread necrosis (viewed after 10 additional days), demonstrating that prostate cancer cells are highly sensitive to caspase-1 activation. (Shown previously**).** Moreover, we injected ADV/CMV-iCaspase-1 into even more malignant tumors at age 32 weeks to see if TRAMP tumors become resistant to Caspase-mediated apoptosis. In those experiments, widespread apoptosis occurred in prostatic ducts in a largely CID-dependent fashion with lesser, but significant apoptosis occurring in the stroma (**Fig. 1**). A manuscript describing this work was published in Cancer Research in May 2005 and appears as appendix one.

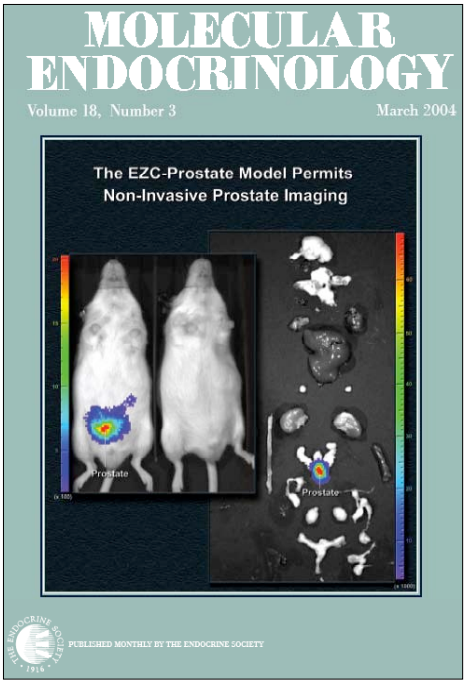

Fig. 2. Cover art from Mol Endo (3/04) showing tissue-specificity of hK2-E3/P promoter *in vivo* driving luciferase activity primarily in the prostate. Transgenic mice were injected with 1 mg D-Luciferin and imaged (for 30'') 15' later (left) with an IVIS-imaging system or ex vivo (right) ~ 45' later.

Over the past year, we built three new viral vectors, **ADV-icp30C9, ADV-ARR$_2$PB-icp30C9**, and **ADV-sHSP70-IRES-icp30C9**, utilizing a new, lower basal activity inducible caspase 9. This version of iCaspase 9 lacks its pro-domain (and hence Apaf-1 binding) and contains a mutation (A330) at position D330 to eliminate a positive feedback-driven caspase 3 cleavage site. There are also several conservative amino acid changes to slightly improve reactivity. Hence the name: Consensus-sequence p30 Caspase 9 ("cp30C9"). These three ADV vectors were amplified and prepared at high titer. Although experiments are still ongoing, initial characterization demonstrates that each kills prostate cancer cells (note: ARR$_2$PB-icp30C9 is androgen receptor (AR)-inducible) in vitro and in vivo in the prostate.

To demonstrate the utility of adenoviruses expressing tissue-restricted iCaspases, we are currently injecting adenovirus ADV/ARR$_2$PB-iCaspase9[2] into the ventral lobes of normal and TRAMP prostates. Moreover, we have made transgenic mice expressing luciferase under the influence of three different prostate-specific promoters, hK2-E3/P[4,5], ARR$_2$PB[6] and a composite PSA-based promoter, PSA-E2/P[2]. In addition to the published EZC-Prostate line based on the human kallikrein 2 promoter, hK2-E3/P (**Fig. 2**)[5], selected founder lines based on the rat probasin-based promoter, ARR$_2$PB, and PSA-E2/P also show high-level tissue-specific reporter expression (**Fig. 3**). A manuscript describing the utility, advantages and disadvantages of the 3 lines will appear in Cancer Research in June (06). Briefly, although there was less site of chromosome integration "position effects" between founder lines that use the hK2-E3/P promoter than the other two, expression was more tissue-specific in mice based on ARR2PB- and PSA-E2/P composite promoters. The PSA-E2/P promoter is bigger than ARR$_2$PB but tends to be stronger and more tissue-

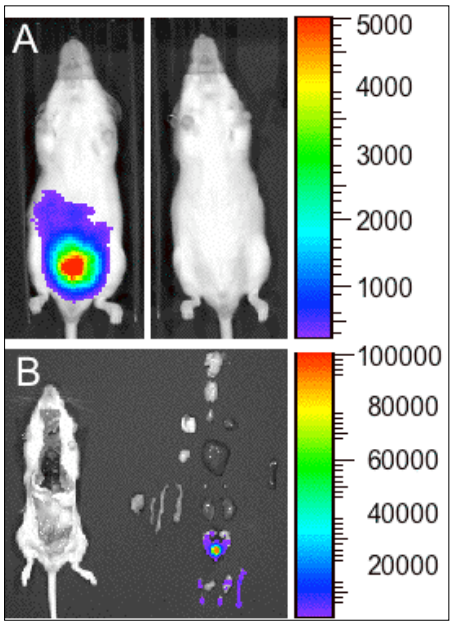

Fig 3. EZC2-Prostate®: Prostate-specific luciferase expression in ARR$_2$PB-luc mice. A. Prostate-localized expression in 12-wk Tg mouse (left). Non-Tg littermate (right) B. Prostate-specific expression viewed *ex vivo*. **Notes:** (i) *Ex vivo* signal ~ 20 x *in vivo* due to tissue, skin, hair absorption (ii) weak ~2% signal in testes and epididymis.

specific. Therefore, adenoviral vectors expressing iCaspase9 for treating prostate cancer should use either of these two promoters. The proofs for this paper are included as an appendix (Seethammagari et al).

Task 2,3. Test the hypotheses that inducing apoptosis in prostate adenocarcinoma cells will induce a T_H1-biased immune response. Test the hypotheses that triggering apoptosis in the context of a T_H1-induced cytokine milieu will evoke or augment an anti-tumor immune response.

Tasks 2 and 3 have been combined and are being tested simultaneously in some experiments. To initially test this hypothesis in s.c. TRAMP tumors, groups (n = 5) of mice bearing small (≤ 35 mm^3) and medium (≤ 100 mm^3) tumors were injected intratumorally with adenovirus expressing iCaspase-1 (as above), ADV-IL-12 (expressing IL-12), both or neither (i.e. ADV/c), and tumor sizes were estimated (via calipers) biweekly. All groups were controlled for total viral particles. Although injection of ADV-IL12 showed some efficacy in small tumors, the combination of iCaspase-1 (+ CID) and IL-12 led to complete elimination of small tumors. No other group, including non-treated tumor-bearing mice, showed any efficacy (**Fig. 4**). Further, CTL activity and IFN-γ producing cells in splenocytes from optimally vaccinated mice showed optimum expansion (**Fig. 5** and not shown). When medium-sized tumors were injected, trends were similar with optimally treated tumors averaging 10% of controls, however only 2/5 mice were completely tumor-free (not shown).

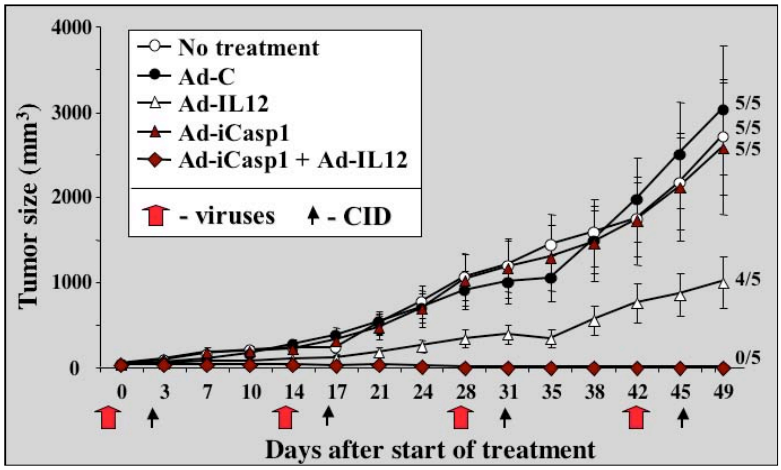

Fig. 4. Treatment of small TRAMP-C2 tumors with Ad-iCasp1 and Ad-IL-12. TRAMP-C2 tumors were established in syngeneic mice following injection of 10^6 cells. When average tumor size was ~ 35 mm^3, tumors were injected with equal numbers of adenovirus, containing IL-12, iCaspase1, both or neither (Ad-c). Control tumors were mock-injected. Tumor sizes were estimated with vernier calipers. Average tumor size ± std dev. shown. Fraction of mice (out of 5) with no tumors is also shown.

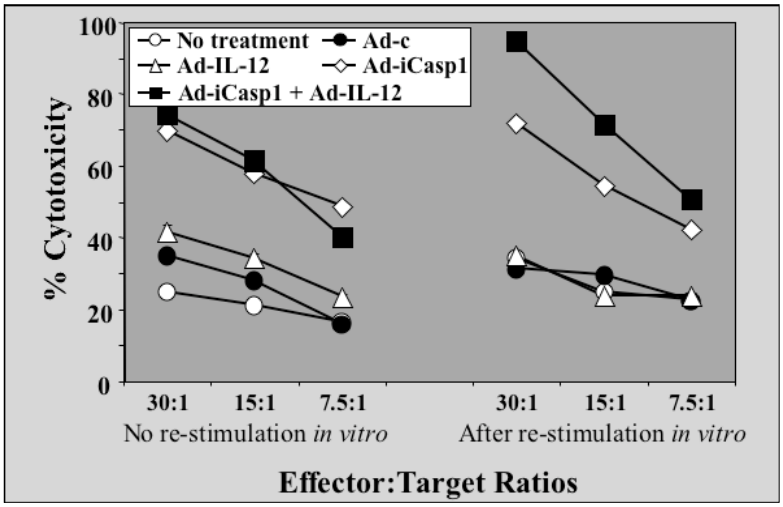

Fig. 5. Treatment of tumors with Ad-iCasp1 and Ad-IL-12 leads to potent CTL activity. Splenocytes from vaccinated mice bearing initially medium-sized tumors (≤ 100 mm^3 at first ADV injection) were cultured for either 7 d in T-Stim® without restimulation or with restimulation by TRAMP-C2-pulsed DCs. % cytotoxicity = % specific release of ^{51}Cr-loaded TRAMP-C2 target cells (pretreated with IFNγ to increase MHC class I expression). Average of 3 mice/group euthanized at conclusion of experiment (~ day 50 after first virus injection) shown.

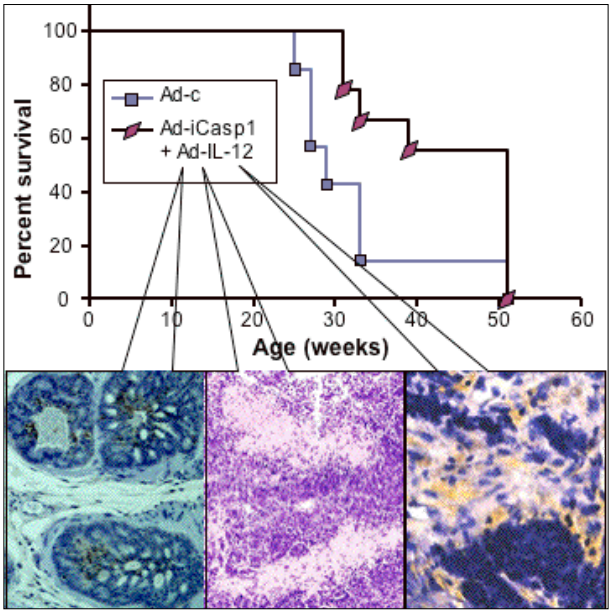

Fig. 6. Treatment of pre-existing PCa with Casp-1/IL-12 therapy. Adenovectors expressing iCaspase-1 and IL-12 or empty control vector were injected into the ventral prostate glands of 12-wk TRAMP mice. A second injection was performed on week 14. Panels: (left) TUNEL assay performed 2d after CID injection. (center) H&E stain shows necrosis. (right) stain for lymphocyte-derived acid phosphatase indicates lymphocyte infiltration.

changes in prostate size in living tumor-prone TRAMP mice and in our inducible prostate cancer model, called JOCK, based on a dimerizer-inducible, prostate-targeted version of FGFR1. Results suggest that as the prostate becomes more hyperplastic and dysplastic luciferase activity actually decreases (~ 5X) perhaps due to changes in promoter activity, vascularity, or both. We also validated Living Image® data with direct anti-luciferase immunohistochemistry. Despite reductions of promoter activity with progression, enough activity remains to justify use of these tissue-specific promoters. This work is included in the appendix.

Task 5. (Optional) Develop novel adenoviral vector, ADV-sHSP70-IRES-icp30Casp-9, coexpressing secreted HSP70 and an improved version of iCaspase-9. Year 2-3.

To test the central hypothesis of this task in autochthonous tumors, we injected 12-week TRAMP mice intraprostaticly with ADV-iCaspase-1 plus ADV-IL-12 or control ADV/C. After two weeks a second injection was performed. Approximately 80% of mice survived the double-survival surgery. While control mice succumbed to late-stage prostate disease and were euthanized or died from high tumor burden, the Caspase/IL-12 vaccinated mice lived significantly longer (**Fig. 6**). Further, there was clear evidence of caspase-mediated apoptosis, necrosis, and infiltrating lymphocytes in caspase/IL-12 treated mice (**Fig. 6**). Nikitina et al describing this work is included as an appendix. Similar experiments will be performed with the new viruses expressing prostate-restricted inducible caspase-9 (i.e. ADV-ARR$_2$PB-iCaspase9) and ADV-IL-12, as this will most likely be the virus used in a clinical trial.

Task 4. (Optional) Test the utility of using the EZC-Prostate model to measure tumor growth *in vivo* following vaccination. Yr 2-3.

We completed assessing the ability to monitor

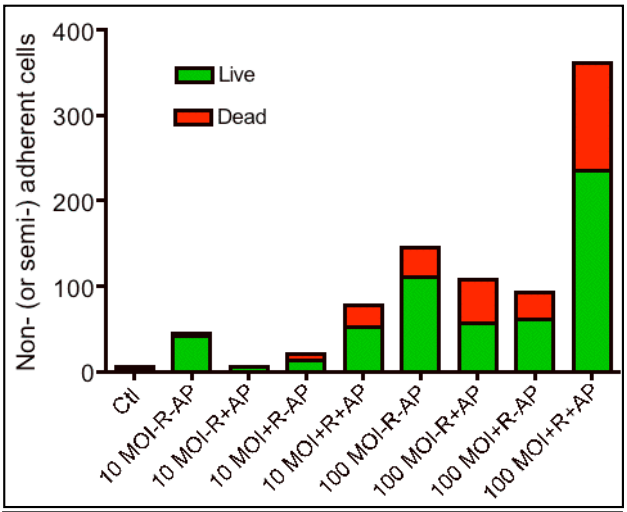

Fig. 7. Androgen and CID-specific effects of ADV-ARR$_2$PB-icp30Casp9 on LNCaP cells. LNCaP cells in charcoal-stripped media were infected with ADV-ARR2PB-icp30C9 at MOI 10 or 100. 24 hours later cells were treated with or without androgen analog R1881 (R; 1 nM), CID AP20187 (AP), or both. 24 hours later, floating cells were assayed for membrane integrity with trypan blue. Cells (x 1000/ml).

Independently, the Chen lab developed a related approach based on release of the potent adjuvant, HSP70, by a conditionally cytolytic virus[7]. Therefore, to compare the efficacy of IL-12, associated with systemic toxicity, with the adjuvant HSP70, we combined in one adenovector, iCaspase-based killing with secreted HSP70. To further improve the system, we shifted from iCaspase-1 use to the more sensitive and less leaky icp30Casp-9. Toward this goal, we made 3 separate adenoviruses. These include ADV-CMV-icp30Caspase-9, ADV-ARR$_2$PB-icp30Caspase-9 and ADV-sHSP70-IRES-icp30Caspase9, expressing secreted HSP70 and iCaspase-9. All three vectors have been tested in culture and are very sensitive to CID administration (**Fig. 7**). Experiments in vivo to treat TRAMP mice or s.c. TRAMP-C2 tumor cells are underway.

KEY RESEARCH ACCOMPLISHMENTS:

- Demonstration that iCaspases can kill prostate adenocarcinoma cells in autochthonous tumors

- Demonstration that combination vaccines with iCaspase-1 and IL-12 can eliminate small sc tumors and greatly retard medium-sized sc TRAMP tumors in syngeneic mice.

- Demonstration that combination vaccines with iCaspase-1 and IL-12 can increase survival of prostate cancer-bearing mice.

- Demonstration that 3 novel adenovectors expressing icp30Caspase9 can kill target prostate tumor cells.

- Demonstration that all three composite prostate cell line-specific promoters, hK2-E3/P, PSA-E2/P and hK2-E3/P are active in prostate cells and prostate cancer cells in reporter transgenic mice and SC tumors. Although the promoters can be somewhat attenuated with progression, they are still active.

REPORTABLE OUTCOMES:

Appendix #:

1. Ekaterina Yu. Nikitina, Smruti A. Desai, Xiuqin Zhao, Weitao Song, Annie Z. Luo, Rama D. Gangula, Kevin M. Slawin and **David M. Spencer.** (2005) Versatile prostate cancer treatment with inducible caspase and interleukin-12, Cancer Research, 65 (10) 4309-19.[8]

2. *Use of iCaspase-9 suicide gene to control T cell survival in vivo. This gene was developed as part of our prostate cancer vaccine:*

Karin Straathof, Martin Pulè, Patricia Yotnda, Gianpietro Dotti, Elio Vanin, Malcolm Brenner, Helen Heslop, **David M. Spencer**, Cliona Rooney (2005) An inducible caspase 9 safety switch for cell therapy, Blood 105 (11) 4247-4254.[9]

3. *Paper describing new prostate reporter mice and crosses with TRAMP and JOCK is in press:*

Seethammagari, M., Xie, X., Greenberg, N.M., and **Spencer, D.M.** (2006) EZC2-Prostate offer both high-sensitivity and specificity for non-invasive imaging of prostate cancer progression and androgen receptor action. Cancer Res., *in press*.

CONCLUSIONS:

Our ultimate goal was to develop an injectable vaccine for advanced prostate disease that does not depend on antigen characterization or *ex vivo* culturing of patient tissue. Towards this goal we demonstrated a combinatorial vaccine based on inducible caspases and the cytokine adjuvant IL-12. These are expressed in an adenoviral vector, which was injected intratumorally. When these vectors are injected into s.c. tumors, complete tumor regression is possible in small tumors and significant regression is seen in larger tumors, corresponding to expansion of tumor-specific CTL and IFNγ-expressing cells from splenocytes of vaccinated mice. We have also developed and began testing delivery of tissue-specific iCaspases to the prostates of TRAMP mice. Towards this goal we built and characterized 3 distinct lines of prostate-specific reporter mice, called EZC-Prostate mice (These mice will be made available to the research community through the NIH MMHCC repository). Initiation of intra-prostatic vaccines based on our initial vectors has shown significant efficacy, triggering apoptosis, anti-tumor immunity and prolonging longevity. During the next year, we will compare IL-12 with secreted HSP70 as adjuvants and characterize improved iCaspases, based on Caspase-9.

These studies should be the basis of a novel vaccine approach that should be easily converted to a clinical protocol provided the results show efficacy. Immunotherapy such as this is likely to be more effective and better tolerated than chemotherapies to eliminate disseminated disease, since androgen-independent metastasis often coincides with increased resistance to chemotherapy.

REFERENCES:

1. Shariat, S.F. et al. Adenovirus-mediated transfer of inducible caspases: a novel "death switch" gene therapeutic approach to prostate cancer. *Cancer Res* **61**, 2562-71. (2001).
2. Xie, X. et al. Adenovirus-mediated tissue-targeted expression of a caspase-9-based artificial death switch for the treatment of prostate cancer. *Cancer Res* **61**, 6795-804. (2001).
3. Kaplan-Lefko, P.J. et al. Pathobiology of autochthonous prostate cancer in a pre-clinical transgenic mouse model. *Prostate* **55**, 219-37 (2003).
4. Xie, X. et al. Robust prostate-specific expression for targeted gene therapy based on the human kallikrein 2 (hK2) promoter. *Hum Gene Ther* **12**, 549-561 (2001).
5. Xie, X., Luo, Z., Slawin, K.M. & Spencer, D.M. The EZC-prostate model: noninvasive prostate imaging in living mice. *Mol Endocrinol* **18**, 722-32 (2004).
6. Zhang, J., Thomas, T.Z., Kasper, S. & Matusik, R.J. A small composite probasin promoter confers high level of prostate-specific gene expression through regulation by androgens and glucocorticoids in vitro and in vivo. *Endocrinology* **141**, 4698-4710 (2000).
7. Huang, X.F. et al. A broadly applicable, personalized heat shock protein-mediated oncolytic tumor vaccine. *Cancer Res* **63**, 7321-9 (2003).
8. Nikitina, E.Y. et al. Versatile prostate cancer treatment with inducible caspase and interleukin-12. *Cancer Res* **65**, 4309-19 (2005).
9. Straathof, K.C. et al. An inducible caspase 9 safety switch for T-cell therapy. *Blood* **105**, 4247-54 (2005).

Versatile Prostate Cancer Treatment with Inducible Caspase and Interleukin-12

Ekaterina Yu. Nikitina,[1] Smruti A. Desai,[1] Xiuqin Zhao,[1,2] Weitao Song,[2] Annie Z. Luo,[2] Rama D. Gangula,[1] Kevin M. Slawin,[2] and David M. Spencer[1]

[1]Department of Immunology and [2]Scott Department of Urology, Baylor College of Medicine, Texas Medical Center, Houston, Texas

Abstract

To establish optimized conditions for immunity against prostate cancer, we compared the efficacy of multiple approaches in autochthonous and s.c. transgenic adenocarcinoma of the mouse prostate (TRAMP)-based models. Mice immunized with interleukin (IL)-12–containing apoptotic, but not necrotic TRAMP-C2 cell–based, vaccines were resistant to TRAMP-C2 tumor challenge and re-challenge, independently of the route of vaccination (s.c. or i.p.). Administration of γ-irradiated TRAMP-C2 cells preinfected with adenovirus containing both B7-1 and IL-12 genes, unlike adenovirus containing B7-1 alone, considerably protected C57BL/6 mice from TRAMP-C2 tumor growth and extended the life span of TRAMP mice. Vaccines that included dendritic cells, instead of IL-12, were equally efficient. Whereas injections of ligand-inducible caspase-1– and IL-12–containing adenoviruses cured small s.c. TRAMP-C2 tumors, nanopump-regulated delivery of viruses led to elimination of much larger tumors. The antitumor immune responses involved $CD4^+$-, $CD8^+$-, and natural killer cells and were strengthened by increasing the number of vaccinations. Intraprostatic administration of inducible caspase-1– and IL-12–containing adenoviruses resulted in local cell death and improved survival of adenocarcinoma-bearing TRAMP mice. Thus, tumor cell apoptosis induced by caspase *in situ* and accompanied by IL-12 is efficient against prostate cancer in a preclinical model. (Cancer Res 2005; 65(10): 4309-19)

Introduction

Due to advances in early detection and treatment of prostate cancer, the death rate from prostate cancer is at its lowest level since the National Cancer Institute began tracking cancer mortality in 1973 (1). Nevertheless, 20% to 25% of patients treated with surgery or radiation for localized prostate adenocarcinoma experience disease progression, presumably associated with occult, micrometastatic cancer. Evidently, a deeper understanding is needed of the immunologic mechanisms that result in prostate cancer prevention or regression in model systems.

An important question of immunotherapeutic design is whether apoptotic or necrotic tumor cells are better as a source of tumor antigens to stimulate specific antitumor immunity. Dendritic cells are 1,000 to 10,000 times more efficient at forming MHC-peptide complexes from phagocytosed cells than at forming them from preprocessed peptides (2). Potentially, both cell lysate-pulsed dendritic cells (3) and those exposed to apoptotic cells (4) induce T-helper 1 cell and CTL reactivity *in vitro* and mediate tumor regression *in vivo*. Because the optimum source of antigens remains a debatable issue (5–8), it may have to be readdressed for each tumor model.

Suicide gene therapy represents an attractive approach to trigger tumor cell death *in situ*, providing a depot of potential tumor antigens while avoiding the side effects of radio- and chemotherapies. Herpes simplex virus type I thymidine kinase (HSV-tk) has been the most widely used suicide gene to date, partially because of its precedence and "bystander effect" (9, 10). However, alternatives are necessary for higher efficiency at killing slowly dividing tumor cells, such as prostate cancer cells. We have previously shown that lipid-permeable dimerizing ligand-inducible caspase–mediated apoptosis is cell cycle-independent, nontoxic to nontargeted cells and a minimally invasive way of creating a large source of dying tumor cells *in vivo* (11, 12). Moreover, inducible caspases can be restricted by tissue-specific promoters. Despite the clear theoretical advantages of inducible caspases, their application to transgenic cancer models and inducible caspase–driven immune responses have never been reported.

In addition to antigens, adjuvant(s), the number, type and activation state of antigen-presenting cells, tumor-specific helper/effector, and regulatory T cells influence the efficacy of immunotherapy (13). In general, inducers of an antitumor immune response must neither tolerize nor overstimulate (13, 14). Potential improvements on an antitumor immune response include the use of costimulatory molecules (e.g., B7-1) to drive T cells towards activation, cytokines [e.g., interleukin (IL)-12] to induce CTL-favoring T-helper 1 differentiation and expansion, and dendritic cells as antigen-presenting cells and an additional source of cytokines.

Intraprostatic administration of therapeutic molecules/cells into mice mimics vector delivery in prostate cancer clinical trials (15, 16). Direct injection into the prostate results in the wide dispersion of adenoviral vectors, especially within the urogenital tract (17, 18), likely providing extra protection against micrometastases. To date, the majority of studies reporting intratumoral treatment of mice have been done in orthotopic preimplanted (19, 20) or s.c. (21) tumor models. The apparent recalcitrance to treat transgenic adenocarcinoma of the mouse prostate (TRAMP) mice intraprostatically (22) is likely related to the heterogeneity of pathology and variability of tumor progression rates in these animals (23, 24). Nevertheless, prostate cancer in TRAMP mice has proven to be sensitive to therapies, when the treatment is started at an appropriate time (23, 25). Depending on the protocol used, the life span of treated TRAMP animals can be extended by 6 to 8 weeks (26), and the incidence of metastasis can be reduced by 30% (27).

Note: Supplementary data for this article are available at Cancer Research Online (http://cancerres.aacrjournals.org/).

Requests for reprints: David M. Spencer, Department of Immunology, Baylor College of Medicine, Texas Medical Center, One Baylor Plaza, BCMM-M929, Houston, TX 77030. Phone: 713-798-6475; Fax: 713-798-3033; E-mail: dspencer@bcm.tmc.edu.

Although extensive apoptosis is capable of promoting dendritic cell maturation (28), modest apoptosis is unlikely to be immunogenic in the absence of exogenous "danger" signals. Therefore, we hypothesized that caspase-killed tumor cells supplemented with IL-12 might trigger robust immune responses against prostate cancer. Accordingly, by systematically testing several variables, including method of killing tumor cells, route of vaccine delivery, presence of a costimulatory molecule, cytokines, and/or dendritic cells, we developed an optimized prostate tumor vaccine protocol. Further, the same protocol was shown to be effective for the treatment of both ectopic and autochthonous prostate tumors in TRAMP-based animal models.

Materials and Methods

Animals. Six- to eight-week-old male C57BL/6 (BL/6) mice were purchased from the Donation Vendor Facility of Baylor College of Medicine (Houston, TX). B6.129S2-Cd4^{tm1Mak} (CD4 knockout), B6.129S2-Cd8^{tm1Mak} (CD8 knockout), and nude (B6.Cg-*Foxn1*^{nu}) mice were purchased from Jackson Laboratory (Bar Harbor, ME). TRAMP mice (BL/6 background) were generously provided by N.M. Greenberg (Baylor College of Medicine). All mice were housed in pathogen-free units in the Transgenic Mouse Facility at Baylor College of Medicine.

Cell lines. TRAMP-based TRAMP-C2 cells (referred to as TC2 in the illustrations), provided by N.M. Greenberg, no longer have detectable SV40 early genes, but still express low levels of androgen receptors and were maintained in high glucose DMEM supplemented with 10^{-8} mol/L dihydrotestosterone, 5 μg/mL insulin, 5% nu-serum IV culture complement (Becton Dickinson, Bedford, MA), 5% fetal bovine serum (FBS), 2 mmol/L L-glutamine, and antibiotics. YAC-1 and B16 cells were obtained from American Type Culture Collection (Manassas, VA). RM-1 cells were a gift from T.C. Thompson (Baylor College of Medicine). YAC-1 cells were cultured in complete culture medium consisting of RPMI 1640, 10% FBS, 2 mmol/L L-glutamine, 20 mmol/L HEPES, and antibiotics, RM-1 and B16 cells—in high glucose DMEM-based complete culture medium.

Generation of dendritic cells. Dendritic cells were generated from bone marrow of naïve BL/6 mice in complete culture medium supplemented with 20 ng/mL recombinant murine (rm) granulocyte-macrophage colony-stimulating factor, 10 ng/mL rmIL-4 and 50 μmol/L 2-mercaptoethanol. After 5 days in culture, cells were enriched by centrifugation over a 13.5% metrizamide gradient (Accurate Chemical & Scientific Corporation, Westbury, NY). The purity of dendritic cells was >80% as determined by flow cytometry based on CD11c, CD11b, B7-2, and I-A^b expression.

Transduction of cells with viral vectors. TRAMP-C2 cells were infected with various adenoviral vectors [multiplicity of infection (MOI) 40, if not indicated otherwise] and cultured for 5 days *prior* to their killing. Ad-B7-1, carrying murine B7-1, Ad-IL-12, expressing IL-12 polypeptide chains p35 and p40, AdBP1, containing B7-1 and IL-12, as well as control adenovirus (Ad-c), were gifts from F.L. Graham (McMaster University, Hamilton, Ontario, Canada; ref. 29). B7-1 expression on the surface of TRAMP-C2 cells and IL-12 secretion were determined by flow cytometry analysis (anti-mouse CD80 antibody; PharMingen, San Diego, CA) and ELISA [OptEIA Mouse IL-12 (p70) set; PharMingen], respectively. Levels of both peaked after 3 days and remained stable for a minimum of 6 days. Adenovirus containing HSV-tk (Ad-HSV-tk) was obtained from the Vector Development Laboratory (Baylor College of Medicine). Ad-iCasp1, containing chemical inducer of dimerization (CID)-inducible caspase-1, was described previously as Ad-G/iCasp1 (30).

Immunization of mice and their challenge with tumor. TRAMP-C2 cells (nontransduced or transduced with adenoviral constructs) were γ-irradiated with 60 Gy using a Gammacell 1000, model C irradiator (Atomic Energy of Canada Ltd., Kanata, Ontario, Canada), washed with Dulbecco's PBS and injected i.p. or s.c. into the hind legs of BL/6, B6.129S2-Cd4^{tm1Mak}, B6.129S2-Cd8^{tm1Mak}, nude, or 6- and 9-week-old TRAMP mice at 2×10^6 cells per mouse. In some experiments, purified dendritic cells were administered at 1.5×10^6 per mouse, alone or together with TRAMP-C2 cells. Control animals were injected with PBS.

Besides γ-irradiation, apoptosis-inducing methods of triggering cell death included infection of cells with Ad-HSV-tk (MOI 10) or Ad-iCasp1 followed by 2-day ganciclovir (100 mmol/L) or CID (200 nmol/L AP20187; ARIAD Pharmaceuticals, Inc., Cambridge, MA) treatment, respectively. Necrosis was induced by three freeze-thaw cycles. In some cases, this was preceded by incubation of cells at 42°C for 30 minutes to induce production of heat-shock proteins followed by a 3-hour recovery period at 37°C.

Immunizations were repeated two to four times as described in Fig. 1*A*. After the last immunization, mice (excluding TRAMP mice) were challenged with viable TRAMP-C2 cells (sufficient to induce tumor growth in 100% of BL/6 mice). Subcutaneous tumors were measured biweekly until animals required euthanasia. Tumor volumes were estimated using the formula: $m_1^2 \times m_2 \times 0.5236$, where m_1 and m_2 represented the maximum diameters of the tumor. Tumor-free mice were observed for at least 60 days following tumor cell rejection. Antitumor immune responses were evaluated 10 to 21 days after final immunization of mice bearing small tumors or reimmunization of tumor-free mice.

Treatment of mice with established tumors. One million viable TRAMP-C2 cells were inoculated s.c. into the hind legs of BL/6 mice. When minimum diameters of tumors reached at least 3, 5, or 5.8 mm, Ad-IL-12 and Ad-iCasp1 were injected intratumorally as indicated in Fig. 1*B*. Ad-c was used alone or added to other viruses, so that each mouse received 3.5×10^{10} total viral particles. A nanopump (model KDS310; KD Scientific, Inc., Holliston, MA) was used to treat the largest tumors by slow administration of viruses (5 μL/minute). Three days after each virus injection, CID (AP20187, 2 mg/kg body weight) or CID carrier (aqueous solution containing 27% polyethylene glycol 400 and 1.5% Tween 80) was given i.p. to mice that had been treated with Ad-iCasp1 or other viruses, respectively. Control animals were injected with PBS. Observation of mice, evaluation of antitumor responses and re-challenge of tumor-free mice were done as described above.

Twelve-week-old TRAMP mice were treated either by s.c. injections with γ-irradiated preinfected TRAMP-C2 cells as described above, or by two virus injections with a 3-week interval into a ventral prostate lobe, followed by CID or CID carrier administration. Doses of intraprostatically injected viruses were 5-fold lower than described in Fig. 1*B*. Long-term mouse survival was determined.

ELISPOT assay for IFN-γ. Ninety-six-well Multi-Screen-HA plates (Millipore, Bedford, MA) were coated with 10 μg/mL purified rat anti-mouse IFN-γ monoclonal antibody (clone R4-6A2; PharMingen) and incubated with 2×10^5 splenocytes per well in complete culture medium supplemented with 5 ng/mL rmIL-2 for 24 hours in the presence or absence of 2×10^3 TRAMP-C2 cells, pretreated with 10 ng/mL rmIFN-γ for 4 days and γ-irradiated with 100 Gy on the eve of the assay. Alternatively, splenocytes were stimulated with 4×10^3 or 2×10^5 dendritic cells preincubated with γ-irradiated (100 Gy) TRAMP-C2 cells at ratio of 1:1 for 24 hours and centrifuged over Lympholyte-M gradient. Pokeweed mitogen (6 μg/mL; Sigma, St. Louis, MO) was used as a positive control. Plates were then incubated overnight at 4°C with 5 μg/mL biotinylated rat anti-mouse IFN-γ monoclonal antibody (clone XMG1.2; PharMingen). Spots were visualized with 5-bromo-4-chloro-3-indolyl phosphate/nitro blue tetrazolium alkaline phosphatase substrate (Sigma) reaction, counted per triplicate well using a stereomicroscope and normalized for 10^6 cells.

CTL assay. Splenocytes were cultured for 7 days in Eagle's MEM containing Earle's salts, 1 mg/mL dextrose, 5 mmol/L L-glutamine, 1 mmol/L sodium pyruvate, 10 mmol/L HEPES, antibiotics, MEM essential amino acids, 0.15 mmol/L MEM nonessential amino acids, 50 μmol/L 2-mercaptoethanol, 10% FBS, and 15% rat T-stim culture supplement without concanavalin A (Becton Dickinson) and every other day provided with 5 ng/mL rmIL-2 starting at day 2. Stimulation was done using 500 dendritic cells per well that had been preincubated with γ-irradiated (100 Gy) TRAMP-C2 cells at a ratio of 1:1 for 24 hours and centrifuged over a Lympholyte-M gradient. Effector cells were then collected and coincubated with 10 ng/mL rmIFN-γ-pretreated ^{51}Cr-labeled TRAMP-C2 cells at ratios of 90:1, 60:1, 30:1, 15:1, and 7.5:1 in triplicate for 6 hours. At a 60:1 ratio, 50 YAC-1 cells were added per ^{51}Cr-labeled target cell.

RM-1 and B16 cells were used as alternative targets. Radioactivity was measured by scintillation counter (Beckman Coulter, LS 6500; Beckman Instruments, Inc., Fullerton, CA). The percentage of cell lysis was calculated as follows: [(experimental release − spontaneous release) / (maximum release − spontaneous release)] × 100%.

Histochemistry. Subcutaneous tumor, prostate, spleen and liver tissues were fixed in 10% buffered formalin, embedded in paraffin, rehydrated and stained with H&E by routine procedure or for leukocyte acid phosphatase using Sigma kit reagents. Terminal deoxynucleotidyl transferase–mediated dUTP nick end-labeling (TUNEL) assay was done according to the manufacturer's instructions (Roche Diagnostics, Mannheim, Germany).

Statistical analyses. Data are presented as mean ± SD. The difference between experimental groups was considered to be significant at $P < 0.05$ as was determined by Student's t test or ANOVA when appropriate. Kaplan-Meier survival curves were analyzed using a log-rank test (GraphPad software).

Results

Comparison of Apoptotic Versus Necrotic Vaccines and Routes of Vaccine Delivery

Because immunization efficacy can depend on the accessibility of the vaccine to antigen-presenting cells, we immunized animals with apoptotic or necrotic tumor cells either i.p. or s.c. The costimulatory molecule, B7-1 (CD80), was tested because of multiple reports of improved immunogenicity of tumor cells expressing B7-1 (31–33), and IL-12 — as a cytokine that enhances a T-helper 1-biased immune response. Before injection, TRAMP-C2 cells were preinfected with AdBP1, expressing B7-1 and IL-12, and killed by one of five methods (Fig. 1*A*) inducing primarily apoptosis, necrosis, or both (HSV-tk/ganciclovir treatment; refs. 9, 34).

All three vaccines based on apoptotic tumor cells offered considerable protection against viable tumor cells, whereas neither the mock-vaccination nor the two necrosis-based vaccines showed any significant protection (Supplemental Fig. 1A). Moreover, there was no significant difference in results between vaccination via i.p. and s.c. routes (data not shown). Eighteen of 20 animals initially resistant to tumor challenge were also resistant to a re-challenge done 2 months later (Supplemental Fig. 1B), indicating long-term immunologic memory. Because secondary necrosis likely accompanied apoptosis, we cannot definitively conclude that apoptosis, in the absence of necrosis, was sufficient to prime the strong antitumor effects. Nevertheless, it is remarkable that even heat-shock did not improve necrosis-based vaccine efficacy. Having shown the equivalency of proapoptotic methods, in subsequent studies examining the immunogenicity of *ex vivo*–killed tumor cells, we used γ-irradiated TRAMP-C2 cells s.c.

IL-12, but not B7-1, Is Necessary for Vaccine Efficacy

To determine the impact, if any, of IL-12 and B7-1 molecules on the observed immunogenicity, cells were either infected with AdBP1 or adenoviruses expressing B7-1 or IL-12 alone, or neither (Ad-c) protein, or were uninfected. IL-12 secretion and B7-1 expression by Ad-IL-12- and Ad-B7-1-transduced cells were comparable to that of AdBP1-infected cells at MOI 10, 20 (data not shown), and 40. At optimum viral dose per cell (MOI 40), 90 ± 5% of TRAMP-C2 cells transduced with Ad-B7-1 and 85.0 ± 2.0% of those transduced with AdBP1 expressed B7-1 ("background" due to nontransduced cells is subtracted) on day 4 after infection. The concentration of IL-12 in TRAMP-C2 cell-conditioned media on day 5 after infection with Ad-IL-12 or AdBP1 fluctuated in the range of

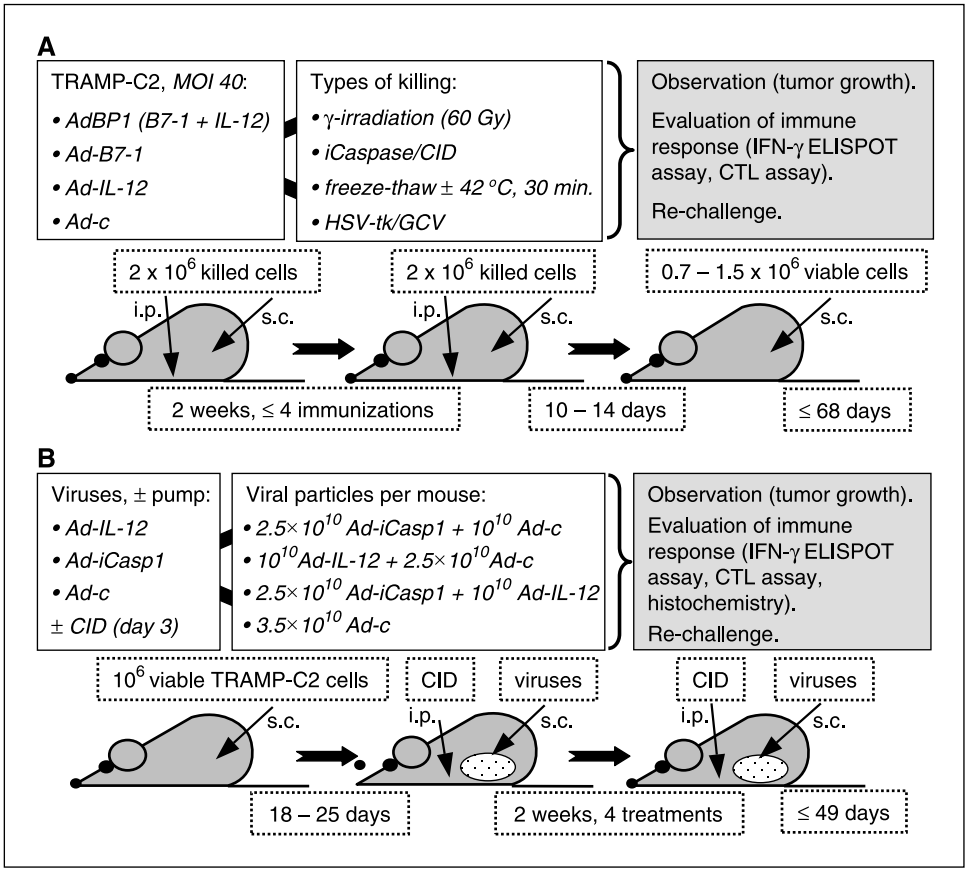

Figure 1. Vaccination and treatment schema. *A,* TRAMP-C2 cells were infected with adenoviral vectors (MOI 40), directing expression of IL-12, B7-1, both (AdBP1), or neither (Ad-c). After 5 days, 2×10^6 transduced γ-irradiated (60 Gy) cells were injected s.c. or i.p. into BL/6 mice. Alternatively, cells were killed by the methods described, which included Ad-iCasp1 (to induce apoptosis), HSV-tk (apoptosis and necrosis), heat-shock in combination with freeze-thaw, or freeze-thaw alone (necrosis). Approximately 2 weeks later, vaccinations were repeated one to three times. Finally, mice were challenged s.c. with 0.7×10^6 to 1.5×10^6 viable TRAMP-C2 cells. *B,* C57BL/6 mice were injected with 10^6 viable TRAMP-C2 cells. Eighteen to 25 days later, established tumors were treated with Ad-IL-12, Ad-iCasp1, both, or Ad-c four times intratumorally followed by i.p. administration of CID or CID carrier and observed.

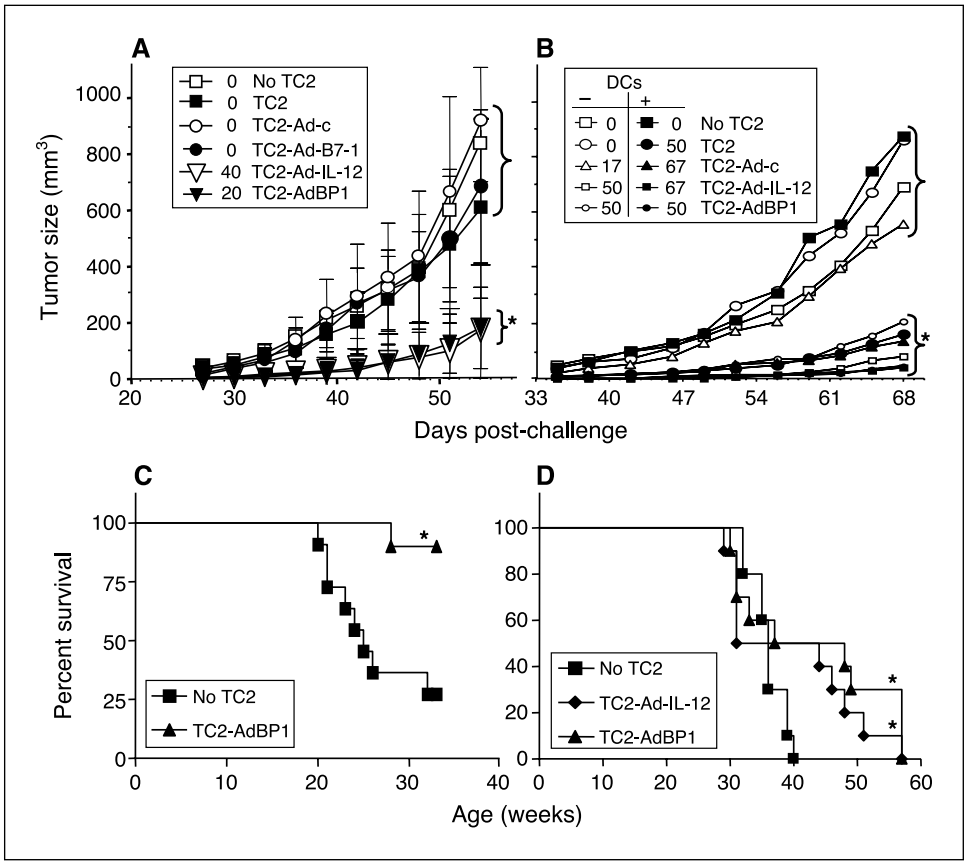

Figure 2. Vaccination and treatment of BL/6 and TRAMP mice with apoptotic TRAMP-C2 cells transduced with IL-12-containing adenoviruses. *A* and *B*, mean tumor volumes for each group of mice at different time points (three independent experiments) are indicated. Percentages of tumor-free animals by the end of the observation are adjacent to the corresponding markers in the legends. *A,* BL/6 mice (n = 10 per group) were vaccinated s.c. twice with noninfected γ-irradiated TRAMP-C2 (TC2) cells or infected with AdBP1, Ad-B7-1, Ad-IL-12, or Ad-c and then challenged with 1.5×10^6 TRAMP-C2 cells. *, statistically significant difference ($P < 0.01$) from mice that did not receive IL-12-containing adenovirus (compared groups are in brackets). *B,* BL/6 mice (6-10 per group) were immunized s.c. four times with γ-irradiated, noninfected, or infected TRAMP-C2 cells in combination with dendritic cells or alone, and then challenged with 0.7×10^6 TRAMP-C2 cells. *, statistically significant difference ($P < 0.01$) between groups in brackets. *DCs*, dendritic cells. *C* and *D*, starting at 16 weeks of age, TRAMP mice were examined weekly for bulky prostate tumors or signs of distress, requiring euthanasia. Percentage of survival is indicated. *C,* 10 mice were vaccinated s.c. with 2×10^6 AdBP1-infected γ-irradiated TRAMP-C2 cells at 9, 13, and 17 weeks of age. A control group of 11 mice was mock-vaccinated with PBS. *, statistically significant difference ($P < 0.01$) from control animals. *D,* TRAMP mice (n = 10) were treated s.c. with either 2×10^6 Ad-IL-12- or AdBP1-infected γ-irradiated TRAMP-C2 cells, or PBS at 12, 14, 16, and 19 weeks of age. *, statistically significant difference ($P < 0.05$) from mock-vaccinated animals.

3,300.0 ± 500.0 ng/10^6 cells (with 64.0 ± 30.0 ng/10^6 cells in media from noninfected cells).

AdBP1- and Ad-IL-12-infected γ-irradiated TRAMP-C2 cells were equally effective in protecting animals from a rigorous (1.5×10^6 cells) tumor challenge (Fig. 2*A*). By contrast, vaccination with Ad-B7-1-infected TRAMP-C2 cells showed no effect relative to uninfected or Ad-c-infected apoptotic TRAMP-C2 cells, or PBS and was therefore not used in further experiments. Thus, IL-12 was a potent adjuvant for apoptotic TRAMP-C2 cell–based vaccines.

Addition of Dendritic Cells Can Optimize TRAMP-C2 Cell–Based Vaccines

To further investigate potential improvements in our immunization design, we added dendritic cells to the vaccines, increased the number of immunizations from two to four and lowered the challenge dose of viable TRAMP-C2 cells from 2×10^6 to 7×10^5 cells per mouse. Controls with no dendritic cells were used for each distinct vaccine.

Vaccination with Ad-c-infected TRAMP-C2 cells had a minor inhibitory effect on tumor growth not previously seen, and notably better results were shown with Ad-IL-12 and AdBP1, likely due to the outlined changes in immunization protocol (Fig. 2*B*). As before, both Ad-IL-12 and AdBP1 had similar efficacy. The addition of immature dendritic cells to γ-irradiated TRAMP-C2 cells improved every vaccine, including nontransduced TRAMP-C2 cells, whereas dendritic cell injections without TRAMP-C2 cells had no significant effect. Remarkably, dendritic cell addition to noninfected TRAMP-C2 cells produced results comparable to those achieved when Ad-IL-12-transduced TRAMP-C2 cells were not supplemented with dendritic cells. The combination of dendritic cells and IL-12-containing TRAMP-C2 cells elicited the lowest mean tumor size, as well as a high proportion of tumor-free mice; however, the differences between outcomes of effective vaccinations were not statistically significant. Regardless of group, animals that rejected their tumors remained cancer-free after tumor re-challenge 2 months later (data not shown).

Apoptotic AdBP1-Transduced TRAMP-C2 Cells Can Prolong the Lives of Mice Bearing Autochthonous Tumors

As a vigorous test for vaccine efficacy, we immunized TRAMP mice with γ-irradiated AdBP1-infected TRAMP-C2 cells at 6, 10,

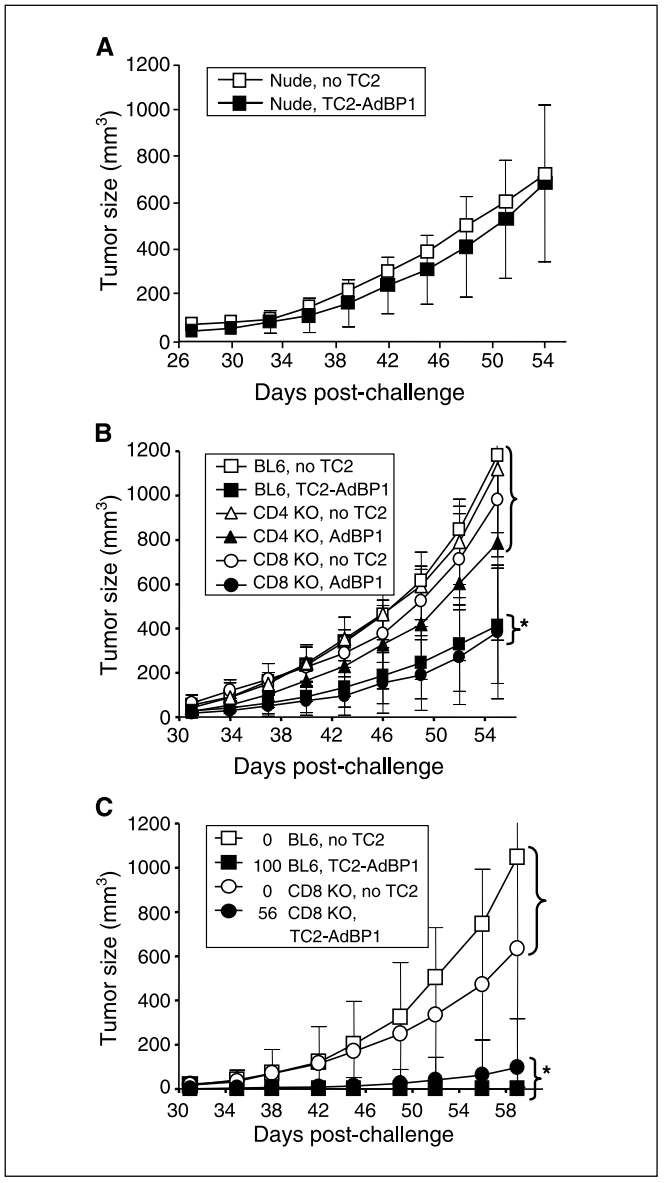

Figure 3. The role for both $CD4^+$- and $CD8^+$-cells in the antitumor effect of the AdBP1-transduced TRAMP-C2 cell–based vaccine. Mice were vaccinated with AdBP1-transduced γ-irradiated TRAMP-C2 cells, then challenged with tumors and observed. Mean tumor volumes for each group at different time points are indicated. *, statistically significant difference ($P < 0.01$) between groups in brackets. *A,* nude mice ($n = 5$) were vaccinated twice, challenged with 1.5×10^6 viable TRAMP-C2 cells and observed for 54 days. Representative of two independent experiments. *B,* wild-type (BL/6), CD4 knockout, and CD8 knockout mice ($n = 10$) were immunized twice followed by challenge with 1.5×10^6 TRAMP-C2 cells and observed for 55 days. *C,* BL/6 ($n = 5$) and CD8 knockout ($n = 8$) mice were immunized thrice followed by challenge with 0.7×10^6 TRAMP-C2 cells and observed for 59 days. Percentages of tumor-free animals by the end of the observation are adjacent to the corresponding markers in the legend. *KO,* knockout.

and 14 weeks of age. A significant reduction in the rate of tumor growth in the vaccinated animals was observed (data not shown). In a more stringent second experiment (Fig. 2*C*), mice were vaccinated in a similar fashion, but the initial vaccination was delayed until 9 weeks of age, at which point most animals display histologic evidence for prostatic intraepithelial neoplasia (35). The average TRAMP male on a BL/6 background requires euthanasia at about 32 weeks (36). However, by 33 weeks of age, only 10% (1 of 10) of vaccinated animals were considered moribund, whereas 72% (8 of 11) of nonvaccinated animals required euthanasia. In addition, the three surviving control animals had large prostate tumors, in contrast to the majority of vaccinated mice with barely palpable tumors. In a third experiment (Fig. 2*D*), mice were treated with γ-irradiated AdBP1- or Ad-IL-12-infected TRAMP-C2 cells four times, starting at 12 weeks of age, when 100% of TRAMP mice reportedly carry adenocarcinoma (23, 35). Initially, we observed a high death rate in all groups, likely due to an incurable stage adenocarcinoma in some mice at the beginning of treatment. Nevertheless, although 100% (10 of 10) of control mice were dead by 40 weeks, 50% of animals in the TRAMP-C2-Ad-IL-12- and TRAMP-C2-AdBP1-treated groups were still alive until 44 and 48 weeks of age, respectively. Again, therapeutic efficiencies of Ad-IL-12- and AdBP1-transduced TRAMP-C2 cells were not statistically different. Thus, IL-12-containing, apoptotic cell–based treatment can significantly prolong the life of mice prone to prostate cancer.

Both $CD4^+$ and $CD8^+$ T Cells Are Required For Maximum Vaccine Efficacy

The utility of IL-12 and resistance of mice to tumor re-challenge implicated T cell involvement. To gain direct evidence for this assumption, we did the immunization in T cell–deficient animals. As expected, vaccination with AdBP1-transduced γ-irradiated TRAMP-C2 cells failed to protect nude mice from TRAMP-C2 tumors (Fig. 3*A*). To investigate the role of T cell subsets in the antitumor response, we vaccinated animals deficient in $CD4^+$ or $CD8^+$ T cells twice. Unexpectedly, no difference was found between mean tumor sizes in vaccinated BL/6 or CD8 knockout mice (Fig. 3*B*). Moreover, 2 of 10 and 3 of 10 animals in these groups, respectively, were tumor-free. Two of 10 immunized CD4 knockout mice also remained tumor-free. However, the mean tumor volume in this group was close to that of nonimmunized mice. To better evaluate the $CD8^+$ T cell requirement, we raised the number of vaccinations and reduced viable tumor cell number. In this case, $CD8^+$ T cell deficiency mildly decreased the resistance of vaccinated mice to TRAMP-C2 cells: 44% of immunized CD8 knockout mice developed tumors, whereas none of the wild-type mice did (Fig. 3*C*). However, tumor growth in CD8 knockout mice was still dramatically slowed. Thus, although both T cell populations were required, $CD4^+$ cells were more critical for efficient antitumor immunity than $CD8^+$ cells.

The Strength of the Antitumor Immune Response Depends on the Number of Immunizations and Type of TRAMP-C2 Cell–Based Vaccine

To further investigate the antitumor effects of the vaccines used, we did ELISPOT and CTL assays with splenocytes isolated from immunized mice.

TRAMP-specific CTL responses. TRAMP-C2 cells express a wide spectrum of mouse homologues of human prostate-specific gene products (37) and are susceptible to lysis by CTLs (38). Accordingly, we found CTL responses in all tumor-challenged (including nonvaccinated) versus naïve animals. However, no statistically significant differences were observed in cytotoxic responses of restimulated *in vitro* splenocytes from mice immunized with different apoptotic TRAMP-C2 cell–based vaccines at the highest effector/target ratios (Fig. 4*A*). Splenocytes from mice immunized with dendritic cell–containing vaccines caused an increased level of TRAMP-C2 cell lysis (up to 40%) even in the absence of restimulation (data not shown).

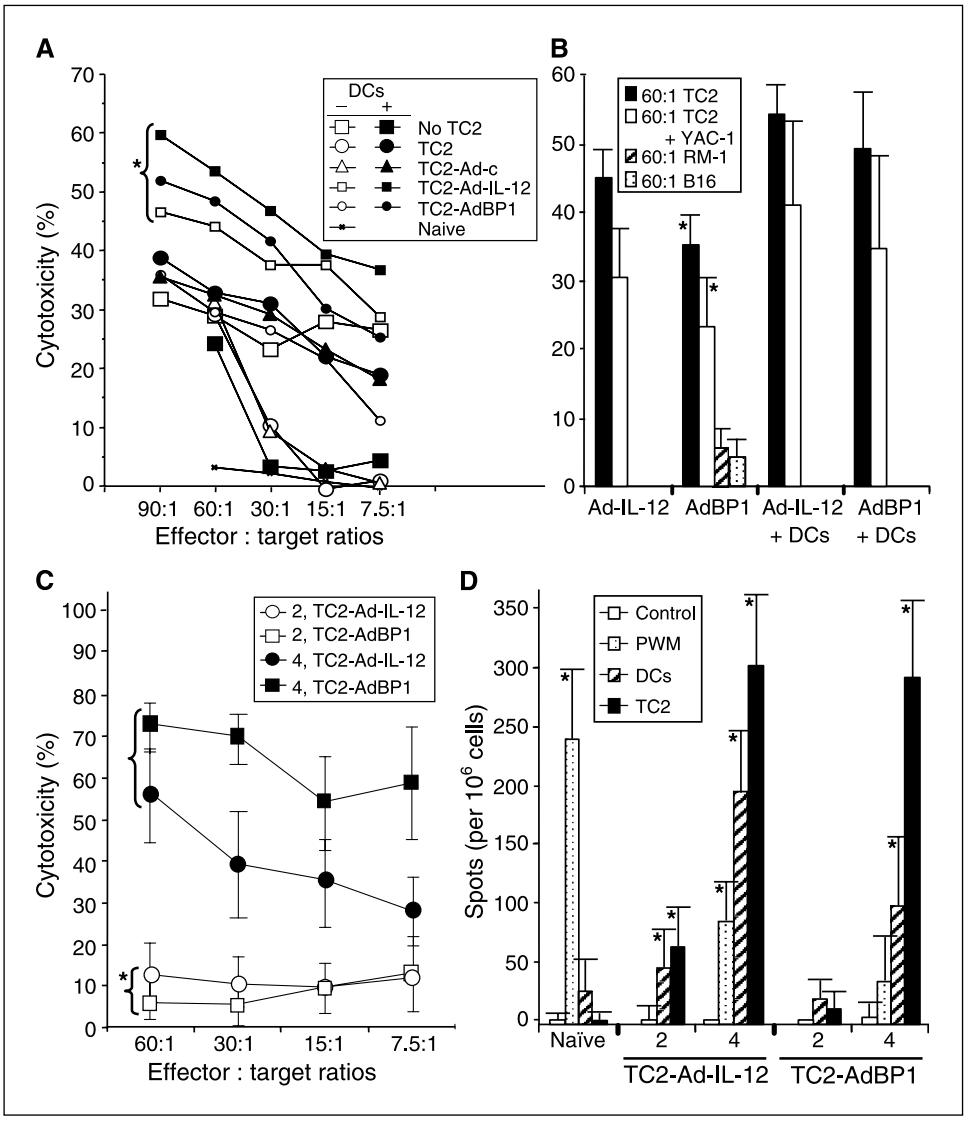

Figure 4. Effect of immunization with apoptotic TRAMP-C2 cell–based vaccines on CTL responses and IFN-γ production by splenocytes of BL/6 mice. *A-C*, animals were immunized as described in the legend to Fig. 2*A* and *B*. A standard 6-hour ^{51}Cr-release assay was done after a 7-day stimulation of splenocytes *in vitro* with dendritic cells exposed to γ-irradiated TRAMP-C2 cells. Six independent experiments were done. Representative of three separate experiments with four mice per group. *A,* CTL responses in mice immunized with different vaccines with or without supplementary dendritic cells are compared. The results are shown as mean percent cytotoxicity against TRAMP-C2 cells at various effector/target ratios. *, statistically significant difference ($P < 0.01$) between groups in bracket and groups that were not vaccinated with TRAMP-C2 cells, calculated at the effector/target ratio 60:1. At this ratio, all groups were different ($P < 0.01$) from naïve animals. *DCs,* dendritic cells. *B,* YAC-1 cells were added at 50-fold excess to splenocytes at an effector/target ratio of 60:1. ^{51}Cr-labeled RM-1 or B16 cells were used as alternative targets for splenocytes from mice immunized with AdBP1-transduced TRAMP-C2 cells. Mean ± SD. *, statistically significant difference ($P < 0.001$) from RM-1 or B16 targets. *C,* cytotoxicity of splenocytes from mice immunized two or four times with TRAMP-C2 cells transduced with either Ad-IL-12 or AdBP1 is represented as mean ± SD. *, statistically significant difference ($P < 0.001$) between groups in brackets, calculated at the effector/target ratio 60:1. *D,* IFN-γ production by freshly isolated splenocytes from mice vaccinated two or four times with γ-irradiated TRAMP-C2 cells transduced with either Ad-IL-12 or AdBP1 was estimated by ELISPOT assay. The responses of splenocytes to 2×10^5 dendritic cells preincubated with γ-irradiated TRAMP-C2 cells, as well as to γ-irradiated TRAMP-C2 cells are represented as mean ± SD spots per 10^6 splenocytes for each group of mice ($n = 6$). IFN-γ secretion was undetectable when TRAMP-C2 cells alone were added to wells; the background due to dendritic cells (no splenocytes) was 24.6 ± 5.2 (data not shown). Pokeweed mitogen (*PWM*) was used as a positive control in naïve and immunized (four times only) animals. *, statistically significant difference ($P < 0.01$) from control (unstimulated splenocytes).

The best results were achieved in mice that were vaccinated with apoptotic TRAMP-C2 cells transduced with IL-12-containing adenoviruses and combined with dendritic cells (Fig. 4*A*). The presence of nonlabeled natural killer (NK)-sensitive YAC-1 cells showed that NK cells were responsible for about one-third of the detected TRAMP-C2 cell lysis, regardless of whether initial vaccines contained AdBP1 or Ad-IL-12 with or without dendritic cells (Fig. 4*B*). At the same time, the observed cytotoxicity was highly specific for TRAMP-C2 cells, because neither syngeneic B16 melanoma nor RM-1 prostate cancer cells were lysed efficiently (Fig. 4*B*). Thus, both CD8 and NK cells contributed to TRAMP-C2 cell killing, stimulated by the apoptosis-based vaccination.

TRAMP-specific IFN-γ production. Dendritic cells are potent inducers of IFN-γ production (39). Consequently, to monitor tumor-specific IFN-γ production in vaccinated mice, splenocytes were coincubated with either γ-irradiated TRAMP-C2 cells or dendritic cells preincubated with γ-irradiated TRAMP-C2 cells.

Dendritic cells preincubated with apoptotic TRAMP-C2 cells had less ability to induce IFN-γ production than did tumor cells (Fig. 4*D*), regardless of the splenocyte/dendritic cell ratio (50:1 and 1:1) used (data not shown). Splenocytes from mice immunized with Ad-IL-12-infected TRAMP-C2 cells responded to TRAMP-C2 cell–exposed dendritic cells insignificantly better than did splenocytes from mice immunized with AdBP1-infected TRAMP-C2 cells (Fig. 4*D*). Furthermore, we compared the numbers of IFN-γ-producing cells among TRAMP-C2 cell–stimulated splenocytes after the various apoptotic cell–based vaccinations. A dramatic difference in the antitumor responses was found only between mice vaccinated with IL-12-expressing TRAMP-C2 cells and nonvaccinated animals (Supplemental Fig. 2). No significant differences were observed between mice immunized with either Ad-IL-12- or AdBP1-transduced TRAMP-C2 cells, or between mice that received the same vaccines with or without supplemental dendritic cells.

TRAMP-specific immune responses after four versus two immunizations. The more robust antitumor effects presented in Figs. 2*B* and 3*C* versus Figs. 2*A* and 3*B* might be explained by additional vaccinations and/or fewer TRAMP-C2 cells for the tumor challenge. To evaluate the role of number of immunizations in the strength of the immune response, we compared the responses of animals vaccinated two or four times with γ-irradiated Ad-IL-12- or AdBP1-transduced TRAMP-C2 cells. Four immunizations of mice with any of these vaccines resulted in greater CTL responses (Fig. 4*C*) and higher ($P < 0.001$) IFN-γ secretion (Fig. 4*D*) than two immunizations.

Intratumoral Administration of IL-12– and Inducible Caspase-1–Containing Adenoviruses Is an Efficient Treatment for Prostate Cancer

Having established the efficacy of the apoptosis- and IL-12-based approach to prostate tumor prophylaxis and eradication, we treated animals with preexisting s.c. or autochthonous tumors with Ad-Casp1/CID and Ad-IL-12.

Treatment of subcutaneous TRAMP-C2 tumors with inducible caspase-1- and IL-12-containing viruses. Intratumoral treatment of BL/6 mice began when their tumors reached either relatively small (4.5 × 5.2 mm or less in maximum diameter) or larger (4.5 × 5.5 mm and greater) sizes (Fig. 5*A* and *B*). All small tumors were rejected following treatment with both Ad-iCasp1 and Ad-IL-12, and one mouse treated with Ad-IL-12 alone also became tumor-free (Fig. 5*A*). Forty percent of mice bearing larger tumors also rejected them after Ad-iCasp1 and Ad-IL-12 treatment, and others showed reduced tumor growth rates (Fig. 5*B*). To test if the critical mass–related limitation of therapeutic efficiency could be partially overcome by improved inoculant delivery, we used a nanopump for slow [5 μL (7-10 × 10^8 viral particles) / minute] virus administration into even larger tumors (5.8 × 7.3 mm and greater). Although these tumors could not be controlled by our standard virus delivery, 40% of mice treated by nanopump with both Ad-iCasp1 and Ad-IL-12 rejected their tumors (Fig. 5*C*). All cured animals remained tumor-free for at least 2 months after re-challenge with TRAMP-C2 tumors (data not shown).

Immune responses in TRAMP-C2 tumor-bearing mice treated with viruses. Mice treated with Ad-Casp1 in combination with Ad-IL-12 had significantly higher numbers of IFN-γ-producing splenocytes than mice in other groups (Fig. 5*D*). These animals, as well as mice, treated with Ad-iCasp1 alone, also showed increased tumor-specific CTL activity (Fig. 5*E*). In contrast to untreated tumors, tissues from animals treated with both Ad-iCasp1 and Ad-IL-12 were characterized by large areas of necrosis and peripheral lymphocyte infiltration intensively stained for acid phosphatase (Supplemental Fig. 3).

Intraprostatic treatment of TRAMP mice with inducible caspase-1- and IL-12-containing viruses. Intraprostatic treatment most accurately imitates clinical applications. Intraprostatically injected Ad-iCasp1 followed by i.p. CID administration, unlike Ad-iCasp1 alone, induces extensive prostate cell death in TRAMP mice that is detected by TUNEL assay 10 (data not shown) and 20 hours (Supplemental Fig. 4) after CID injection. Due to anesthesia-related mortality of animals, treatment with Ad-iCasp1 and Ad-IL-12 was limited to two prostate ventral lobe injections into TRAMP mice starting at 12 weeks of age. Nevertheless, this prolonged TRAMP mouse life span significantly beyond that of animals injected with Ad-c (Fig. 6*A*). H&E staining revealed larger areas of coagulative necrosis in treated than in untreated prostate tissues (Fig. 6*C* and *B*, respectively). Additionally, we observed lymphocyte infiltration, often surrounding these areas, and on the periphery of tumors. The infiltrated regions were saturated with acid phosphatase granules (Fig. 6*G*, *H* versus *F*), mainly characteristic of activated lymphocytes, including NK cells (40). Although frozen tumor sections have been analyzed previously for leukocyte acid phosphatase (41, 42), no reports on staining of formalin-fixed and paraffin-embedded organ tissues, as well as any tissues other than breast tumors for this enzyme have been found. To confirm the relevance and accuracy of our method, we examined spleen (Fig. 6*D*) and liver (Fig. 6*E*) sections. Whereas normal spleen tissues were heavily impregnated with acid phosphatase, representing both diffuse and granular patterns of its distribution, liver tissues were negative for acid phosphatase.

Thus, intratumoral administration of Ad-iCasp1 in combination with Ad-IL-12 treats both s.c. and orthotopic prostate adenocarcinomas, leading to considerably strengthened immune responses, dramatic suppression of tumor growth, and increased mouse survival.

Discussion

The use of dendritic cells in the induction of antitumor responses against poorly immunogenic tumors and in advanced disease is gaining support in clinical trials (43, 44). However, fiscal realities of our health care system dictate that any viable immunotherapeutic strategy should avoid the need to individualize therapy, relying instead on "off-the-shelf" reagents that reduce both time and cost. Because inducible caspases, which can create a source of tumor antigens *in situ* in tumor-bearing hosts, potentially satisfy this requirement, we compared an inducible caspase–based method with several well-described approaches to induce tumor cell death. High efficacy of apoptosis-inducing methods in a TRAMP-based model did not depend on the route of vaccine delivery and was consistent with Scheffer and colleagues' study, showing immunity to apoptotic, but not necrotic, tumor cells (8).

Seeking an optimum combination of inducible caspases with an adjuvant to trigger long-lasting immune responses, we tested B7-1 and IL-12. Conclusions about the comparative efficacy of distinct apoptotic TRAMP-C2 cell–based vaccines were founded on multiple criteria, including tumor growth, level of IFN-γ production and CTL activity. Despite previous observations of the positive therapeutic effects of B7-1 expression by tumor cells (31), especially when $CD28^+$ NK and NKT cells had been activated by IL-12 (32, 33, 45), high levels of B7-1 (approximately 100-fold higher than on nontransduced cells)

on Ad-B7-1-infected TRAMP-C2 cells *prior* to irradiation had no detectable antitumor effects. Whereas low-level B7-1 expression could favor down-regulation of T cell responses (46), excessive costimulation might, in turn, bias T cell responses towards a T-helper 2 phenotype and even so-called "high zone tolerance" (i.e. clonal exhaustion; ref. 47). It is also possible that B7-1 is useful as an adjuvant only when targeted to viable tumor cells (31).

In contrast to B7-1, IL-12 had a dramatic positive effect in TRAMP-based models, and Ad-IL-12 was at least as effective as AdBP1 in both C57BL/6 and TRAMP animals. Although previous studies found that the combination of IL-12 and B7-1 was more efficient than B7-1 or IL-12 alone when respective adenoviral constructs were injected into mouse prostate or mammary adenocarcinomas (29, 48), our observation is in accordance with Aruga and colleagues' report of tumor cells expressing IL-12 having higher immunogenicity than B7-1 (49). This may also support the ability of IL-12 to abrogate T cell tolerance induced by B7-1-CTLA-4 binding (50).

Reported effects of IL-12 include stimulation of $CD4^+$-lymphocyte differentiation, NK activation, IFN-γ secretion by different cells, and CTL activation (51). Because these effects are dose- and model-dependent (52), the existing information regarding IL-12 applications to prostate cancer immunity (10, 48, 52–54) may not be generalizable or fully relevant to findings in TRAMP-based models, and immune responses in each particular study may require careful evaluation. We analyzed antitumor responses at least 2 weeks after the final vaccination to avoid transient T-, B-lymphocyte and antigen-presenting cell depletion following IL-12 administration (55, 56). *In vivo* protection from tumor re-challenge of up to 100% of vaccinated animals showed the efficiency of the apoptotic cell- and IL-12-based approach. Predictably, NK cells contributed significantly to protection against TRAMP-C2 tumors, especially in CD8-deficient mice (57). However, despite the expected role of CTLs (that accounted for approximately two-thirds of the total detected cytotoxicity), the

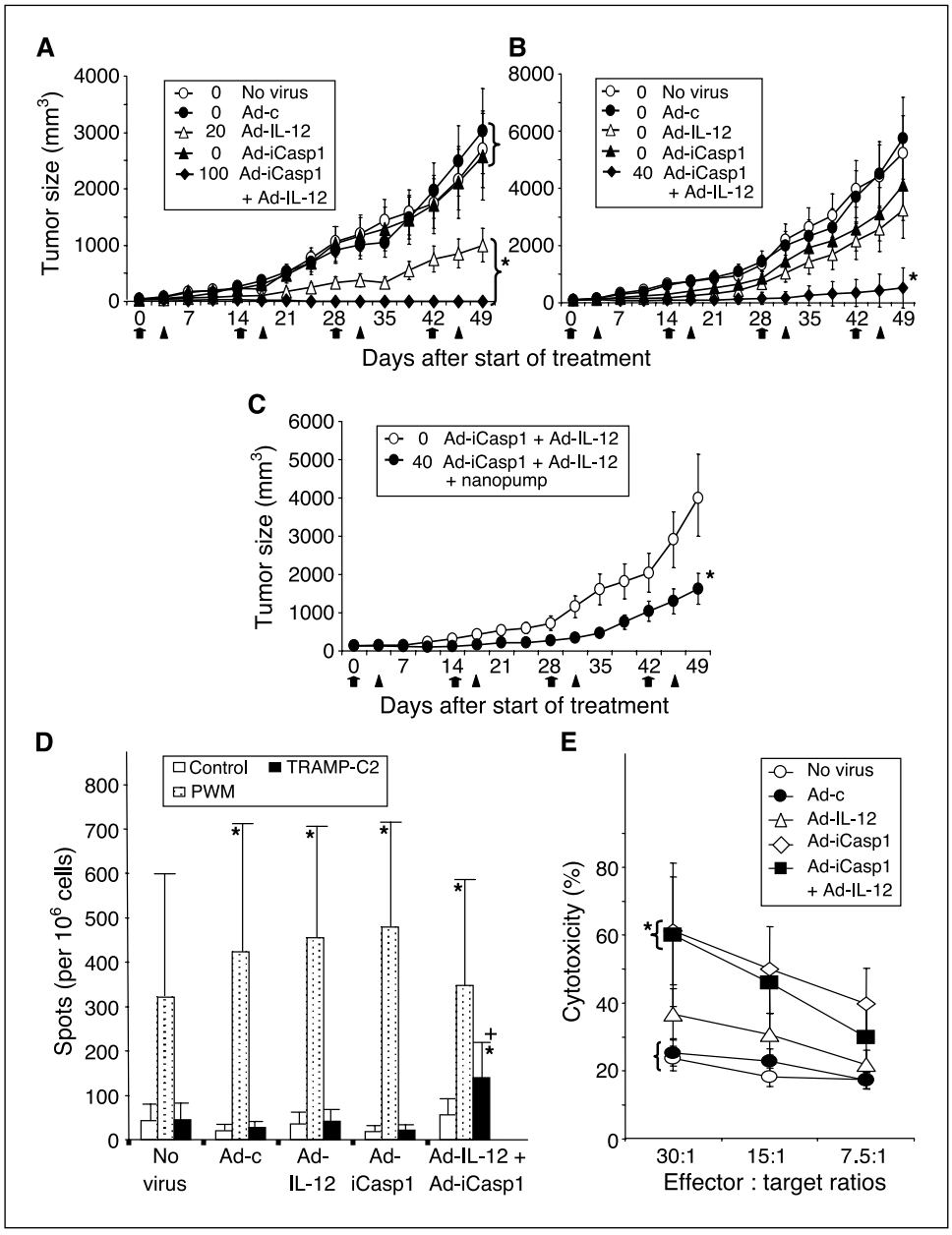

Figure 5. Treatment of s.c. TRAMP-C2 tumors with intratumoral injections of Ad-iCasp1 and Ad-IL-12 and its effect on CTL responses and IFN-γ production by splenocytes. *A-C*, TRAMP-C2 tumor-bearing BL/6 mice were treated intratumorally with either Ad-iCasp1/CID, Ad-IL-12/CID carrier, both, or Ad-c/CID carrier four times. Average tumor volumes at the beginning of the experiments were: (*A*) 37.3 ± 22.7 mm^3, (*B*) 97.8 ± 37.6 mm^3, (*C*) 139.5 ± 29.5 mm^3. Mean ± SD for each group of mice (n = 5) at different time points are shown. Percentages of tumor-free animals by the end of the observation are adjacent to the corresponding markers in the legends. *Arrows,* days of treatment with viruses; *arrowheads,* treatment with CID or CID carrier; *, statistically significant difference (P < 0.01) between groups in brackets (*A*) or from all other groups (*B* and *C*). *D* and *E*, the results are representative of two independent experiments with six mice per group. *D,* IFN-γ production by freshly isolated splenocytes in response to γ-irradiated TRAMP-C2 cells was estimated by ELISPOT assay and is shown as mean ± SD spots per 10^6 splenocytes for each group of mice. *, statistically significant difference (P < 0.05) from control (unstimulated splenocytes); +, statistically significant difference (P < 0.05) from responses to γ-irradiated TRAMP-C2 cells in other groups of mice. *E,* ^{51}Cr-release assay was done after a 7-day stimulation of splenocytes *in vitro* with dendritic cells exposed to γ-irradiated TRAMP-C2 cells. The levels of tumor-specific cytotoxicity are represented as mean ± SD. *, statistically significant difference (P < 0.05) between groups in brackets at effector/target ratio 30:1.

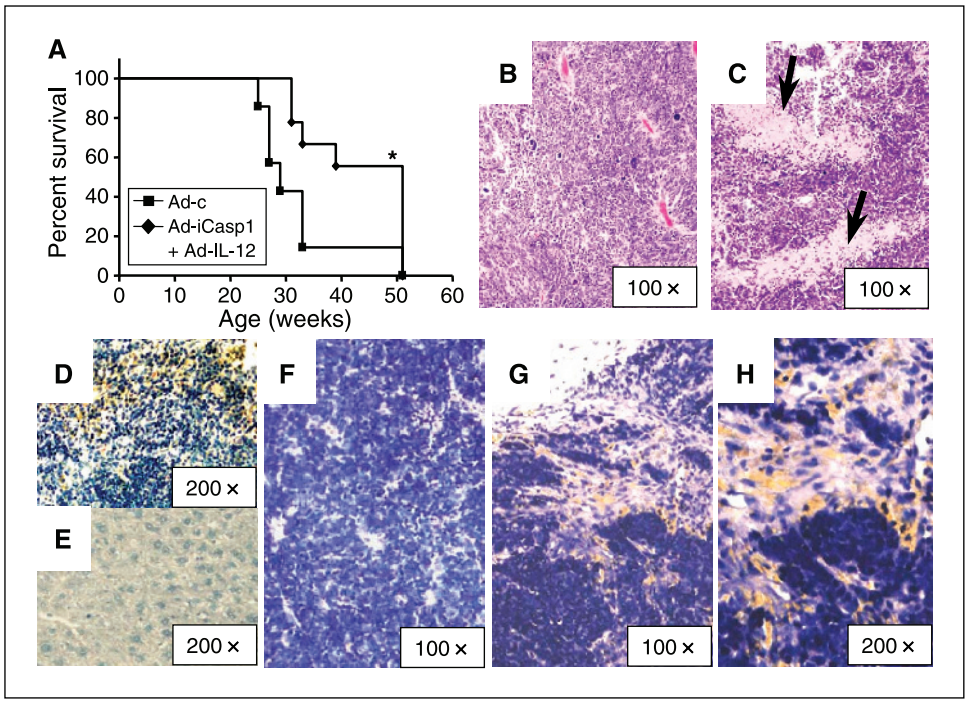

Figure 6. Treatment of TRAMP mice with intraprostatic injections of Ad-iCasp1 in combination with Ad-IL-12. *A,* TRAMP mice (n = 9) were treated intraprostatically at 12 and 15 weeks of age with Ad-iCasp1/CID and Ad-IL-12. A control group (n = 7) was treated with Ad-c/carrier. Starting at 16 weeks of age, mice were examined weekly for bulky prostate tumors or signs of distress and were correspondingly euthanized. The percentage of survival is indicated. *, statistically significant difference (P = 0.03) from control animals. *B*, *C*, *F*, *G*, and *H*, prostates were removed 10 days after a single treatment of 20-week-old TRAMP mice with either Ad-c/CID carrier (*B* and *F*) or Ad-iCasp1/CID together with Ad-IL-12 (*C*, *G*, and *H*). *B* and *C*, H&E staining. Arrows, areas of coagulative necrosis. *D*, *E*, *F*, *G*, and *H*, staining for leukocyte acid phosphatase (yellow granular and diffuse impregnation). Counterstaining with hematoxylin. *D,* spleen tissue. *E,* liver tissue. Magnification shown.

absence of $CD8^+$ cells did not affect vaccine efficacy as dramatically as lack of $CD4^+$ cells. Recently discovered insufficiency of $CD8^+$-responses in CD4 knockout mice seemingly explains this observation (58). At the same time, prominent compensation of MHC class II-restricted immune responses in CD4 knockout mice (58) provided by $CD8^+$ cells suggests the high probability of reciprocal compensatory MHC class I-restricted responses in CD8 knockout mice as well. In fact, although all vaccinated CD8 knockout mice eventually developed tumors by day 80 after tumor challenge (data not shown), tumor growth was retarded, confirming the presence of protective mechanisms (57).

To improve the vaccine microenvironment, we expanded the reservoir of dendritic cells. In addition to cytokine production and antigen presentation (2, 5), dendritic cells transfer antigens from live cells (59) and reduce tumor mass by direct cytotoxicity towards tumor cells (60), followed by phagocytosis of dead cells without consequent immunosuppression (61). Indeed, even without exogenous IL-12, dendritic cell addition dramatically slowed tumor growth in mice vaccinated with TRAMP-C2 cells. Apparently, additional adjuvants are no longer essential to trigger maturation of administered and preexisting dendritic cells when a large number of apoptotic cells is present at the site of injection (28). However, the total IL-12 amount may still be critical for involvement of distinct NK cell populations (45). Thus, although less economical than adenovirus injection alone, use of dendritic cells may have additive benefits for some prostate cancer patients.

We previously shown that inducible caspases could efficiently kill slowly dividing, prostate tumor–derived cells (12). We also reported that intratumoral injections of Ad-iCasp1 led to significant, but transient, reduction in TRAMP-C2 tumor growth and volume (30), and the survival of LNCaP tumor-bearing athymic mice was considerably prolonged by treatment with Ad-iCasp-9 (12). In the present study, we modified that approach for a standardized comparison with other vaccines. The results indicate that the efficiency of TRAMP-C2 cells pretreated with Ad-iCasp1 and CID *in vitro* was as high as the efficiency of HSV-tk-infected TRAMP-C2 cells. Furthermore, having suggested that IL-12 might improve outcome of cancer treatment with inducible caspases, we established the most rigorous test for therapeutic efficacy by evaluating the treatment of different-sized tumors. Apparently, 96 to 101 mm^3 tumors were very close to or had reached a critical mass at which they became incurable with Ad-iCasp1 and Ad-IL-12. Coll et al. have shown that slow (20 μL/minute) delivery of a vector raised the level and duration of transgene expression (62), possibly due to better diffusion and weaker reflux of the inoculant along the needle track. In our experiments, the use of a nanopump expanded the range of treatable tumors and resulted in rejection of 40% of tumors with average volumes of 136 to 143 mm^3. Markedly, although the IFN-γ release by splenocytes from mice treated with Ad-iCasp1 alone was significantly lower than in the case of virus combination, the level of TRAMP-C2-specific CTL activity was similar in both cases. Large central areas of coagulative necrosis and peripheral lymphocyte infiltration were present in tumors treated with both Ad-iCasp1 and Ad-IL-12. *In situ* induction of apoptosis by caspases could eliminate the need for costly and complicated preparation of patient's cells and potentially sustain the high level of apoptosis in prostate tumor tissue between irradiations or when irradiation is unwarranted.

Serendipitously, we found that, in the absence of commercially available anti-CD8 and anti-CD3 antibodies efficiently binding to formalin-fixed tissues, staining for leukocyte acid phosphatase is useful for the retrospective screening of archived tissue samples. Leukocyte acid phosphatase content increases dramatically in activated lymphocytes (63), followed by its redistribution from a mostly diffuse to a more granular pattern (64). Leukocyte acid phosphatase plays a role in NK cell cytotoxicity (65), and the number of blood lymphocytes with granular acid phosphatase reaction is often significantly lower in patients with malignancies than in healthy subjects (66). Although tumor cell death can lead to formation of acid phosphatase–rich granules and

vacuoles inside cells in certain cases (67), in our experiments, untreated tumor tissues, surrounding necrotic areas and/or exhibiting signs of apoptosis, seemed to be negative for acid phosphatase. Positive staining for acid phosphatase was found in those areas of treated tumors that were infiltrated by lymphocytes, based on the results of parallel staining of adjacent sections with H&E.

Although autochthonous prostate tumors can potentially promote immune responses distinct from that induced by s.c. tumors, vaccination with apoptotic IL-12-containing TRAMP-C2 cells significantly increased survival of 6-, 9- and 12-week-old TRAMP mice. As expected based on Hurwitz et al.'s report (25), older mice seemed to be more resistant to the therapy applied. In part, because of the poor accessibility of the mouse prostate gland, intraprostatic immunotherapy in orthotopic prostate cancer models has been attempted in only a few studies. Those that involved IL-12 reported the result of a single virus injection into one of the dorsolateral prostate lobes of BL/6 mice with preestablished RM-9 tumors (48, 54). Although, TRAMP mice usually exhibit nonfocal patterns of adenocarcinoma development (23), notably, in our study, two injections of Ad-iCasp1 and Ad-IL-12 into a single ventral lobe were sufficient to initiate leukocyte infiltration of the prostate and to extend life span of >50% of animals by 12 weeks. Because the ventral lobes of the majority of TRAMP mice undergo malignant transformation at later stages than other prostate lobes, this indicated the induction of a generalized immune response.

For patients with clinically localized disease, intraprostatic injections of inducible caspases in combination with adjuvants may serve as a nonmutagenic presurgical treatment or an alternative to established forms of local therapy, such as radical prostatectomy and γ-irradiation. At the same time, an approach based on *ex vivo* γ-irradiation of excised tumor cells potentially could be used for postsurgical boosting of antitumor immunity against micrometastases in patients at high risk for or experiencing disease recurrence.

Acknowledgments

Received 8/27/2004; revised 2/3/2005; accepted 2/25/2005.

Grant support: NIH grant #R01-CA77266 and DOD grant #PC020062.

The costs of publication of this article were defrayed in part by the payment of page charges. This article must therefore be hereby marked *advertisement* in accordance with 18 U.S.C. Section 1734 solely to indicate this fact.

We thank Dorothy E. Lewis, Richard Cook, and Carolyn Schum for a critical reading of the manuscript; Arthur A. Hurwitz, Margaretha M. Guenther, Alexander V. Selutin, and John R. Rodgers for technical advice; and Michael M. Ittmann for the help in histologic examination of some tissues.

References

1. Chu KC, Tarone RE, Freeman HP. Trends in prostate cancer mortality among Black men and White men in the United States. Cancer 2003;97:1507–16.
2. Inaba K, Turley S, Yamaide F, et al. Efficient presentation of phagocytosed cellular fragments on the major histocompatibility complex class II products of dendritic cells. J Exp Med 1998;188:2163–73.
3. Fields RC, Shimizu K, Mulé JJ. Murine dendritic cells pulsed with whole tumor lysates mediate potent antitumor immune responses *in vitro* and *in vivo*. Proc Natl Acad Sci U S A 1995;95:9482–7.
4. Nouri-Shirazi M, Banchereau J, Bell D, et al. Dendritic cells capture killed tumor cells and present their antigens to elicit tumor-specific immune responses. J Immunol 2000;165:3797–803.
5. Larsson M, Fonteneau JF, Bhardwaj N. Dendritic cells resurrect antigens from dead cells. Trends Immunol 2001;22:141–8.
6. Basu S, Binder RJ, Suto R, et al. Necrotic but not apoptotic cell death releases heat shock proteins, which deliver a partial maturation signal to dendritic cells and activate the NF-κB pathway. Int Immunol 2000;12:1539–46.
7. Kotera Y, Shimizu K, Mulé JJ. Comparative analysis of necrotic and apoptotic tumor cells as a source of antigen(s) in dendritic cell-based immunization. Cancer Res 2001;61:8105–9.
8. Scheffer SR, Have H, Korangy F, et al. Apoptotic, but not necrotic, tumor cell vaccines induce a potent immune response *in vivo*. Int J Cancer 2003;103:205–11.
9. Ramesh R, Munshi A, Marrogi AJ, Freeman SM. Enhancement of tumor killing using a combination of tumor immunization and HSV-tk suicide gene therapy. Int J Cancer 1999;80:380–6.
10. Hall SJ, Canfield SE, Yan Y, et al. A novel bystander effect involving tumor cell-derived Fas and FasL interactions following Ad.HSV-tk and Ad.mIL-12 gene therapies in experimental prostate cancer. Gene Ther 2002;9:511–7.
11. Fan L, Freeman KW, Khan T, et al. Improved artificial death switches based on caspases and FADD. Hum Gene Ther 1999;10:2273–85.
12. Xie X, Zhao X, Liu Y, et al. Adenovirus-mediated tissue-targeted expression of a caspase-9-based artificial death switch for the treatment of prostate cancer. Cancer Res 2001;61:6795–804.
13. Morel PA, Feili-Hariri M, Coates PT, Thomson AW. Dendritic cells, T tolerance and therapy of adverse immune reactions. Clin Exp Immunol 2003;133:1–10.
14. Overwijk WW, Restifo N. Creating therapeutic cancer vaccines: notes from the battlefield. Trends Immunol 2001;22:5–7.
15. Trudel S, Trachtenberg J, Toi A, et al. A phase I trial of adenovector-mediated delivery of interleukin-2 (AdIL-2) in high-risk localized prostate cancer. Cancer Gene Ther 2003;10:755–63.
16. Satoh T, Teh BS, Timme TL, et al. Enhanced systemic T-cell activation after *in situ* gene therapy with radiotherapy in prostate cancer patients. Int J Radiat Oncol Biol Phys 2004;59:562–71.
17. Timme TL, Hall SJ, Barrios R, et al. Local inflammatory response and vector spread after direct intraprostatic injection of a recombinant adenovirus containing the herpes simplex virus thymidine kinase gene and ganciclovir therapy in mice. Cancer Gene Ther 1998;5:74–82.
18. Paielli DL, Wing MS, Rogulski KR, et al. Evaluation of the biodistribution, persistence, toxicity, and potential of germ-line transmission of a replication-competent human adenovirus following intraprostatic administration in the mouse. Mol Ther 2000;1:263–74.
19. Somers K, Brown RR, Holterman DA, et al. Orthotopic treatment model of prostate cancer and metastasis in the immunocompetent mouse: efficacy of flt3 ligand immunotherapy. Int J Cancer 2003;107:773–80.
20. Eastham JA, Grafton W, Martin CM, Williams BJ. Suppression of primary tumor growth and the progression to metastasis with p53 adenovirus in human prostate cancer. J Urol 2000;164:814–9.
21. Voeks D, Martiniello-Wilks R, Madden V, et al. Gene therapy for prostate cancer delivered by ovine adenovirus and mediated by purine nucleoside phosphorylase and fludarabine in mouse models. Gene Ther 2002;9:759–68.
22. Martiniello-Wilks R, Dane A, Voeks DJ, et al. Gene-directed enzyme prodrug therapy for prostate cancer in a mouse model that imitates the development of human disease. J Gene Med 2004;6:43–54.
23. Kaplan-Lefko PJ, Chen TM, Ittmann MM, et al. Pathobiology of autochthonous prostate cancer in a pre-clinical transgenic mouse model. Prostate 2003;55:219–37.
24. Martiniello-Wilks R, Dane A, Mortensen E, et al. Application of the transgenic adenocarcinoma mouse prostate (TRAMP) model for pre-clinical therapeutic studies. Anticancer Res 2003;23:2633–42.
25. Hurwitz AA, Foster BA, Kwon ED, et al. Combination immunotherapy of primary prostate cancer in a transgenic mouse model using CTLA-4 blockade. Cancer Res 2000;60:2444–8.
26. Arap W, Haedicke W, Bernasconi M, et al. Targeting the prostate for destruction through a vascular address. Proc Natl Acad Sci U S A 2002;99:1527–31.
27. Wechter WJ, Leipold DD, Murray ED Jr, et al. E-7869 (R-flurbiprofen) inhibits progression of prostate cancer in the TRAMP mouse. Cancer Res 2000;60:2203–8.
28. Rovere P, Vallinoto C, Bondanza A, et al. Cutting edge: bystander apoptosis triggers dendritic cell maturation and antigen-presenting function. J Immunol 1998;161:4467–71.
29. Pützer BM, Hitt M, Muller WJ, et al. Interleukin 12 and B7-1 costimulatory molecule expressed by an adenovirus vector act synergistically to facilitate tumor regression. Proc Natl Acad Sci U S A 1997;94:10880–94.
30. Shariat SF, Desai S, Song W, et al. Adenovirus-mediated transfer of inducible caspases: a novel "death switch" gene therapeutic approach to prostate cancer. Cancer Res 2001;61:2562–71.
31. Townsend SE, Allison JP. Tumor rejection after direct costimulation of CD8+ T cells by B7-transfected melanoma cells. Science 1993;259:368–70.
32. Yeh K-Y, Pulaski BA, Woods ML, et al. B7-1 enhances natural killer cell-mediated cytotoxicity and inhibits tumor growth of a poorly immunogenic murine carcinoma. Cell Immunol 1995;165:217–24.
33. Dessureault S, Graham FL, Gallinger S. Autologous lymphocyte responses to adenovirus-B7-1-transduced human cancer cells. Cancer Gene Ther 1999;6:195–208.
34. Freeman SM, Ramesh R, Shastri M, et al. The role of cytokines in mediating the bystander effect using HSV-TK xenogeneic cells. Cancer Lett 1995;92:167–74.
35. Gingrich JR, Barrios RJ, Foster BA, Greenberg NM. Pathologic progression of autochthonous prostate cancer in the TRAMP model. Prostate Cancer Prostatic Dis 1999;2:70–5.
36. Gingrich JR, Barrios RJ, Kattan MW, et al. Androgen-independent prostate cancer progression in the TRAMP model. Cancer Res 1997;57:4687–91.

37. Yang D, Holt GE, Velders MP, et al. Murine six-transmembrane epithelial antigen of the prostate, prostate stem cell antigen, and prostate-specific membrane antigen: prostate-specific cell-surface antigens highly expressed in prostate cancer of transgenic adenocarcinoma mouse prostate mice. Cancer Res 2001;61:5857–60.

38. Grossmann ME, Wood M, Celis E. Expression, specificity and immunotherapy potential of prostate-associated genes in murine cell lines. World J Urol 2001;19:365–70.

39. Albert ML, Jegathesan M, Darnell RB. Dendritic cell maturation is required for the cross-tolerization of CD8+ T cells. Nat Immunol 2001;2:1010–7.

40. Astaldi G, Lisiewicz J. Lymphocytes—structure, production, functions. Naples: Casa Editrice Idelson; 1971. p. 48–55.

41. Lauder I, Aherne W, Stewart J, Sainsbury R. Macrophage infiltration of breast tumours: a prospective study. J Clin Pathol 1977;30:563–8.

42. Hurlimann J, Saraga P. Mononuclear cells infiltrating human mammary carcinomas: immunohistochemical analysis with monoclonal antibodies. Int J Cancer 1985;35:753–62.

43. Stift A, Friedl J, Dubsky P, et al. Dendritic cell-based vaccination in solid cancer. J Clin Oncol 2003;21:135–42.

44. Burch PA, Croghan GA, Gastineau DA, et al. Immunotherapy (APC8015, Provenge) targeting prostatic acid phosphatase can induce durable remission of metastatic androgen-independent prostate cancer: a phase 2 trial. Prostate 2004;60:197–204.

45. Smyth MJ, Crowe NY, Hayakawa Y, et al. NKT cells—conductors of tumor immunity? Curr Opin Immunol 2002;14:165–71.

46. McAdam AJ, Schweitzer AN, Sharpe AH. The role of B7 co-stimulation in activation and differentiation of CD4+ and CD8+ T cells. Immunol Rev 1998;165:231–47.

47. Lenschow DJ, Walunas TL, Bluestone JA. CD28/B7 system of T cell costimulation. Annu Rev Immunol 1996;14:233–58.

48. Hull GW, McCurdy MA, Nasu Y, et al. Prostate cancer gene therapy: comparison of adenovirus-mediated expression of interleukin 12 with interleukin 12 plus B7-1 for *in situ* gene therapy and gene-modified, cell-based vaccines. Clin Cancer Res 2000;6:4101–9.

49. Aruga E, Aruga A, Arca MJ, et al. Immune responsiveness to a murine mammary carcinoma modified to express B7-1, interleukin-12, or GM-CSF. Cancer Gene Ther 1997;4:157–66.

50. Van Parijs L, Perez VL, Biuckians A, et al. Role of interleukin 12 and costimulators in T cell anergy *in vivo*. J Exp Med 1997;186:1119–28.

51. Trinchieri G. Interleukin-12 and the regulation of innate resistance and adaptive immunity. Nat Rev Immunol 2003;3:133–46.

52. Smyth MJ, Taniguchi M, Street SEA. The anti-tumor activity of IL-12: mechanisms of innate immunity that are model and dose dependent. J Immunol 2000;165:2665–70.

53. Sanford MA, Yan Y, Canfield SE, et al. Independent contributions of GR-1+ leukocytes and Fas/FasL interactions to induce apoptosis following interleukin-12 gene therapy in a metastatic model of prostate cancer. Hum Gene Ther 2001;12:1485–98.

54. Nasu Y, Bangma CH, Hull GW, et al. Adenovirus-mediated interleukin-12 gene therapy for prostate cancer: suppression of orthotopic tumor growth and pre-established lung metastases in an orthotopic model. Gene Ther 1999;6:338–49.

55. Peter K, Brunda MJ, Corradin G. IL-12 administration leads to a transient depletion of T cells, B cells, and APCs and concomitant abrogation of the HLA-A2.1-restricted CTL response in transgenic mice. J Immunol 2002;169:63–7.

56. Kurzawa H, Wysocka M, Aruga E, et al. Recombinant interleukin 12 enhances cellular immune responses to vaccination only after a period of suppression. Cancer Res 1998;58:491–9.

57. Ribas A, Wargo JA, Comin-Anduix B, et al. Enhanced tumor responses to dendritic cells in the absence of CD8-positive cells. J Immunol 2004;172:4762–9.

58. Tyznik AJ, Sun JC, Bevan MJ. The CD8 population in CD4-deficient mice is heavily contaminated with MHC class II-restricted T cells. J Exp Med 2004;199:559–65.

59. Harshyne LA, Zimmer MI, Watkins SC, Barratt-Boyes SM. A role for class A scavenger receptor in dendritic cell nibbling from live cells. J Immunol 2003;170:2302–9.

60. Janjic BM, Lu G, Pimenov A, et al. Innate direct anticancer effector function of human immature dendritic cells. I. Involvement of an apoptosis-inducing pathway. J Immunol 2002;168.

61. Stuart LM, Lucas M, Simpson C, et al. Inhibitory effects of apoptotic cell ingestion upon endotoxin-driven myeloid dendritic cell maturation. J Immunol 2002;168:1627–35.

62. Coll J-L, Chollet P, Brambilla E, et al. *In vivo* delivery to tumors of DNA complexed with linear polyethylenimine. Hum Gene Ther 1999;10:1659–66.

63. Astaldi G, Lisiewicz J, Cichocki T, Burlina A. The lysosomal enzymes in lymphocytes. Part II. Activated lymphocytes. Acta Vitaminol Enzymol 1973;27:197–206.

64. Hirschhorn R, Kaplan JM, Goldberg AF, et al. Acid-phosphatase-rich granules in human lymphocytes induced by phytohemagglutinin. Science 1965;147:55–7.

65. Mysliwska J, Bigda J, Mysliwski A. Activity of acid phosphatase in target binding cells expressing NK cytotoxic potential. Acta Histochem 1987;82:127–31.

66. Lisiewicz J, Moszczynski P, Sulowicz W. The lymphocyte acid phosphatase-positive lysosomes in patients with malignancies. Scand J Haematol 1985;34:181–3.

67. Komatsu F, Masuda T. Cell-cell adhesion-independent killing due to lymphokine-activated killer cells against glioblastoma cell lines. Oncol Res 2001;12:371–81.

An inducible caspase 9 safety switch for T-cell therapy

Karin C. Straathof, Martin A. Pulè, Patricia Yotnda, Gianpietro Dotti, Elio F. Vanin, Malcolm K. Brenner, Helen E. Heslop, David M. Spencer, and Cliona M. Rooney

The efficacy of adoptive T-cell therapy as treatment for malignancies may be enhanced by genetic modification of infused cells. However, oncogenic events due to vector/transgene integration, and toxicities due to the infused cells themselves, have tempered enthusiasm. A safe and efficient means of removing aberrant cells in vivo would ameliorate these concerns. We describe a "safety switch" that can be stably and efficiently expressed in human T cells without impairing phenotype, function, or antigen specificity. This reagent is based on a modified human caspase 9 fused to a human FK506 binding protein (FKBP) to allow conditional dimerization using a small molecule pharmaceutical. A single 10-nM dose of synthetic dimerizer drug induces apoptosis in 99% of transduced cells selected for high transgene expression in vitro and in vivo. This system has several advantages over currently available suicide genes. First, it consists of human gene products with low potential immunogenicity. Second, administration of dimerizer drug has no effects other than the selective elimination of transduced T cells. Third, inducible caspase 9 maintains function in T cells overexpressing antiapoptotic molecules. These characteristics favor incorporation of inducible caspase 9 as a safety feature in human T-cell therapies. (Blood. 2005;105:4247-4254)

Introduction

Cellular therapies hold great promise for the treatment of human disease, and this promise may be extended if the cells are first genetically modified to alter or augment function. Unfortunately, significant toxicities from the cells themselves or from their transgene products have hampered clinical investigation. There is considerable interest in developing means by which infused cells may be ablated should problems arise from their use. Most experience with safety-switch genes to date has been in T lymphocytes since immunotherapy with these cells has proved efficacious as treatment for viral infections and malignancies.[1-4]

The herpes simplex virus I–derived thymidine kinase (HSV-TK) gene has been used as an in vivo suicide switch in donor T-cell infusions to treat recurrent malignancy and Epstein Barr virus (EBV) lymphoproliferation after hemopoietic stem cell transplantation.[5,6] However, destruction of T cells causing graft-versus-host disease was incomplete, and the use of ganciclovir (or analogs) as a pro-drug to activate HSV-TK precludes administration of ganciclovir as an antiviral drug for cytomegalovirus infections. Moreover, HSV-TK–directed immune responses have resulted in elimination of HSV-TK–transduced cells, even in immunosuppressed human immunodeficiency virus and bone marrow transplant patients, compromising the persistence and hence efficacy of the infused T cells.[5,7] The *E coli*–derived cytosine deaminase gene has also been used clinically,[8] but as a xenoantigen it is also likely to be immunogenic and thus incompatible with T-cell–based therapies that require long-term persistence.

Transgenic human CD20, which can be activated by a monoclonal chimeric anti–CD20 antibody, has been proposed as a nonimmunogenic safety system.[9] However, it results in the unwanted loss of normal B cells for 6 months or more. An alternative suicide gene strategy is based on human proapoptotic molecules fused with an FKBP variant that is optimized to bind a chemical inducer of dimerization (CID),[10] AP1903, a synthetic drug that has proven safe in healthy volunteers.[11] Administration of this small molecule results in cross-linking and activation of the proapoptotic target molecules. The application of this inducible system in human T lymphocytes has been explored using Fas or the death effector domain (DED) of the Fas-associated death domain–containing protein (FADD) as proapoptotic molecules. Up to 90% of T cells transduced with these inducible death molecules underwent apoptosis after administration of CID.[12-16]

While these results are promising, elimination of 90% of transduced cells may be insufficient to ensure safety of genetically modified cells in vivo. Moreover, death molecules that act downstream of most apoptosis inhibitors may be effective in a wider range of cells. The activity of membrane proximal apoptosis initiators such as Fas and FADD may be impaired when cellular inhibitors of apoptosis such as c-FLIP, bcl-2, and bcl-x_L are upregulated (Figure 1)—a frequent early event in malignant transformation and in the long-term maintenance of memory T cells.[17,18] Hence, the most deleterious cells may be inadvertently spared.

From the Center for Cell and Gene Therapy; the Departments of Pediatrics, Medicine, Immunology, and Molecular Virology and Microbiology, Baylor College of Medicine; the Methodist Hospital; and Texas Children's Hospital, Houston, TX.

Submitted December 1, 2004; accepted January 31, 2005. Prepublished online as *Blood* First Edition Paper, February 22, 2005; DOI 10.1182/blood-2004-11-4564.

Supported in part by grants from The Dutch Cancer Foundation, The Royal Dutch Academy for Science, The Ank van Vlissingen Foundation (K.C.S.); The British Society for Haematology Society Fellowship (M.A.P.); DOD no. PC020 062 (D.M.S.), NCI PO1 CA94 237, a Specialized Centre of Research Award from the Leukemia Lymphoma Society, a Translational Research Award from the Leukemia Lymphoma Society (C.M.R.), and a Doris Duke Distinguished Clinical Scientist Award (H.E.H.).

The online version of this article contains a data supplement.

Reprints: Cliona M. Rooney, Center for Cell and Gene Therapy, 1102 Bates St, Suite 750.09, Houston, TX 77030; e-mail: crooney@bcm.tmc.edu.

The publication costs of this article were defrayed in part by page charge payment. Therefore, and solely to indicate this fact, this article is hereby marked "advertisement" in accordance with 18 U.S.C. section 1734.

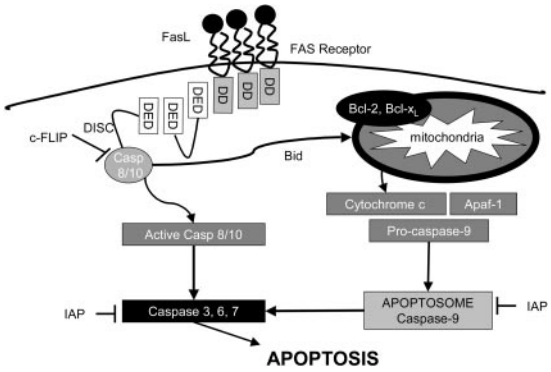

Figure 1. Antiapoptotic molecules regulate the sensitivity to apoptotic signals. In human lymphocytes apoptosis can be induced through at least 2 pathways. Stimulation of the Fas receptor results in recruitment of the initiator caspase 8, through interaction with the adaptor molecule Fas-associated death domain protein (FADD) by means of its death domains (DDs) and death effector domains (DEDs). In turn, activated caspase 8 activates the effector caspases 3, 6, and 7. Alternatively, disruption of the mitochondrial membrane results in the release of cytochrome c, which activates caspase 9 through interaction with the adaptor molecule, apoptotic protease-activating factor 1 (Apaf-1). Caspase 9 is then able to activate caspase 3. The death receptor–activated extrinsic pathway can crosstalk to the intrinsic mitochondrial pathway through the caspase 8–mediated cleavage of Bid (BH3 interacting domain death agonist). Inhibitors of apoptosis that engage at different steps of these pathways regulate the balance between apoptosis and survival. FLIP prevents the full activation of caspase 8. Antiapoptotic bcl-2 (B-cell CLL/lymphoma-2) family members prevent apoptosis initiated via the mitochondria. Inhibitors of apoptosis proteins (IAPs including X-linked IAP [XIAP]) can either prevent activation of caspases 3, 7, and 9 or inhibit their activated forms. DISC indicates death-inducing signaling complex; FasL, Fas ligand; c-FLIP, cellular FLICE-like inhibitory protein.

The efficacy of adoptive immunotherapy may be enhanced by rendering the therapeutic T cells resistant to immune evasion strategies employed by tumor cells. In vitro studies have shown that this can be achieved by transduction with a dominant-negative receptor or an immunomodulatory cytokine.[19,20] Moreover, transfer of antigen-specific T-cell receptors allows for the application of T-cell therapy to a broader range of tumors.[21,22] We therefore chose to develop and test a suicide system for engineered human T cells to allow their subsequent use in clinical studies. Here we describe how a modification of a late-stage apoptosis pathway molecule, caspase 9, can be stably expressed in human T lymphocytes without compromising their functional and phenotypic characteristics while demonstrating exquisite sensitivity to CID, even in T cells that have upregulated antiapoptotic molecules.

Materials and methods

Plasmids

Full-length inducible caspase 9 (F'F-C-Casp9.I.GFP) consists of full-length caspase 9, including its caspase recruitment domain (CARD; GenBank NM001 229) linked to 2 12-kDa human FK506 binding proteins (FKBP12; GenBank AH002 818) that contain an F36V mutation (Figure 2A).[10] The inducer of dimerization used in this study, AP20187 (generous gift of ARIAD Pharmaceuticals, Cambridge, MA), is a nontoxic synthetic FK506 analog that has been modified to reduce interactions with endogenous FKBPs, while enhancing binding to this FK506-BP12 variant. Administration of the CID results in the aggregation of inducible caspase 9 molecules, leading to their activation. Caspase 9 will subsequently activate downstream effector caspases, such as caspase 3, and ultimately induce apoptosis (Figure 1). Silent mutations in the third base of multiple codons have been introduced into the first FKBP segment to prevent homologous recombination between the coding sequences of the 2 linked FKBPs in our retroviral system[12] and a short Ser-Gly-Gly-Gly-Ser linker connects the FKBPs and caspase 9 to enhance flexibility.[14] Inducible Fas consists of the extracellular and transmembrane domains of human low-affinity nerve growth factor receptor (ΔNGFR), 2 $FKBP12_{V36}$s, and the cytoplasmic domains of human Fas as described by Thomis et al.[12] The cDNA for the p40 and p35 subunit of human interleukin 12 (IL-12) connected with a flexible linker was cloned from pcDNA3.1, a kind gift from Robert Anderson and Grant Prentice, Royal Free Hospital, London, United Kingdom.[23] All constructs were cloned into the retroviral vector MSCV.IRES.GFP.

Western blot

Transfected 293T cells were resuspended in lysis buffer (50% Tris/Gly, 10% sodium dodecyl sulfate [SDS], 4% beta-mercaptoethanol, 10% glycerol, 12% water, 4% bromophenol blue at 0.5%) containing aprotinin, leupeptin, and phenylmethylsulfonyl fluoride (Boehringer, Ingelheim, Germany) and incubated for 30 minutes on ice. After a 30-minute centrifugation, supernatant was harvested, mixed 1:2 with Laemmli buffer (Bio-Rad, Hercules, CA), boiled and loaded on a 10% SDS–polyacrylamide gel. The membrane was probed with rabbit anti–caspase 9 (amino acid residues 299-318) immunoglobulin G (IgG; Affinity BioReagents, Golden, CO; 1:500) and with mouse anti–GFP IgG (Covance, Berkeley, CA; 1:25 000). Blots were then exposed to appropriate peroxidase-coupled secondary antibodies and protein expression was detected with enhanced chemiluminescence (ECL; Amersham, Arlington Heights, IL). The membrane was

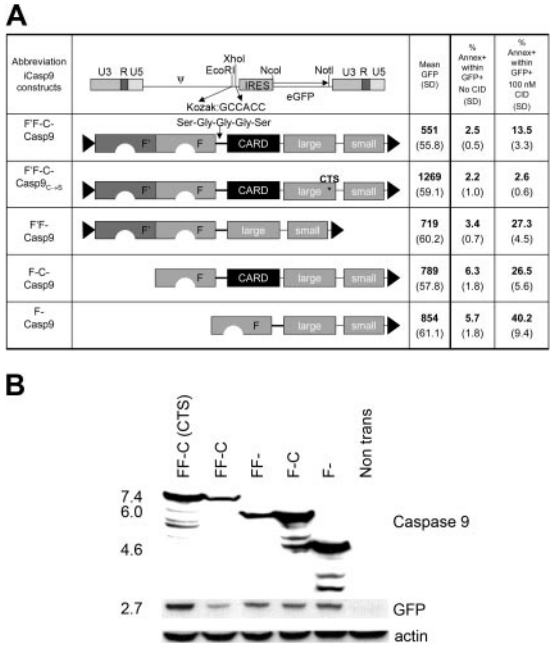

Figure 2. Modifications of full-length inducible caspase 9. (A) The full-length inducible caspase 9 molecule (F'-F-C-Casp9) consists of 2 FK506 binding proteins (FKBPs) linked with a Ser-Gly-Gly-Gly-Ser linker to the small and large subunit of the caspase molecule. The amino acid sequence of one of the FKBPs (F') is codon-wobbled to prevent homologous recombination when expressed in a retrovirus. F'F-C-$Casp9_{C\rightarrow S}$ contains a cysteine to serine mutation at position 287 that disrupts its activation site. In constructs F'F-Casp9, F-C-Casp9, and F'-Casp9, either the caspase activation domain (CARD), one FKBP, or both, were deleted respectively. All constructs were cloned into MSCV.IRES.GFP as *Eco*RI-*Xho*I fragments. 293T cells were transfected with each of these constructs and 48 hours after transduction expression of the marker gene GFP was analyzed by flow cytometry. In addition, 24 hours after transfection, 293T cells were incubated overnight with 100 nM CID and subsequently stained with the apoptosis marker annexin V. The mean and standard deviation of transgene expression level (mean GFP) and number of apoptotic cells before and after exposure to CID (% annexin V within GFP^+ cells) from 4 separate experiments are shown. (B) Coexpression of the inducible caspase 9 constructs of the expected size with the marker gene GFP in transfected 293T cells was demonstrated by Western blot using a caspase 9 antibody specific for amino acid residues 299-318, present both in the full-length and truncated caspase molecules as well as a GFP-specific antibody. Additional smaller size bands likely represent degradation products. Degradation products for the F'F-C-Casp9 and F'F-Casp9 constructs may not be detected due to a lower expression level of these constructs as a result of their basal activity. Equal loading was confirmed by blotting for actin.

then stripped and reprobed with goat polyclonal antiactin (Santa Cruz Biotechnology; 1:500) to check equality of loading.

Cell lines

B95-8 EBV transformed B-cell lines (LCLs), Jurkat, and MT-2 cells (kindly provided by Dr S. Marriott, Baylor College of Medicine, Houston, TX) were cultured in RPMI 1640 (Hyclone, Logan, UT) containing 10% fetal bovine serum (FBS; Hyclone). Polyclonal EBV-specific T-cell lines were cultured in 45% RPMI/45% Clicks (Irvine Scientific, Santa Ana, CA)/10% FBS and generated as previously reported.[2] Briefly, peripheral blood mononuclear cells (2×10^6 per well of a 24-well plate) were stimulated with autologous LCLs irradiated at 4000 rads at a responder-to-stimulator (R/S) ratio of 40:1. After 9 to 12 days, viable cells were restimulated with irradiated LCLs at an R/S ratio of 4:1. Subsequently, cytotoxic T cells (CTLs) were expanded by weekly restimulation with LCLs in the presence of 40 U/mL to 100 U/mL recombinant human interleukin-2 (rhIL-2; Proleukin; Chiron, Emeryville, CA).

Retrovirus transduction

For the transient production of retrovirus, 293T cells were transfected with iCasp9/iFas constructs, along with plasmids encoding gag-pol and RD114 envelope using GeneJuice transfection reagent (Novagen, Madison, WI). Virus was harvested 48 to 72 hours after transfection, snap frozen, and stored at −80°C until use. A stable FLYRD18-derived retroviral producer line was generated by multiple transductions with VSV-G pseudotyped transient retroviral supernatant.[24] FLYRD18 cells with highest transgene expression were single-cell sorted, and the clone that produced the highest virus titer was expanded and used to produce virus for lymphocyte transduction. The transgene expression, function, and retroviral titer of this clone was maintained during continuous culture for more than 8 weeks. For transduction of human lymphocytes, a non–tissue-culture–treated 24-well plate (Becton Dickinson, San Jose, CA) was coated with recombinant fibronectin fragment (FN CH-296; Retronectin; Takara Shuzo, Otsu, Japan; 4 μg/mL in PBS, overnight at 4°C) and incubated twice with 0.5 mL retrovirus per well for 30 minutes at 37°C. Subsequently, 3×10^5 to 5×10^5 T cells per well were transduced for 48 to 72 hours using 1 mL virus per well in the presence of 100 U/mL IL-2. Transduction efficiency was determined by analysis of expression of the coexpressed marker gene green fluorescent protein (GFP) on a FACScan flow cytometer (Becton Dickinson). For functional studies, transduced CTLs were either nonselected or segregated into populations with low, intermediate, or high GFP expression using a MoFlo cytometer (Dako Cytomation, Ft Collins, CO) as indicated.

Induction and analysis of apoptosis

CID (AP20187; ARIAD Pharmaceuticals) at indicated concentrations was added to transfected 293T cells or transduced CTLs. Adherent and nonadherent cells were harvested and washed with annexin binding buffer (BD Pharmingen, San Jose, CA). Cells were stained with annexin-V and 7-amino-actinomycin D (7-AAD) for 15 minutes according to the manufacturer's instructions (BD Pharmingen). Within 1 hour after staining, cells were analyzed by flow cytometry using CellQuest software (Becton Dickinson).

Cytotoxicity assay

The cytotoxic activity of each CTL line was evaluated in a standard 4-hour ^{51}Cr release assay, as previously described.[25] Target cells included autologous LCLs, human leukocyte antigen (HLA) class I–mismatched LCLs and the lymphokine-activated killer cell–sensitive T-cell lymphoma line HSB-2. Target cells incubated in complete medium or 1% Triton X-100 (Sigma, St Louis, MO) were used to determine spontaneous and maximum ^{51}Cr release, respectively. The mean percentage of specific lysis of triplicate wells was calculated as 100 × (experimental release − spontaneous release) / (maximal release − spontaneous release).

Phenotyping

Cell-surface phenotype was investigated using the following monoclonal antibodies: CD3, CD4, CD8, (Becton Dickinson) and CD56 and TCR-α/β (Immunotech, Miami, FL). ΔNGFR-iFas was detected using anti–NGFR antibody (Chromaprobe, Aptos, CA). Appropriate matched isotype controls (Becton Dickinson) were used in each experiment. Cells were analyzed with a FACSscan flow cytometer (Becton Dickinson).

Analysis of cytokine production

The concentration of interferon-γ (IFN-γ), IL-2, IL-4, IL-5, IL-10, and tumor necrosis factor-α (TNFα) in CTL culture supernatants was measured using the Human Th1/Th2 cytokine cytometric Bead Array (BD Pharmingen) and the concentration of IL-12 in the culture supernatants was measured by enzyme-linked immunosorbent assay (ELISA; R&D Systems, Minneapolis, MN) according to the instructions of the manufacturer.

In vivo experiments

Nonobese diabetic severe combined immunodeficient (NOD/SCID) mice, 6 to 8 weeks of age, were irradiated (250 rad) and injected subcutaneously in the right flank with 10×10^6 to 15×10^6 LCLs resuspended in Matrigel (BD Bioscience). Two weeks later mice bearing tumors that were approximately 0.5 cm in diameter were injected into the tail vein with a 1:1 mixture of nontransduced and iCasp9.I.GFP_{high}-transduced EBV CTLs (total 15×10^6). At 4 to 6 hours prior and 3 days after CTL infusion, mice were injected intraperitoneally with recombinant hIL-2 (2000 U; Proleukin; Chiron). On day 4, the mice were randomly segregated in 2 groups: 1 group received CID (50 μg AP20 187, intraperitoneally) and 1 group received carrier only (16.7% propanediol, 22.5% PEG400, and 1.25% Tween 80, intraperitoneally). On day 7, all mice were killed. Tumors were homogenized and stained with antihuman CD3 (BD Pharmingen). By FACS analysis, the number of GFP^+ cells within the gated $CD3^+$ population was evaluated. Tumors from a control group of mice that received only nontransduced CTLs (total 15×10^6) were used as a negative control in the analysis of $CD3^+/GFP^+$ cells.

Results

Optimization of expression and function of inducible caspase 9

We initially screened previously described caspases 3, 7, and 9 for their suitability as inducible safety-switch molecules both in transfected 293T cells and in transduced human T cells.[14] Only inducible caspase 9 (iCasp9) could be expressed at levels sufficient to confer sensitivity to CID (data not shown). However, even the initially tested iCasp9 could not be maintained stably at high levels in T cells, and we hypothesized that basal activity of the transgene was eliminating transduced cells. The CARD domain is responsible for physiologic dimerization of caspase 9 molecules, by a cytochrome C and adenosine triphosphate (ATP)–driven interaction with apoptotic protease-activating factor 1 (Apaf-1). Hence the CARD domain appears superfluous in this context and its removal might reduce basal activity. Given that only dimerization rather than multimerization is required for activation of caspase 9, we also reasoned that a single FKBP domain might be adequate to effect activation. We therefore compared the activity of iCasp9 derivatives in which either the CARD domain, or one of the 2 FKBP domains, or both, had been removed. A construct with a disrupted activation site, F'F-C-$Casp9_{C \rightarrow S}$, provided a nonfunctional control (Figure 2A). All constructs were cloned into the retroviral vector MSCV[26] in which retroviral long terminal repeats (LTRs) direct transgene expression and enhanced GFP is coexpressed from the same mRNA by use of an internal ribosomal entry site (IRES). In transfected 293T cells, expression of all inducible caspase 9

constructs at the expected size as well as coexpression of GFP was demonstrated by Western blot (Figure 2B). Protein expression (estimated by mean fluorescence of GFP and visualized on Western blot) was highest in the nonfunctional construct F'F-C-Casp9$_{C\rightarrow S}$ and greatly diminished in the full-length construct F'F-C-Casp9. Removal of the CARD (F'F-Casp9), one FKBP (F-C-Casp9), or both (F-Casp9) resulted in progressively higher expression of both inducible caspase 9 and GFP, and correspondingly enhanced sensitivity to CID (Figure 2A). Based on these results, the F-Casp9 construct (henceforth referred to as iCasp9$_M$) was used for further study in human T lymphocytes.

Stable expression of iCasp9$_M$ in human T lymphocytes

The long-term stability of suicide gene expression is of utmost importance, since suicide genes must be expressed for as long as the genetically engineered cells persist. For T-cell transduction, a FLYRD18-derived retroviral producer clone that produces high-titer RD114-pseudotyped virus was generated to facilitate the transduction of T cells.[24] We evaluated iCasp9$_M$ expression in EBV-specific CTL lines (EBV-CTL), since these have well-characterized function and specificity and are already being used as in vivo therapy for prevention and treatment of EBV-associated malignancies.[2,27] Consistent transduction efficiencies of EBV-CTLs of more than 70% (mean, 75.3%; range, 71.4%-83.0% in 5 different donors) were obtained after a single transduction with retrovirus. The expression of iCasp9$_M$ in EBV-CTLs was stable for at least 4 weeks after transduction without selection or loss of transgene function (data not shown).

iCasp9$_M$ does not alter transduced T-cell characteristics

To ensure that expression of iCasp9$_M$ did not alter T-cell characteristics, we compared the phenotype, antigen-specificity, proliferative potential, and function of nontransduced or nonfunctional iCasp9$_{C\rightarrow S}$-transduced EBV-CTLs, with that of iCasp9$_M$-transduced EBV-CTLs. In 4 separate donors, transduced and nontransduced CTLs consisted of equal numbers of CD4$^+$, CD8$^+$, CD56$^+$, and TCR$\alpha\beta^+$ cells (Figure 3A). Similarly, production of cytokines including IFN-γ, TNFα, IL-10, IL-4, IL-5, and IL-2 was unaltered by iCasp9$_M$ expression (Figure 3B). iCasp9$_M$-transduced EBV-CTLs specifically lysed autologous LCLs comparable to nontransduced and control-transduced CTLs (Figure 3C). Expression of iCasp9$_M$ did not affect the growth characteristics of exponentially growing CTLs, and importantly, dependence on antigen and IL-2 for proliferation was preserved (Figure 3D).

Elimination of more than 99% of T lymphocytes selected for high transgene expression in vitro

To provide an effective safety switch, suicide gene induction should eliminate all gene-modified cells. Therefore, iCasp9$_M$ proficiency in CTLs was tested by monitoring loss of GFP-expressing cells after administration of CID; 91.3% (range, 89.5%-92.6% in 5 different donors) of GFP$^+$ cells were eliminated after a single 10-nM dose of CID (Figure 4A). Similar results were obtained regardless of exposure time to CID (range, 1 hour-continuous; data not shown). In all experiments, CTLs that survived CID treatment had low transgene expression with a 70% (range, 55%-82%) reduction in mean fluorescence intensity of GFP after CID. No further elimination of the surviving GFP$^+$ T cells could be obtained by an antigenic stimulation followed by a second 10-nM dose of CID (data not shown). Therefore, the nonresponding CTLs most likely expressed insufficient iCasp9$_M$ for functional

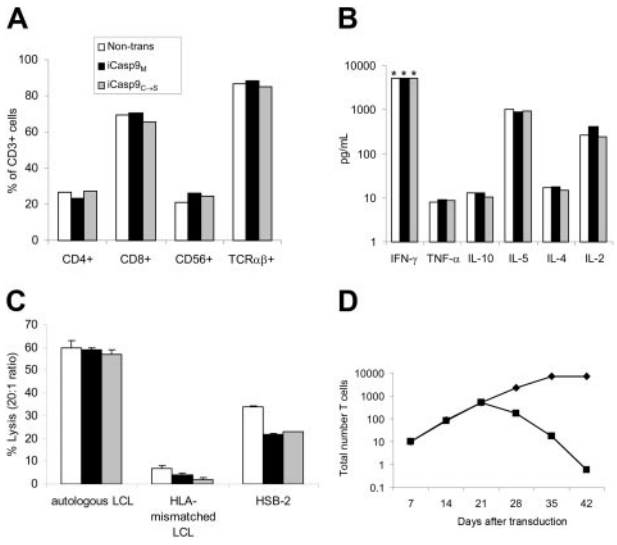

Figure 3. Expression of iCasp9$_M$ does not affect the phenotype or function of EBV-CTLs. Phenotype (A) and secretion (B) of Th1- and Th2-type cytokines upon antigen stimulation, and (C) cytolytic activity against autologous EBV-transformed lymphoblastoid B-cell line (LCL), HLA-mismatched LCL, and HSB-2 (a LAK cell target) were compared in nontransduced (□), F-Casp9$_M$-transduced (■), and F'F-C-Casp9$_{C\rightarrow S}$-transduced (▤) EBV-specific CTLs (EBV-CTLs) on day 15 to day 18 after transduction (2 antigenic stimulations after transduction). The mean and standard deviation of triplicate wells are shown. Examples of experiments using EBV-CTLs from 4 different donors are shown. *Greater than 5000 pg/mL. (D) On day 21 after transduction the normal weekly antigenic stimulation with autologous LCLs and IL-2 was continued (♦) or discontinued (■) to evaluate the antigen dependence of iCasp9$_M$-transduced CTLs.

activation by CID. To test this hypothesis CTLs were sorted for low, intermediate, and high expression of the linked marker gene GFP and mixed 1:1 with nontransduced CTLs from the same donor to allow for an accurate quantitation of the number of transduced T cells responding to CID-induced apoptosis. The number of transduced T cells eliminated increased with the level of GFP transgene expression (Figure S1; see the Supplemental Figure link at the top of the online article on the *Blood* website). For GFP$_{high}$-selected cells, 10 nM CID led to deletion of 99.1% (range, 98.7%-99.4%) of transduced cells (Figure 4A). Rapid induction of apoptosis in these GFP$_{high}$-selected cells is demonstrated by apoptotic characteristics such as cell shrinkage and fragmentation within 14 hours of CID administration (Figure 4B). Of these T cells, 64% (range, 59%-69%) had an apoptotic (annexin-V$^+$/7-AAD$^-$) and 30% (range, 26%-32%) had a necrotic (annexin-V$^+$/7-AAD$^+$) phenotype (Figure 4C). In contrast, the induction of apoptosis was significantly lower in T cells selected for intermediate or low GFP expression (Figure S1). For clinical applications therefore, transduced cells may have to be sorted for sufficient transgene expression before administration. CID-induced apoptosis was inhibited by the pan-caspase inhibitor zVAD-fmk (100 μM for 1 hour prior to adding CID; data not shown). Titration of CID showed that 1 nM CID was sufficient to obtain the maximal deletion effect (Figure 4D). This dose response remained unchanged for at least 4 weeks after transduction (data not shown).

iCasp9$_M$ is functional in malignant cells that express antiapoptotic molecules

We had selected caspase 9 as an inducible proapoptotic molecule for clinical use rather than previously described iFas[12] and iFADD,[16] since caspase 9 acts relatively late in apoptosis signaling and should be less susceptible to inhibition by apoptosis inhibitors. Thus, suicide function should be preserved not only in malignant,

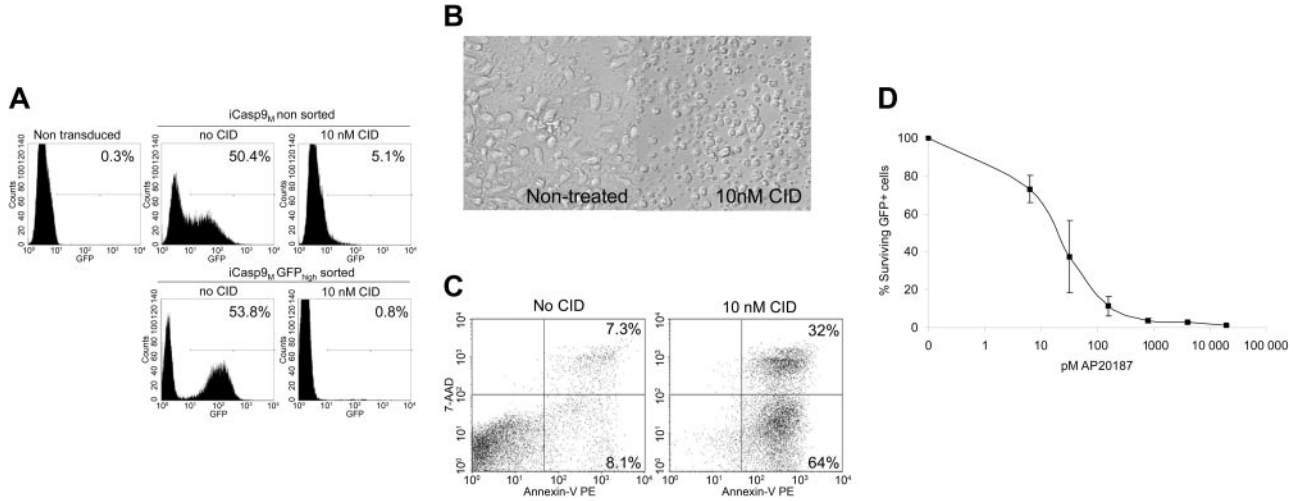

Figure 4. Administration of CID eliminates iCasp9$_M$-expressing T cells. (A) On the day of antigen stimulation, F-Casp9$_M$.I.GFP-transduced CTLs were either untreated or treated with 10 nM CID. Seven days later, the response to CID was measured by flow cytometry for GFP. The percentage of transduced T cells was adjusted to 50% to allow for an accurate measurement of residual GFP$^+$ cells after CID treatment. The responses to CID in unselected (top row) and GFP$_{high}$-selected CTLs (bottom row) was compared. The percentage of residual GFP$^+$ cells is indicated. (B) After overnight incubation with 10 nM CID, F-Casp9$_M$.I.GFP$_{high}$-transduced T cells had apoptotic characteristics such as cell shrinkage and fragmentation by microscopic evaluation. (C) Staining with markers of apoptosis showed that 64% of T cells had an apoptotic phenotype (annexin V$^+$, 7-AAD$^-$, lower right quadrant) and 32% a necrotic phenotype (annexin V$^+$, 7-AAD$^+$, upper right quadrant). A representative example of 3 separate experiments is shown. (D) A dose-response curve using the indicated amounts of CID (AP20187) shows the sensitivity of F-Casp9$_M$.I.GFP$_{high}$ to CID. Survival of GFP$^+$ cells is measured on day 7 after administration of the indicated amount of CID. Shown are mean and standard deviation. Similar results were obtained using AP1903, which has proven safe in a clinical trial in healthy volunteers.[11]

transformed T-cell lines that express antiapoptotic molecules,[28,29] but also in subpopulations of normal T cells that express elevated antiapoptotic molecules as part of the process to ensure long-term preservation of memory cells.[18,30] To test this hypothesis we first compared the function of iCasp9$_M$ and iFas in EBV-CTLs. Like iCasp9, inducible Fas[12] was expressed by the MSCV.IRES.GFP vector. For these experiments both ΔNGFR.iFas.I.GFP and iCasp9$_M$.I.GFP-transduced CTLs were sorted for GFP$_{high}$ expression and mixed with nontransduced CTLs at a 1:1 ratio to obtain cell populations that expressed either iFas or iCasp9$_M$ at equal proportions and at similar levels (Figure 5A). Elimination of GFP$^+$ cells after administration of 10 nM CID was more rapid and more efficient in iCasp9$_M$ than in iFas-transduced CTLs (99.2% ± 0.14% of iCasp9$_M$-transduced cells compared with 89.3% ± 4.9% of iFas-transduced cells at day 7 after CID; $P < .05$; Figure 5B).

Second, we compared the function of iCasp9$_M$ and iFas in 2 malignant T-cell lines: Jurkat, an apoptosis-sensitive T-cell leukemia line, and MT-2, an apoptosis-resistant T-cell line, due to c-FLIP and bcl-x$_L$ expression.[31,32] Jurkat cells and MT-2 cells were transduced with iFas and iCasp9$_M$ with similar efficiencies (92% vs 84% in Jurkat, 76% vs 70% in MT-2) and were cultured in the presence of 10 nM CID for 8 hours. Annexin-V staining showed that although iFas and iCasp9$_M$ induced apoptosis in an equivalent number of Jurkat cells (56.4% ± 15.6% and 57.2% ± 18.9%, respectively), only activation of iCasp9$_M$ resulted in apoptosis of MT-2 cells (19.3% ± 8.4% and 57.9% ± 11.9% for iFas and iCasp9$_M$, respectively; Figure 5C). These results demonstrate that in T cells overexpressing apoptosis-inhibiting molecules, the function of iFas can be blocked, while iCasp9$_M$ can still effectively induce apoptosis.

iCasp9$_M$-mediated elimination of T cells expressing an immunomodulatory transgene

To determine whether iCasp9$_M$ could effectively destroy cells genetically modified to express an active transgene product, we measured the ability of iCasp9$_M$ to eliminate EBV-CTLs stably expressing IL-12 to enhance their antitumor activity.[20] While IL-12 was undetectable in the supernatant of nontransduced and iCasp9$_M$.IRES.GFP-transduced CTLs, the supernatant of iCasp9$_M$.IRES.IL-12–transduced cells contained 324 pg/mL to

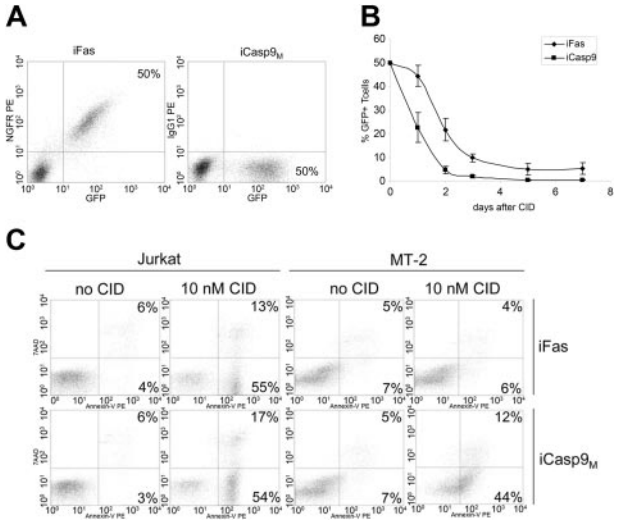

Figure 5. Comparison of functionality of iFas and iCasp9$_M$ in T cells. (A) EBV-CTLs were transduced with ΔNGFR-iFas.I.GFP (left) or iCasp9$_M$.I.GFP (right) and sorted for high GFP expression. Transduced CTLs were then mixed 1:1 with nontransduced CTLs. The percentages of ΔNGFR$^+$/GFP$^+$ and GFP$^+$ T cells are indicated. (B) On the day of LCL stimulation, 10 nM CID was administered, and GFP was measured at the time points indicated to determine the response to CID. ◆ indicates ΔNGFR-iFas.I.GFP; ■, iCasp9$_M$.I.GFP. Mean and standard deviation of 3 experiments are shown. (C) The human T-cell lines Jurkat (left) and MT-2 (right) were transduced with ΔNGFR-iFas.I.GFP (top row) or iCasp9$_M$.I.GFP (bottom row). An equal percentage of T cells was transduced with each of the suicide genes: 92% for ΔNGFR-iFas.I.GFP versus 84% for iCasp9$_M$.I.GFP in Jurkat, and 76% for ΔNGFR-iFas.I.GFP versus 70% for iCasp9$_M$.I.GFP in MT-2 (data not shown). T cells were either nontreated or incubated with 10 nM CID. Eight hours after exposure to CID, apoptosis was measured by staining for annexin V and 7-AAD. Representative example of 3 experiments is shown. PE indicates phycoerythrin.

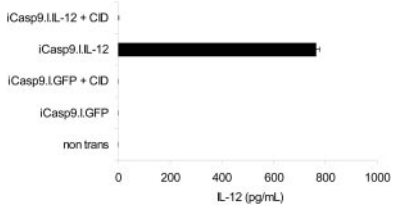

Figure 6. Function of iCasp9$_M$ when coexpressed with IL-12. The marker gene GFP in the iCasp9$_M$.I.GFP constructs was replaced by flexi IL-12, encoding the p40 and p35 subunits of human IL-12. iCasp9$_M$.I.GFP- and iCasp9$_M$.I.IL-12–transduced EBV-CTLs were stimulated with LCLs, and then left untreated or exposed to 10 nM CID. Three days after a second antigenic stimulation, IL-12 in the culture supernatant was measured by IL-12 ELISA (detection limit of this assay is 7.8 pg/mL). The mean and standard deviation of triplicate wells are indicated. Results of 1 of 2 experiments with CTLs from 2 different donors are shown.

762 pg/mL IL-12. After administration of 10 nM CID, however, the IL-12 in the supernatant fell to undetectable levels (< 7.8 pg/mL). Hence, even without prior sorting for high transgene–expressing cells, activation of iCasp9$_M$ is sufficient to completely eliminate all T cells producing biologically relevant levels of IL-12 (Figure 6).

Elimination of more than 99% of T cells selected for high transgene expression in vivo

Finally, to evaluate the function of iCasp9$_M$ in transduced EBV-CTLs in vivo, we used a SCID mouse–human xenograft model for adoptive immunotherapy.[33] After intravenous infusion of a 1:1 mixture of nontransduced and iCasp9$_M$.IRES.GFP$_{high}$-transduced CTLs into SCID mice bearing an autologous LCL xenograft, mice were treated either with a single dose of CID or carrier only. Three days after CID/carrier administration, tumors were analyzed for human CD3$^+$/GFP$^+$ cells. Detection of the nontransduced component of the infusion product using human anti–CD3 antibodies confirmed the success of the tail-vein infusion in mice that received CID. In mice treated with CID, there was a more than 99% reduction in the number of human CD3$^+$/GFP$^+$ T cells, compared with infused mice treated with carrier alone, demonstrating equally high sensitivity of iCasp9$_M$-transduced T cells in vivo and in vitro (Figure 7).

Discussion

A suicide gene designed to eliminate gene-modified T cells in vivo ideally should be coexpressed stably in all cells carrying the modifying gene, at levels high enough to elicit cell death. Thus, it must have low basal activity along with high specific activity, together with minimal susceptibility to endogenous antiapoptotic molecules. We have developed an inducible caspase 9, iCasp9$_M$, which has low basal activity allowing stable expression for more than 4 weeks in human T cells. A single 10-nM dose of CID is sufficient to kill more than 99% of iCasp9$_M$-transduced cells selected for high transgene expression both in vitro and in vivo. Moreover, when coexpressed with the pivotal Th1 cytokine IL-12, activation of iCasp9$_M$ eliminated all detectable IL-12–producing cells, even without selection for high transgene expression. As caspase 9 acts downstream of most antiapoptotic molecules, a high sensitivity to CID is preserved regardless of the presence of increased levels of antiapoptotic molecules of the bcl-2 family. Thus, iCasp9$_M$ should induce destruction even of transformed T cells and memory T cells that are relatively resistant to apoptosis.

Recent insights into caspase 9 activation allow us to propose a molecular mechanism of iCasp9$_M$ activation.[34] In contrast to other caspase molecules, proteolysis appears to be insufficient and unnecessary for activation of caspase 9.[35,36] Crystallographic and functional data indicate that dimerization of inactive caspase 9 monomers leads to conformational change–induced activation.[37] In a physiologic setting the concentration of pro-caspase 9 is in the 20 nM range,[35] well below dimerization threshold. According to the proposed model, the energetic barrier to dimerization is overcome by homophilic interactions between the CARD domains of Apaf-1 and caspase 9, driven by cytochrome C and ATP.[37] Overexpression of caspase 9 joined to 2 FKBPs results in a situation where spontaneous dimerization might occur and account for the observed toxicity of the initial construct. Removal of one FKBP resulted in increased gene expression probably by reducing spontaneous dimerization and hence toxicity. While multimerization is required for activation of surface death receptors, this model predicts that dimerization should be sufficient to mediate activation of caspase 9. Indeed, iCasp9 constructs with a single FKBP function as effectively as those with 2 FKBPs. Increased sensitivity to dimerizer by removal of the CARD domain probably represents a reduction in the energetic threshold of dimerization upon CID binding. In short, our final construct simply represents replacement of one dimerization/activation module (CARD) with another (FKBP12).

Unwanted immune responses against cells expressing virus- or bacteria-derived lethal genes such as HSV-TK and cytosine deaminase can impair their persistence.[5,7] The FKBPs and proapoptotic molecules that form the components of iCasp9$_M$ are human-derived molecules and are therefore less likely to induce an immune response. Although the linker between FKBP and caspase 9 and the single point mutation in the FKBP domain introduce novel amino acid sequences, the latter was not immunologically recognized by macaque recipients of iFas-transduced T cells.[15] Moreover, unlike virus-derived proteins such as HSV-TK, no memory T cells specific for these junctional sequences should be present, reducing the risk of immune response–mediated elimination of iCasp9$_M$-transduced T cells.

Elimination of all cells expressing the therapeutic transgene is a prerequisite for a safety switch for clinical applications. Previous studies using inducible Fas or DED of FADD showed that approximately 10% of transduced cells were unresponsive to activation of the destructive gene.[12,15,16] One explanation for unresponsiveness to CID is low expression of the transgene: both iCasp9$_M$-transduced T cells in our study and iFas-transduced T cells in studies by others[12,16] that survived after CID administration

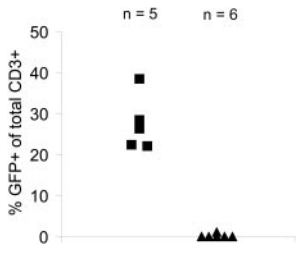

Figure 7. Function of iCasp9$_M$ in vivo. NOD/SCID mice were irradiated and injected subcutaneously with 10 × 10^6 to 15 × 10^6 LCLs. After 14 days, mice bearing tumors of 0.5 cm in diameter received a total of 15 × 10^6 EBV-CTLs (50% of these cells were nontransduced and 50% were transduced with iCasp9$_M$.I.GFP and sorted for high GFP expression). On day 3 after CTL administration, mice received either CID (50 μg AP20187; ▲, n=6) or carrier only (■, n=5) and on day 6 the presence of human CD3$^+$/GFP$^+$ T cells in the tumors was analyzed. Human CD3$^+$ T cells isolated from the tumors of a control group of mice that received only nontransduced CTLs (15 × 10^6 CTLs; n= 4) were used as a negative control for the analysis of CD3$^+$/GFP$^+$ T cells within the tumors.

had low levels of transgene expression. We interpreted this as a retroviral "positional effect" and attempted to achieve more homogeneous expression of transgene by flanking retroviral integrants with the chicken beta-globin chromatin insulator.[38] This modification dramatically increased the homogeneity of expression in transduced 293T cells, but had no significant effect in transduced primary T cells (data not shown). Selection of T cells with high expression levels minimized variability of response to the dimerizer. Over 99% of transduced T cells sorted for high GFP expression were eliminated after a single 10-nM CID dose. This demonstration supports the hypothesis that cells expressing high levels of suicide gene can be isolated using a selectable marker. Although a very small number of residual cells may cause resurgence of toxicity, a deletion efficiency of up to 2 logs will significantly decrease this possibility. For clinical use, coexpression with a nonimmunogenic selectable marker such as truncated human NGFR, CD20, or CD34 instead of GFP will allow for selection of high transgene–expressing T cells.[39-41] Coexpression of such a selectable marker can be obtained using either an IRES or posttranslational modification of a fusion protein containing a self-cleaving (eg, 2A) sequence.[42] In contrast, in situations where the sole safety concern is the transgene-mediated (eg, artificial T-cell receptors, cytokines) toxicity, this selection step may be unnecessary, as tight linkage between $iCasp9_M$ and transgene expression ensures elimination of those cells that are expressing biologically relevant levels of the therapeutic transgene. We demonstrated this by coexpressing $iCasp9_M$ with IL-12; activation of $iCasp9_M$ completely abolished measurable IL-12 production. However, this may depend on the function and the activity of the transgene.

The other explanation for unresponsiveness to CID is that high levels of apoptosis inhibitors may attenuate CID-mediated apoptosis. These include c-FLIP, bcl-2 family members, and inhibitors of apoptosis proteins (IAPs), which normally regulate the balance between apoptosis and survival. For instance, upregulation of c-FLIP and bcl-2 render a subpopulation of T cells, destined to establish the memory pool, resistant to activation-induced cell death in response to cognate target or antigen-presenting cells.[18,30] In several T-lymphoid tumors, the physiologic balance between apoptosis and survival is disrupted in favor of cell survival.[28,29] A suicide gene should delete all transduced T cells including memory and malignantly transformed cells. Thus, to ensure safety, preserved function of the inducible suicide gene in the presence of increased levels of antiapoptotic molecules is critical. The apical location of iFas (or iFADD) in the apoptosis signaling pathway may leave it especially vulnerable to inhibitors of apoptosis and these molecules are therefore less suited to being the key component of an apoptotic safety switch. While caspase 3 or 7 as terminal effector molecules appear to be ideal candidates, we were unable to express either in primary human T cells at functional levels (data not shown). One possible explanation is that caspase 3 and 7, unlike caspase 9, make poor substrates for themselves and thus require prohibitively high cellular concentrations for cleavage.[14] We therefore chose caspase 9, which bypasses the inhibitory effects of c-FLIP and antiapoptotic bcl-2 family members and could be expressed stably at functional levels. Although X-linked inhibitor of apoptosis (XIAP) could in theory reduce spontaneous caspase 9 activation (Figure 1),[43] the high affinity of AP20187 (or AP1903) for $FKBP_{V36}$ likely displaces this noncovalently associated XIAP. Indeed, in contrast to iFas, $iCasp9_M$ remained functional in a transformed T-cell line that overexpresses antiapoptotic molecules, including bcl-x_L.

We have described a new inducible safety switch, designed specifically for expression from an oncoretroviral vector by human T cells. $iCasp9_M$ can be activated by AP1903 (or analogs), a small chemical inducer of dimerization that has proven safe at the required dose for optimum deletional effect,[11] and unlike ganciclovir or rituximab has no other biologic effects in vivo. Therefore, expression of this suicide gene in T cells for adoptive transfer will increase safety and hence broaden the scope of clinical applications.

References

1. Walter EA, Greenberg PD, Gilbert MJ, et al. Reconstitution of cellular immunity against cytomegalovirus in recipients of allogeneic bone marrow by transfer of T-cell clones from the donor. N Engl J Med. 1995;333:1038-1044.
2. Rooney CM, Smith CA, Ng CY, et al. Infusion of cytotoxic T cells for the prevention and treatment of Epstein-Barr virus-induced lymphoma in allogeneic transplant recipients. Blood. 1998;92:1549-1555.
3. Dudley ME, Wunderlich JR, Robbins PF, et al. Cancer regression and autoimmunity in patients after clonal repopulation with antitumor lymphocytes. Science. 2002;298:850-854.
4. Marijt WA, Heemskerk MH, Kloosterboer FM, et al. Hematopoiesis-restricted minor histocompatibility antigens HA-1- or HA-2-specific T cells can induce complete remissions of relapsed leukemia. Proc Natl Acad Sci U S A. 2003;100:2742-2747.
5. Bonini C, Ferrari G, Verzeletti S, et al. HSV-TK gene transfer into donor lymphocytes for control of allogeneic graft-versus-leukemia. Science. 1997;276:1719-1724.
6. Tiberghien P, Ferrand C, Lioure B, et al. Administration of herpes simplex-thymidine kinase-expressing donor T cells with a T-cell-depleted allogeneic marrow graft. Blood. 2001;97:63-72.
7. Riddell SR, Elliott M, Lewinsohn DA, et al. T-cell mediated rejection of gene-modified HIV-specific cytotoxic T lymphocytes in HIV-infected patients. Nat Med. 1996;2:216-223.
8. Freytag SO, Khil M, Stricker H, et al. Phase I study of replication-competent adenovirus-mediated double suicide gene therapy for the treatment of locally recurrent prostate cancer. Cancer Res. 2002;62:4968-4976.
9. Introna M, Barbui AM, Bambacioni F, et al. Genetic modification of human T cells with CD20: a strategy to purify and lyse transduced cells with anti-CD20 antibodies. Hum Gene Ther. 2000;11:611-620.
10. Clackson T, Yang W, Rozamus LW, et al. Redesigning an FKBP-ligand interface to generate chemical dimerizers with novel specificity. Proc Natl Acad Sci U S A. 1998;95:10437-10442.
11. Iuliucci JD, Oliver SD, Morley S, et al. Intravenous safety and pharmacokinetics of a novel dimerizer drug, AP1903, in healthy volunteers. J Clin Pharmacol. 2001;41:870-879.
12. Thomis DC, Marktel S, Bonini C, et al. A Fas-based suicide switch in human T cells for the treatment of graft-versus-host disease. Blood. 2001;97:1249-1257.
13. Spencer DM, Belshaw PJ, Chen L, et al. Functional analysis of Fas signaling in vivo using synthetic inducers of dimerization. Curr Biol. 1996;6:839-847.
14. Fan L, Freeman KW, Khan T, Pham E, Spencer DM. Improved artificial death switches based on caspases and FADD. Hum Gene Ther. 1999;10:2273-2285.
15. Berger C, Blau CA, Huang ML, et al. Pharmacologically regulated Fas-mediated death of adoptively transferred T cells in a nonhuman primate model. Blood. 2004;103:1261-1269.
16. Junker K, Koehl U, Zimmerman S, et al. Kinetics of cell death in T lymphocytes genetically modified with two novel suicide fusion genes. Gene Ther. 2003;10:1189-1197.
17. Yu J, Zhang L. Apoptosis in human cancer cells. Curr Opin Oncol. 2004;16:19-24.
18. Grayson JM, Zajac AJ, Altman JD, Ahmed R. Cutting edge: increased expression of Bcl-2 in antigen-specific memory $CD8^+$ T cells. J Immunol. 2000;164:3950-3954.
19. Bollard CM, Rossig C, Calonge MJ, et al. Adapting a transforming growth factor beta-related tumor protection strategy to enhance antitumor immunity. Blood. 2002;99:3179-3187.
20. Wagner HJ, Bollard CM, Vigouroux S, et al. A strategy for treatment of Epstein-Barr virus-positive Hodgkin's disease by targeting interleukin 12 to the tumor environment using tumor antigen-specific T cells. Cancer Gene Ther. 2004;11:81-91.
21. Pule M, Finney H, Lawson A. Artificial T-cell receptors. Cytotherapy. 2003;5:211-226.
22. Schumacher TN. T-cell-receptor gene therapy. Nat Rev Immunol. 2002;2:512-519.
23. Anderson R, Macdonald I, Corbett T, et al. Construction and biological characterization of an interleukin-12 fusion protein (Flexi-12): delivery to acute myeloid leukemic blasts using adeno-associated virus. Hum Gene Ther. 1997;8:1125-1135.

24. Cosset FL, Takeuchi Y, Battini JL, Weiss RA, Collins MK. High-titer packaging cells producing recombinant retroviruses resistant to human serum. J Virol. 1995;69:7430-7436.
25. Smith CA, Ng CY, Heslop HE, et al. Production of genetically modified Epstein-Barr virus-specific cytotoxic T cells for adoptive transfer to patients at high risk of EBV-associated lymphoproliferative disease. J Hematother. 1995;4:73-79.
26. Hawley RG, Hawley TS, Fong AZ, et al. Thrombopoietic potential and serial repopulating ability of murine hematopoietic stem cells constitutively expressing interleukin 11. Proc Natl Acad Sci U S A. 1996;93:10297-10302.
27. Gottschalk S, Heslop HE, Roon CM. Treatment of Epstein-Barr virus-associated malignancies with specific T cells. Adv Cancer Res. 2002;84:175-201.
28. Schattner EJ. Apoptosis in lymphocytic leukemias and lymphomas. Cancer Invest. 2002;20:737-748.
29. Nakatsuka S, Takakuwa T, Tomita Y, et al. Hypermethylation of death-associated protein (DAP) kinase CpG island is frequent not only in B-cell but also in T- and natural killer (NK)/T-cell malignancies. Cancer Sci. 2003;94:87-91.
30. Kirchhoff S, Muller WW, Li-Weber M, Krammer PH. Up-regulation of c-FLIPshort and reduction of activation-induced cell death in CD28-costimulated human T cells. Eur J Immunol. 2000;30:2765-2774.
31. Zehender G, Varchetta S, De Maddalena C, et al. Resistance to Fas-mediated apoptosis of human T-cell lines expressing human T-lymphotropic virus type-2 (HTLV-2) Tax protein. Virology. 2001;281:43-50.
32. Kongphanich A, Hieda M, Kurokawa K, Murata T, Kobayashi N. Overcoming the blockade at the upstream of caspase cascade in Fas-resistant HTLV-I-infected T cells by cycloheximide. Biochem Biophys Res Commun. 2002;294:714-718.
33. Lacerda JF, Ladanyi M, Louie DC, et al. Human Epstein-Barr virus (EBV)–specific cytotoxic T lymphocytes home preferentially to and induce selective regressions of autologous EBV-induced B cell lymphoproliferations in xenografted C.B-17 scid/scid mice. J Exp Med. 1996;183:1215-1228.
34. Boatright KM, Salvesen GS. Mechanisms of caspase activation. Curr Opin Cell Biol. 2003;15:725-731.
35. Stennicke HR, Deveraux QL, Humke EW, et al. Caspase-9 can be activated without proteolytic processing. J Biol Chem. 1999;274:8359-8362.
36. Boatright KM, Renatus M, Scott FL, et al. A unified model for apical caspase activation. Mol Cell. 2003;11:529-541.
37. Renatus M, Stennicke HR, Scott FL, Liddington RC, Salvesen GS. Dimer formation drives the activation of the cell death protease caspase 9. Proc Natl Acad Sci U S A. 2001;98:14250-14255.
38. Emery DW, Yannaki E, Tubb J, Stamatoyannopoulos G. A chromatin insulator protects retrovirus vectors from chromosomal position effects. Proc Natl Acad Sci U S A. 2000;97:9150-9155.
39. Deola S, Scaramuzza S, Birolo RS, et al. Mobilized blood CD34$^+$ cells transduced and selected with a clinically applicable protocol reconstitute lymphopoiesis in SCID-Hu mice. Hum Gene Ther. 2004;15:305-311.
40. Fehse B, Kustikova OS, Li Z, et al. A novel 'sort-suicide' fusion gene vector for T cell manipulation. Gene Ther. 2002;9:1633-1638.
41. Serafini M, Manganini M, Borleri G, et al. Characterization of CD20-transduced T lymphocytes as an alternative suicide gene therapy approach for the treatment of graft-versus-host disease. Hum Gene Ther. 2004;15:63-76.
42. Szymczak AL, Workman CJ, Wang Y, et al. Correction of multi-gene deficiency in vivo using a single 'self-cleaving' 2A peptide-based retroviral vector. Nat Biotechnol. 2004;22:589-594.
43. Srinivasula SM, Hegde R, Saleh A, et al. A conserved XIAP-interaction motif in caspase-9 and Smac/DIABLO regulates caspase activity and apoptosis. Nature. 2001;410:112-116.

Research Article

EZC-Prostate Models Offer High Sensitivity and Specificity for Noninvasive Imaging of Prostate Cancer Progression and Androgen Receptor Action

Mamatha Seethammagari,[1] Xiaoming Xie,[1] Norman M. Greenberg,[2] and David M. Spencer[1]

[1]Baylor College of Medicine, Houston, Texas and [2]Fred Hutchinson Cancer Research Center, Seattle, Washington

Abstract

In vivo **imaging advances have greatly expanded the use of animal cancer models. Herein, we describe two new models that permit prostate imaging** ***ex vivo, in vivo*****, and** ***in utero*****. Further, we show the use of these models for detecting small metastasis and testing reagents that modulate the androgen receptor (AR) axis. A luciferase reporter gene was directed to the prostate epithelium using three composite promoters called human kallikrein 2 (hK2)-E3/P, PSA-E2/P, and ARR_2PB, derived from hK2, PSA, and rat probasin regulatory elements, to generate the EZC1, EZC2, and EZC3-prostate mice, respectively. EZC2 and EZC3-prostate display robust expression in the prostate with only minimal detectable expression in other organs, including testes and epididymis. Luciferase expression was detected as early as embryonic day 13 (E13) in the urogenital track. To image prostate cancer progression, lines of EZC mice were bred with prostate cancer models TRAMP and JOCK1, and imaged longitudinally. When crossed with prostate cancer models, EZC3 facilitated detection of metastatic lesions although total prostate luciferase expression was static or reduced due to weakening of AR-regulated promoters. Castration reduced luciferase expression by 90% and 97% in EZC2 and EZC3 mice, respectively, and use of GnRH antagonist also led to extensive inhibition of reporter activity. The EZC-prostate model permits prostate imaging** ***in vivo*** **and should be useful for imaging prostate development, growth, metastasis, and response to treatment noninvasively and longitudinally. These models also provide powerful new reagents for developing improved drugs that inhibit the AR axis.** (Cancer Res 2006; 66(12): 1-11)

Introduction

Animal models that reflect the natural history of human disease and/or human pathobiology can help elucidate the molecular basis of disease pathogenesis and accelerate the pace of drug development. There is now an increasing repertoire of animal models for numerous distinct types of cancer, such as prostate cancer (reviewed in refs. 1, 2). Because autochthonous models develop progressive disease over time, advances in molecular and optical imaging now permit imaging of early tumor growth or metastasis. These new noninvasive techniques can complement results obtained by direct methods at the study end point, thereby hastening the pace of research while reducing the number of animals required (reviewed in ref. 3).

Approaches to noninvasive imaging differ by a number of key variables, such as spatial resolution, depth, imaging times, sensitivity, type of probe, cost, and others (reviewed in ref. 4). The highest spatial resolution is obtained with magnetic resonance imaging and computed tomography that can get close to 25 μm with long (>15 minutes) scan times. Molecular imaging using positron emission tomography (PET) and techniques based on detection of γ-rays produced by radiolabeled probes can provide resolution near 1 to 2 mm, but these methods require expensive equipment and relatively slow throughput. A new three-dimensional ultrasound microimaging technology has been developed with very good spatial resolution at low cost that has been used to image spontaneous models of prostate cancer (5). Alternatively, advances in charged coupled devices (CCD) have made optical imaging quite feasible for both fluorescence and especially bioluminescence imaging (BLI), where typically the oxidation of D-luciferin [D-(−)-2-(6′-hydroxy-2′-benzothiazolyl) thiazone-4-carboxylic acid] is observed following the Mg-ATP- and O_2-dependent catalysis by firefly luciferase (6). The main advantages of BLI is sensitivity: Background is virtually absent in mammals imaged in light-tight specimen chambers attached to cryogenically cooled (≤−105°C) CCD cameras. Another advantage of BLI is speed, as multiple animals can be scanned simultaneously in seconds to minutes in a single image acquisition with minimal postprocessing. Drawbacks include the partial opacity of highly vascularized tissue and melanin-pigmented skin, light scattering from tissue membranes and hair of most visible light, and planar two-dimensional images lacking depth information; however, newer "red-shifted" reporter proteins (i.e., producing light >600 nm) and other technologies may overcome these obstacles (7–10). Despite these limitations, imaging of as few as 100 tumor cells in the peritoneal cavity has been shown (10).

We previously reported development and characterization of a mouse model originally named EZC-prostate based on prostate epithelial-directed firefly (*Photinus pyralis*) luciferase and enhanced green fluorescent protein (EGFP) expression (11). The majority of expression was directed by prostate, with minor confounding signals coming from the testes and intestines. Longitudinal measurements showed strong androgen receptor (AR) responsiveness of luciferase reporter driven by the composite human kallikrein 2 (hK2) promoter, hk2-E3/P (12). In the present study, we describe two new prostate-directed expression systems that were used to build new luciferase reporter models, called EZC2-prostate and EZC3-prostate, based on the composite probasin promoter, ARR_2PB (13), and a composite prostate-specific antigen promoter, PSA-E2/P (14), respectively. These new models direct even more exquisite prostate specificity than the original model, allowing for detection of distant soft-tissue metastasis when bred

Note: Supplementary data for this article are available at Cancer Research Online (http://cancerres.aacrjournals.org/).

Requests for reprints: David M. Spencer, Baylor College of Medicine, One Baylor Plaza/M929, Houston, TX 77030. Phone: 713-798-6475; Fax: 713-798-3033; E-mail: dspencer@bcm.edu.

doi:10.1158/0008-5472.CAN-05-3954

unto the TRAMP prostate cancer background (15, 16). Early detection of distant metastasis in living mice should greatly reduce the number of animals required in some studies. Moreover, localization of metastasis *ex vivo* should facilitate histologic analysis.

The use of AR-responsive reporter models also allows remote appraisal of AR activity during development and prostate tumor progression. Although AR levels are maintained or even elevated in the majority of cells within human prostate metastasis (17), AR levels typically drop in a subset of cells or poorly differentiated tumors, especially those displaying neuroendocrine markers (18–20). This observation has been used to suggest that AR signaling maintains the differentiated state of prostate epithelial cells, but loss of this signaling axis in the presence of other genetic and epigenetic events can drive dedifferentiation or reprogramming of cells in both human and animal models (reviewed in ref. 21). Consistent with this hypothesis, we observed a sharp decrease in reporter activity during cancer progression in bigenic models on both the TRAMP background and the JOCK1 model (22). Moreover, distant metastasis in bigenic EZC3-prostate × TRAMP (i.e., EZC-TRAMP) mice have low-level (but detectable) reporter signal, consistent with their prostatic origin.

Although palliative therapies can extend life span by several years, virtually all patients treated with surgical or medical androgen deprivation, combined with AR blockade, eventually succumb to an aggressive hormone-refractory prostate cancer (reviewed by ref. 23). Targets of androgen action include blockade of GnRH/LH-RH signaling (e.g., leuprolide, Abarelix), blockade of 5α-reductase that converts testosterone to the more potent androgen, 5α-dihydrotestosterone (e.g., finasteride, dutasteride), nonsteroidal antiandrogens that act as AR antagonist (e.g., flutamide, bicalutamide), and selective AR modulators that likely prevent tissue-specific coactivator function (24, 25). To test the use of the EZC system in predicting response to hormone withdrawal therapy, we show that the GnRH antagonist, PPI-258, can almost completely eliminate prostate-directed reporter activity to levels comparable with that of castration (up to 3 orders of magnitude).

These new genetically engineered mouse models should accelerate the pace of drug development and our understanding of the role of AR signaling during prostate cancer progression.

Materials and Methods

Constructs. pARR$_2$PB-KBPA-Luc and pPSA-E2/P-KBPA-Luc were composed of the ~500 bp composite ARR$_2$PB promoter originally from pSK/ARR$_2$PB (13) or the ~2.9 kb PSA-E2/P promoter (12), respectively, cloned upstream of the KCR intron in KBPA (26), which is, in turn, upstream of the modified firefly (*Photinus* sp.) luciferase gene from pGL3-Basic (Promega, Madison, WI) and a polyadenylic acid site from bovine growth hormone. Briefly, IRES-EGFP was released from plasmid phK2-E3/P-IRES-EGFP (11) by *Eco*RI digestion and religation to give phK2-E3/P-KBPA-Luc. To get pARR$_2$PB-KBPA-Luc, the *Xba*I/*Spe*I ARR$_2$PB fragment from pAdlox/ARR$_2$PB-EGFP (27) was blunt ligated into the *Not*I/*Bam*HI sites of phK2.E3/P-KBPA-Luc. Similarly, the *Not*I/*Xba*I (blunt) PSA-E2/P fragment from pSH1/PSA-E2/P-SEAP (27) was ligated into *Not*I/*Bam*HI (blunt)–digested phK2.E3/P-KBPA-Luc to produce pPSA-E2/P-KBPA-Luc.

Generation and screening of transgenic mice. The minimal eukaryotic-derived fragments were released from plasmids pARR$_2$PB-KBPA-Luc and pPSA-E2/P-KBPA-Luc with *Bss*HII and gel-purified with Gene Clean kit (Bio101, Vista, CA). The EZC2-prostate (ARR$_2$PB-luc) and EZC3-prostate (PSA-E2/P-luc) transgenic mice were generated by microinjection of purified fragments into the male pronuclei of fertilized FVB oocytes by the Transgenic Core Lab at Baylor College of Medicine. EZC-prostate mice based on plasmid hK2-E3/P-Luc-IRES-EGFP were previously described (11). Mice were maintained in the Transgenic Mouse Facility, a pathogen-free environment, in compliance with Baylor College of Medicine policy. Mouse tail DNA was extracted using the DNeasy Tissue kit (Qiagen, Inc., Valencia, CA) and screened by PCR using primers for the firefly luciferase genes *Luc-P1*, 5′-AGCCAGCATGGAAGACGCCAAAAAC-3′, and *Luc-P2*, 5′-ATCGCAGTATCCGGAATGATTTGATTGC-3′. DNA quality control primers for mouse casein: forward, 5′-GATGTGCTCCAGGC-TAAAGTT-3′, and reverse, 5′-AGAAACGGAATGTTGTGGAGT-3′.

Luciferase assays. To assay tissue-derived luciferase activity, animals were euthanized and dissected. Tissue specimens from the ventral, dorsolateral, and anterior prostate lobes were microdissected and stored temporarily on ice before homogenization in lysis buffer. Other tissue specimens, including testes, epididymis, seminal vesicle, penis, as well as brain, salivary glands, thymus, lung, heart, stomach, cecum, small intestine, large intestine, liver, adrenal gland, kidney, pancreas, and spleen were also analyzed to determine the tissue specificity of the EZC, EZC2, and EZC3 promoters. Tissues were homogenized with a PRO250 homogenizer (Pro Scientific, Inc., Oxford, CT) in 300 μL luciferase lysis buffer (Promega) containing 1/100 diluted protein inhibitor cocktail (Roche). Specimens were centrifuged at 8,000 rpm for 5 minutes and placed temporarily on ice. Luciferase activity of the cell lysates was measured with a TD 20/20 luminometer (Turner Designs, Inc., Mt. View, CA) and the protein concentration was determined using the detergent-compatible protein assay system (Bio-Rad, Hercules, CA) in a Beckman DU-640 spectrophotometer (Beckman Instruments). The luminescence results are reported as relative light units per milligram of protein.

Histologic and immunohistochemical examination. The microdissected prostate parts and other tissues indicated above were fixed overnight in 10% formaldehyde and transferred to 1:1 formaldehyde/ethanol for 1 hour followed by transfer to 70% ethanol until processing. Tissues were processed in a series of increasing ethanol concentrations and embedded in paraffin wax. Five-micrometer sections were cut and stained with H&E. Immunostaining for firefly luciferase was also done. Briefly, sections were deparaffinized in xylene, rehydrated in decreasing ethanol from 100% to 80%, microwaved for 10 minutes in 10 mmol/L citrate buffer (pH 6.0) at 95°C to 99°C for antigen retrieval, and finally endogenous peroxidase activity was quenched with 3% hydrogen peroxide. Nonspecific binding was abolished with 10% Power Blocker (BioGenex, San Ramon, CA) for 10 minutes. Tissue sections were incubated overnight at 4°C with a 1:2,000 dilution of 10 mg/mL biotin-conjugated goat anti–firefly luciferase antibody (Abcam, Hartford, CT). After four PBS washes with 0.1% Tween 20 for 2 hours, sections were incubated with horseradish peroxidase–conjugated streptavidin using the Vectastin Elites ABC kit (Vector Laboratories, Inc., Burlingame, CA) for 45 minutes at room temperature. Peroxidase activity was revealed with 3′,3′-diaminobenzidine (DAB) tetrahydrochlorate using a DAB kit (Vector Laboratories) according to the protocol provided. Finally, sections were washed in distilled water for terminating the reaction, counterstained with 1% methyl green, dehydrated, and mounted.

Imaging and quantification of bioluminescence data. Mice were anesthetized with a mixture of 1.5% isoflurane/air using an Inhalation Anesthesia System (VetEquip, Inc., Pleasant Hill, CA). D-Luciferin (Xenogen, Alameda, CA) was i.p. injected at 40 mg/kg mouse body weight (unless otherwise specified). Ten minutes after D-luciferin injection, mice were imaged with an IVIS Imaging System (Xenogen) with continuous 1% to 2% isoflurane exposure. Imaging variables were maintained for comparative analysis. Gray scale–reflected images and pseudocolorized images reflecting bioluminescence were superimposed and analyzed using the Living Image software (Xenogen). A region of interest (ROI) was manually selected over relevant regions of signal intensity. The area of the ROI was kept constant within experiments and the intensity was recorded as total photon counts per second per cm^2 within a ROI. In some experiments, after imaging living mice, animals were euthanized and organs of interest were removed, arranged on black, bioluminescence-free paper, and *ex vivo* imaged within 30 minutes.

Castration of mice and administration of reagents. To study the effect of androgen ablation on EZC2-Prosate-driven firefly luciferase

expression, 20-week-old male mice, were anesthetized with Rodent Combo Anesthetic III (37.6 mg/mL ketamine, 1.92 mg/mL xylazine, and 0.38 mg/mL acepromazine) at 240 mg/kg mouse weight, and cleaned around the scrotum with 70% ethanol. A 1-cm median incision was made at the tip of the scrotum. The testes lying in the sacs can be seen by placing pressure on the lower abdomen. A 5-mm incision was made into each sac, and the testes, epididymis, vas deferens, and spermatic blood vessels were pulled out. A single ligature was placed around the spermatic blood vessels and vas deferens. The testes and epididymis were removed by severing the blood vessels and vas deferens distal to the ligature. The remaining vas deferens was pushed back into the sac and the incision was sutured. The castrated mice were put on a heating pad until recovery and were given injectable Buprenex (buprenorphine hydrochloride; Reckitt Benckiser Healthcare UK, Ltd., England, United Kingdom). Sham-operated, age-matched males were used as controls. The orchiectomized mice were imaged biweekly until day 16 postcastration when animals were given testosterone pellets (10 mg/21-day release-Innovative Research of America, Sarasota, FL) for experimental groups and placebo for control groups. The mouse was shaved on dorsal side and cleaned with 70% ethanol. A 5-mm incision was made in the center of the back, the pellet was placed under the skin with forceps and the incision was clipped with surgical staples. The mice were measured biweekly and after 2 weeks animals were euthanized and imaged *ex vivo* as above. Mice treated with GnRH antagonist, PPI-258 (Praecis Pharma, Waltham, MA), were treated with a single s.c. 50 mg/kg dose (5 mg/mL 0.9% saline) of PPI-258-CMC, suspended in a time-release depot, designed to last for at least 4 weeks. For treatment of EZC-JOCK mice with chemical inducer of dimerization (CID), AP20187 was dissolved in 16.7% propanediol, 22.5% PEG400, 1.25% Tween 80, and injected i.p. biweekly at 2 mg/kg. Alternatively, carrier alone was injected.

Statistical analysis. Statistical significance was determined between indicated groups primarily using a nonpaired, two-sided Student's *t* test (Microsoft Excel 2004).

Results

Development of EZC-prostate models. We previously reported that *in vivo* chemiluminescent imaging of the prostate was possible (11). Although reporter expression driven by the composite hK2-based promoter, hK2-E3/P, was primarily (>98%) specific for prostate tissue, low-level androgen-independent expression in the cecum and lower intestines of some animals produced a disproportionate confounding signal during living imaging. Therefore, we have now developed two models that expressed luciferase under the transcriptional regulation of the alternative prostate-epithelial-targeted promoters, namely ARR_2PB, based on the rat probasin promoter (13) and PSA-E2/P, based on the prostate-specific antigen promoter (12).

We were able to select new founder lines using both ARR_2PB (one of three) and PSA-E2/P (two of four) that showed highly robust and prostate-specific expression, and have named them EZC2-prostate (EZC2) and EZC3-prostate (EZC3), respectively. Both new lines showed extremely high luminescence in the lower abdomen of living mice, requiring only seconds for imaging (Fig. 1*A*). Dissection of these lines and *ex vivo* imaging of tissues confirmed that the major luminescence was derived from the relatively small (~20 mg) ventral prostate lobes. Moreover, luciferase expression was almost undetectable in the intestines and all internal organs of both new lines (Fig. 1*B*). Additional relatively weak signals in the extremities of EZC3 mice are distant from the prostate and likely target tissues of prostate cancer metastasis in mice, such as draining lymph nodes, lungs, and liver. Thus, EZC2- and EZC3-prostate models reflect the highest overall signal intensity and tissue specificity ever seen in a prostate-directed bioluminescence model. F1

Tissue-specific and temporal regulation of reporter expression. To quantitate the tissue specificity of these new lines, we conducted sensitive luciferase assays on a broad panel of tissues from 12-week-old mice from each line (Fig. 2*A-C*). This analysis further confirmed that the major reporter signal from each line was derived from the ventral prostate with minor signals coming from various other sources. For EZC2, minor relative signals (>0.1%) were detected in the epididymis (2.1%), dorsolateral prostate (0.7%), and penis (0.4%; Fig. 2*B*). For EZC3, minor signals (>0.1%) were detected in dorsolateral prostate (1.6%), testes (1.1%), and anterior prostate (0.2%). In contrast, for the original EZC-prostate (renamed EZC1), minor signals (≥0.5%) came from a larger number of tissues, including dorsolateral prostate (7.8%), cecum (6.1%), anterior prostate (3.2%), large intestines (2.0%), testes (1.4%), spleen (1.4%), small intestines (1.1%), penis (0.5%), and F2

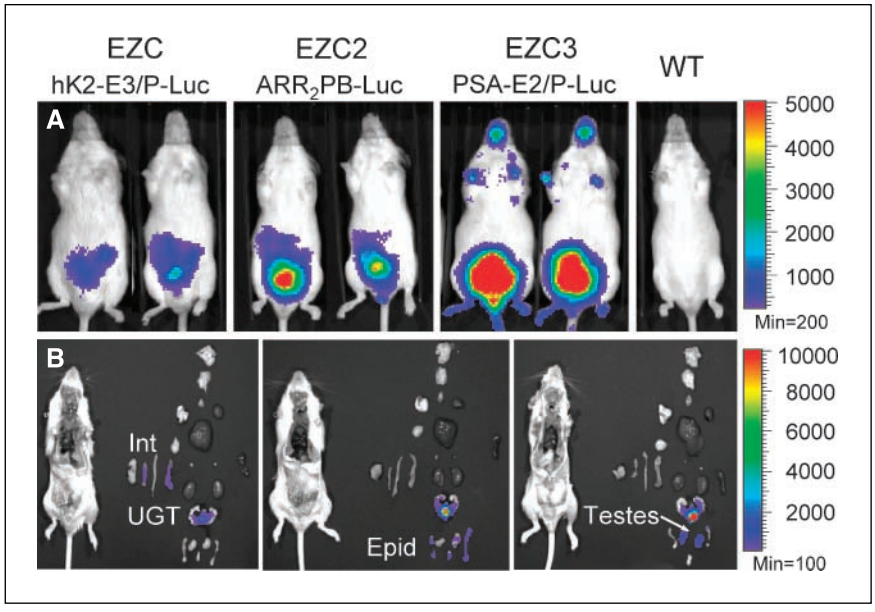

Figure 1. Comparison of three distinct prostate-specific promoters in transgenic mice. *A,* male 12-week-old transgenic mice were anesthetized and chemiluminescence was imaged using an IVIS imaging system 10 minutes after i.p. injection with D-luciferin (40 mg/kg). Two representative mice per line and one wild-type (*WT*) nontransgenic mouse are shown. *B,* mice were immediately euthanized and dissected. Isolated organs were laid out on nonluminescent paper in anatomically relevant order and imaged within 45 minutes. Most highly chemiluminescent organs are labeled. *Int,* intestines; *UGT,* urogenital tract; *Epid,* epididymis.

thymus (0.4%; Fig. 2*C*). Thus, careful tissue analysis confirmed the robust expression and prostate specificity of EZC2 and EZC3.

An advantage of live imaging is the ability to undertake longitudinal analysis of reporter activity. In accordance with the large increase in testosterone production and prostate size during puberty, all three distinct EZC-prostate lines showed an increase in AR-driven reporter activity in living mice after 4 weeks of age (Fig. 3*A* and *B*). Moreover, in EZC2 mice, the amount of luciferase per milligram prostate tissue showed a very large (~100-fold) increase from 4 to 8 weeks (Fig. 3*C*). A somewhat more conservative increase was observed during puberty in EZC3-prostates (Supplementary Fig. S1), perhaps reflecting greater sensitivity of the PSA-E2/P promoter to lower testosterone levels. In EZC1 mice, the biggest temporal increase in reporter signal occurred earlier, between 3 and 4 weeks, although off-target reporter expression in their intestines may have partially confounded pubertal changes in AR activity during prostate development (data not shown). Thus, in all three of the EZC series of prostate models, AR activity in the prostate could be measured as a surrogate marker for prostate growth and development.

To determine whether the EZC system was active *in utero*, gravid, nontransgenic female mice bearing embryonic day 10 (E10) to E19 EZC2 embryos were administered D-luciferin. Although the signal intensity was weak relative to adult transgenic mice, by 10 minutes after substrate injection, fetal signals were readily detected after E14 in some mice (Fig. 4*A*). Although some intermouse variability was seen, likely due to positioning of embryos and stochastic efficiency of substrate delivery, in general the average signal intensity peaked at E17 and dropped steadily until birth (data not shown). Removal of the uterine horn 15 or 19 days *post coitis* confirmed that all of the detectable signals came from transgenic embryos although the absolute levels of luciferase activity varied per embryo (Fig. 4*B*). Also, we were unable to find a significant correlation between signal intensity and gender or fetus position in the uterus (Fig. 4*C*). The weakest signals, however, did originate from the smallest embryos. Luminescence was localized to the urogenital tract of both male and female embryos, as well as from other tissues, including the penis, vagina, upper and lower jaws (and other head regions), and the upper limbs (Fig. 4*D*). In contrast, as in adults, there did not seem to be reporter gene expression in the internal organs, including the liver, lungs, and intestines.

The signals we detected at the ends of the upper and lower jaws and the upper limbs (likely from skeletal muscle) at E15 and E19 were essentially undetectable by neonatal day 1 or 2 (Fig. 4*E*). Similarly, the urogenital tract–derived signal was difficult to detect after day 3, commensurate with the predicted drop in circulating androgens. Interestingly, reporter activity in the lower abdomen continued to increase in intensity during early development despite near undetectable signaling from the urogenital sinus (Fig. 4*F*). Dissection and *ex vivo* imaging showed that this weak signal came primarily from the intestines, and leveled off following puberty. Thus, these very sensitive androgen-responsive promoters can drive a spatiotemporal program of expression during development that may differ from adults, likely reflecting changes in both AR levels and coactivators.

Imaging prostate cancer progression and metastasis with EZC-prostate models. One of the primary goals of generating organ-specific reporter mice is the ability to noninvasively image changes in the gland during normal development or pathologic states, such as neoplasia. To test whether the EZC-prostate model could be used to measure prostate hyperplasia and cancer progression. EZC1-, EZC2-, and EZC3-prostate mice were bred with two distinct animal models, the recently described inducible prostate intraepithelial neoplasia model, JOCK1 (22), and the well-characterized TRAMP model (15, 20). In the JOCK-1 model, administration of a lipid-permeable dimerizing drug leads to cross-linking and activation of a prostate-targeted isoform of FGFR-1 that carries cytoplasmic tyrosine kinase domains linked to tandem dimerizer drug-binding domains but lacks any extracellular native ligand-binding capacity. Signaling ensues within minutes of dimerizer delivery and proliferation is detectable within 24 hours. Hyperplasia is evident within 2 weeks of biweekly dimerizer administration; by 6 to 8 weeks, the ducts are filled with dysplastic cells, and by 24 weeks high-grade prostate intraepithelial neoplasia is widespread. Further, within 40 weeks of treatment, adenocarcinoma is reproducibly seen.[3] Despite a large increase in cellular content, we did not detect a concomitant increase in reporter activity in bigenic mice treated with dimerizer drug for up to 40 weeks (Fig. 5*A* and *B*). Histologic analysis showed a reduction

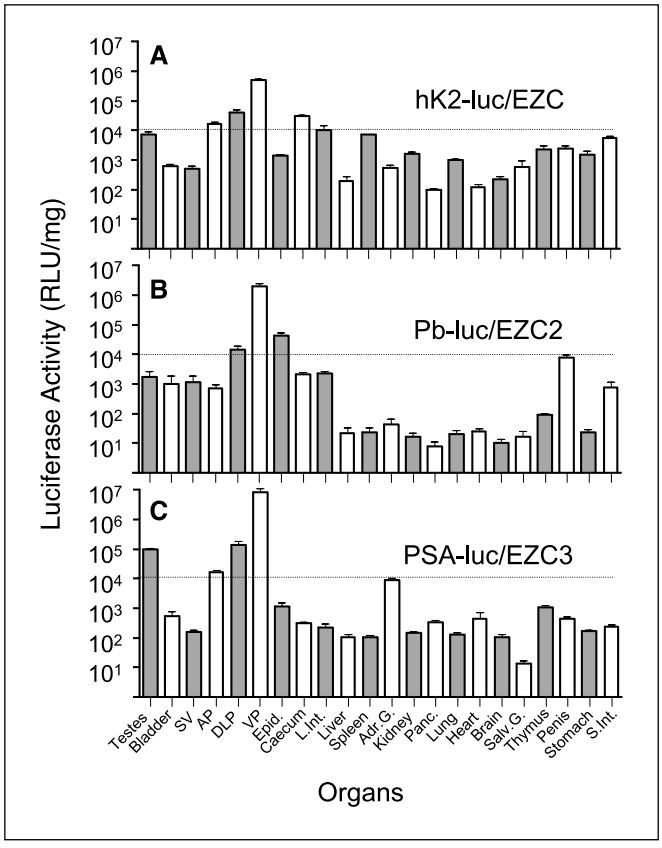

Figure 2. Tissue-specific reporter expression in three EZC-prostate lines. *A* to *C,* three 12-week-old EZC-prostate (*A*), EZC2-prostate (*B*), or EZC3-prostate (*C*) transgenic mice were microdissected and organs were homogenized. Luciferase activity was quantitated in each tissue extract using a standard luminometer. *Columns,* mean luciferase activity (*RLU,* relative luciferase units) per milligram of total protein; *bars,* SD. *SV,* seminal vesicle; *AP,* anterior prostate; *DLP,* dorsolateral prostate; *VP,* ventral prostate; *L.int.,* large intestines; *Adr.G.,* adrenal gland; *Panc.,* pancreas; *Salv.G.,* salivary gland; *S.Int.,* small intestines.

[3] D.M. Spencer, E.N., and V.A., unpublished results.

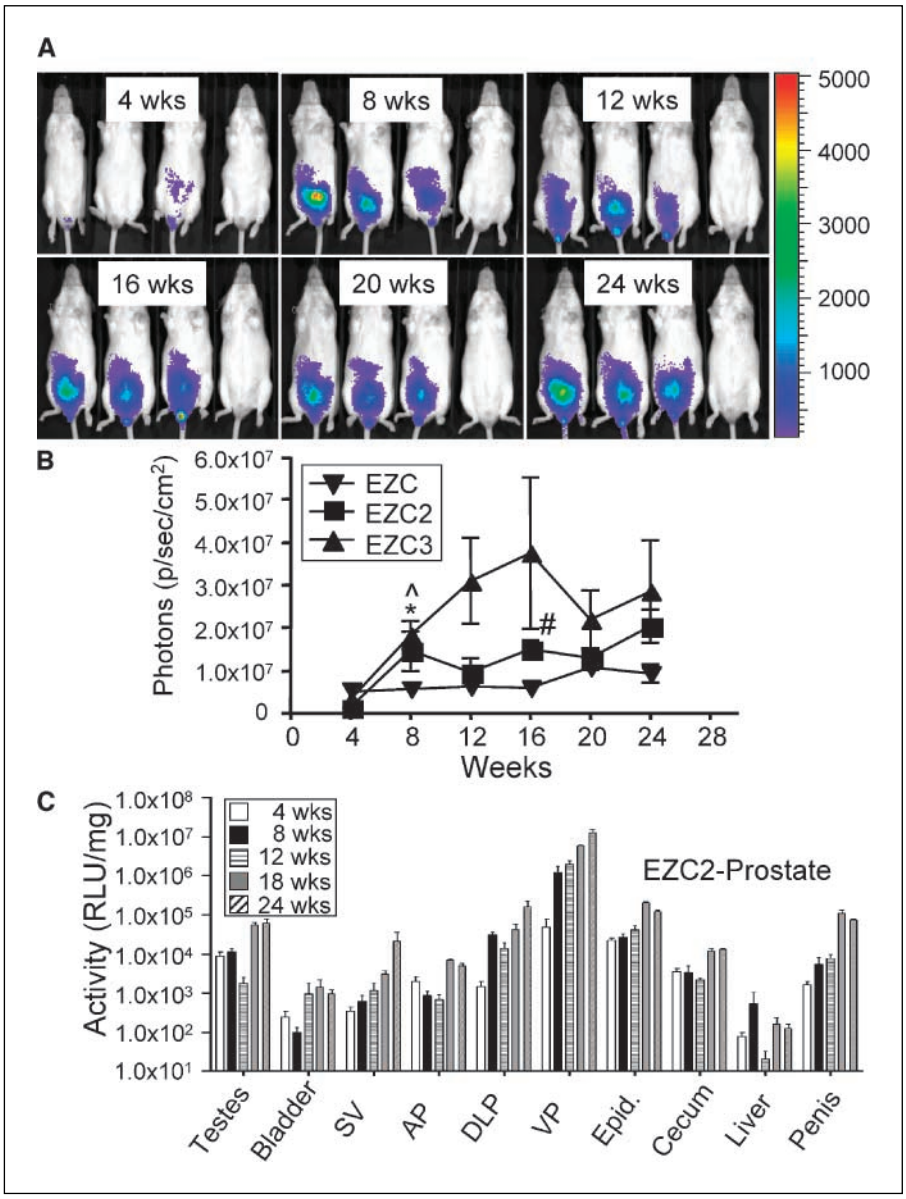

Figure 3. Kinetics of luciferase expression in EZC-prostate mice. *A,* male EZC2-prostate mice were anesthetized and chemiluminescence was imaged 10 minutes after i.p. injection with D-luciferin (40 mg/kg) at the ages shown. Three representative mice and one nontransgenic mouse are shown. *B,* reporter activity at various ages for all three EZC-prostate lines. *Points,* mean photon counts ($n = 3$) summed over the entire chemiluminescent lower half of each mouse; *bars,* SD. *, $P < 0.05$, EZC3 versus EZC1; #, $P < 0.05$, EZC2 versus EZC1; ^, $P < 0.05$, EZC3 (8 versus 4 weeks). Kinetics of tissue-specific reporter expression in EZC2-prostate mice. Luciferase activity was quantitated in each tissue extract using a luminometer. *Columns,* mean luciferase activity (relative luciferase units per milligram of total protein); *bars,* SD.

SF2 in luciferase expression per cell following FGFR1-mediated hyperplasia and dysplasia (Supplementary Fig. S2). *Ex vivo* chemiluminescent imaging of 60-week-old EZC2-JOCK prostates (from above) also shows that AR activity is diminished per cell during FGFR1-stimulated progression, which increases total prostate volume, leading to an overall ~5-fold decrease in reporter activity *ex vivo* (Fig. 5*C*).

In the TRAMP model, histologic well-differentiated adenocarcinoma can be detected by 12 weeks of age that progresses to poorly differentiated adenocarcinoma with metastasis over the next 12 to 18 weeks (20). Although skin and hair pigment from the C57BL/6 background lower reporter activity by at least 10-fold, chemiluminescence was readily detected in the lower abdomen of
F6F7 SF3 living mice in all three models (Figs. 6 and 7; Supplementary Fig. S3). Despite reproducible tumor progression, we were unable to detect significant concomitant increases in reporter activity in living mice (Fig. 6*A, B* and 7; Supplementary Fig. S3), consistent with a loss of promoter activity as a function of tumor progression. Higher reporter variability in the EZC1-TRAMP model (i.e., hK2-E3/P-luc × TRAMP) over time versus EZC2-TRAMP is apparently due to unpredictable tumor-mediated displacements of the faintly glowing intestines in the EZC1 model, which luminesce as a function of surface proximity (Fig. 6*A* and *C*). The decrease in reporter activity in the prostates of tumor-bearing mice may be due to a number of factors, including reduced blood flow and hypoxia in necrotic tissue, decreases in AR expression during dedifferentiation, and possible changes in coactivator function. Interestingly, reporter activity can still be seen in the less involved anterior prostate even when other prostate lobes become fused within a large tumor mass (Fig. 6*C*).

Imaging metastasis with the EZC-prostate models. In a minority of EZC1-TRAMP and EZC2-TRAMP mice (10-20%), distant site metastasis is visible at necropsy (Fig. 6*D*). Although reporter activity in the ventral prostate of normal EZC1-prostate mice is ~20-fold greater per milligram of tissue than in the intestines (Fig. 2), reporter activity in distant metastasis in EZC1-TRAMP

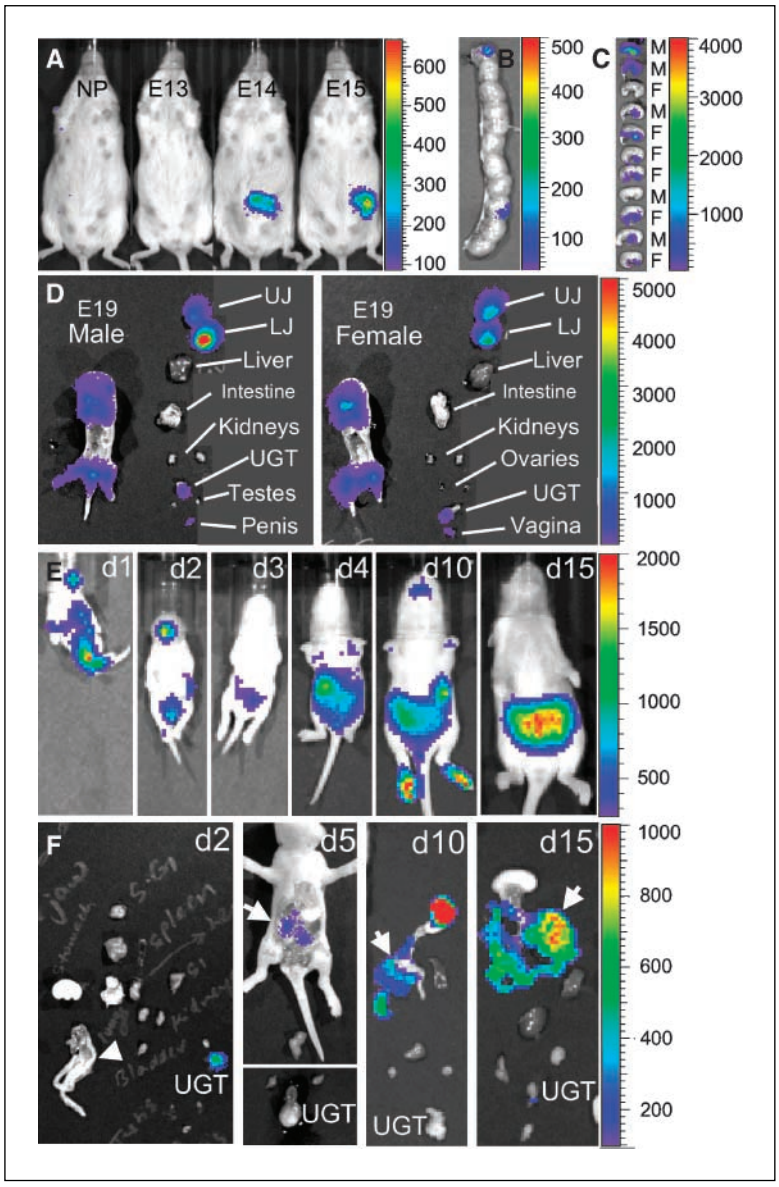

Figure 4. Kinetics of luciferase expression during development in EZC2-prostate mice. *A,* embryonic E13 to E15 expression viewed from within nontransgenic females. *NP,* not pregnant. *B,* uterine horn containing transgenic E19 embryos. *C,* embryos imaged separately in birth order. Gender (*M/F*) is indicated based on genotype. *D,* representative embryos 4 (*left*) and 5 (*right*) were dissected, showing reporter-expressing urogenital tract and upper (*UJ*) and lower (*LJ*) jaws. *E,* reporter expression *in vivo* during early development. Age in days (*d*) is shown. Amount of D-luciferin injected based on weight. *F,* dissected male EZC2-prostate mice at various ages showing UGT and intestinal signal (*arrows*). Scale, counts in all panels. All panels are representative of at least three age-matched mice.

mice is actually weaker than that of intestinal tissue. However, lowering the pseudocolor threshold reveals reporter activity in the easily visible hypochromic metastatic tumors, consistent with prostate epithelial origin, and this bioluminescence follows the outline of the gross metastasis (Fig. 6*E*). Imaging tissues *ex vivo* can also reveal metastasis within tissues, such as in the enlarged spleen of this animal despite the absence of metastatic nodules on the surface. Therefore, although imaging of prostate metastasis in living mice may be challenging when AR-regulated promoters are used to express luciferase activity, prostate metastasis in distant organs can be easily detected *ex vivo*.

As opposed to EZC1 and, to a lesser extent, EZC2 mice, the near absence of detectable extraprostatic reporter activity in the abdominal region of EZC3 mice led to the prediction that distant metastasis should be easily detectable in the EZC3-TRAMP model. Similar to EZC1- and EZC2-TRAMP, reporter activity from the lower abdomen of EZC3-TRAMP dropped with age in 40% (4 of 10) of animals imaged fortnightly until euthanasia [due to age (up to 32 weeks), distress, or prohibitive tumor size], consistent with prostate cancer progression (Fig. 7*A* and Supplementary Fig. S3*A, C, E*, and *F*). Moreover, in 50% of mice analyzed until euthanasia, we witnessed a large increase in disseminated reporter activity in living mice (Fig. 7*A* and Supplementary Fig. S3*A, B, C, E*, and *F*). Upon autopsy, we observed reporter activity in numerous tissues, including pancreas (10 of 10) para-aortic (prostate draining) and mesenteric lymph nodes (6 of 10), kidneys (3 of 10), adrenal glands (2 of 10), liver (2 of 10), spleen (2 of 10), and salivary glands (1 of 10). Histologic analysis confirmed that putative tumors imaged in living mice were present in suspect organs (Fig. 7*C-F*). Thus, the EZC3-prostate model can be used to identify prostate metastasis in living mice and to localize metastasis to specific organ sites *ex vivo*.

***In vivo* imaging of AR activity.** The three EZC-prostate models were based on highly AR-responsive promoters, leading to the prediction that they should permit remote determination of AR activity in living mice. To test this hypothesis, we compared *in vivo* reporter activity between castrated and intact mice. Circulating DHT levels in intact mice varied widely (from 50 to 3,000 pg/mL),

but dropped below detection (<5 pg/mL) in all castrated mice (data not shown). Although there was some variability in signal intensity in intact mice, likely due to these large variations in circulating androgen levels in cohabitating male animals, the luminescence of castrate mice were quite reproducible and dropped rapidly (3-4 days) to ~10% of total intact levels in living EZC2-prostate mice (Fig. 8*A* and *C*). Ectopic delivery of testosterone (10 mg/pellet/21 days) led to recovery of intact reporter levels over a 3-week period. The lengthened time required for reporter rebound versus suppression was likely due to the additional time needed for restoring prostate cellularity. Addition of testosterone pellets to intact mice led to only a slight increase in average reporter levels (Fig. 8*A*), likely reflecting intact homeostatic regulation of circulating testosterone levels in intact mice. Thus, EZC-prostate mice permit high-throughput appraisal of AR activity in mouse prostates, which could be used to facilitate the characterization and development of drugs that target the AR axis.

As a proof-of-principle of this novel assay for AR activity, we treated EZC2-prostate mice with a 20-day depot (50 mg/kg total) of the gonadotropin-releasing hormone antagonist, PPI-258. Similar to castration, PPI-258 administration led to a relatively rapid drop in total (lower abdomen) reporter activity to ~10% of untreated mice (Fig. 8*B* and *C*). As above, addition of testosterone during GnRH blockade led to reporter rebound, consistent with the mechanism for GnRH antagonist function, which targets leutenizing hormone production in the pituitary gland. Thus, the EZC2-prostate model should provide a convenient model for testing some classes of new drugs targeting the AR axis.

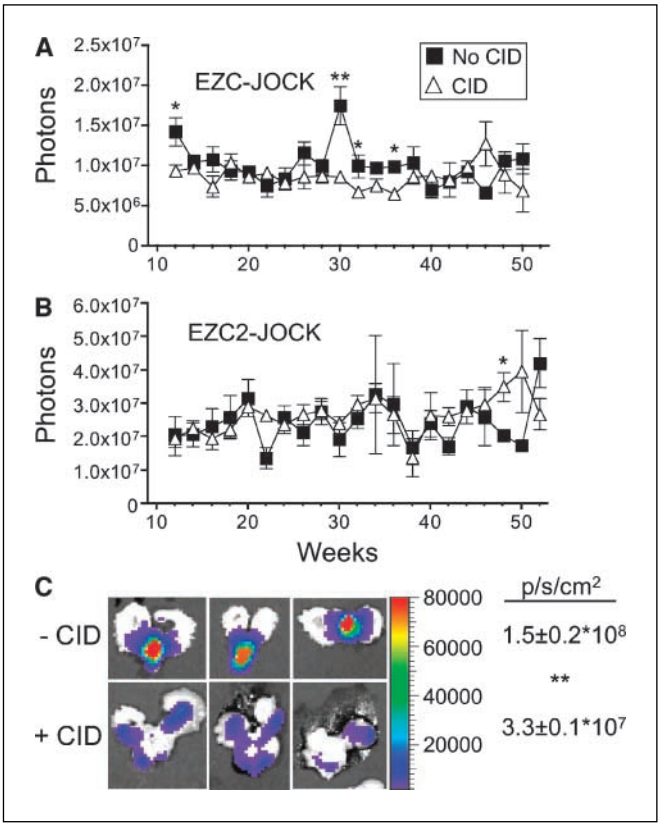

Figure 5. Imaging the prostates of EZC-JOCK mice. Living imaging of equivalent regions of interest (covering lower abdomens) of bigenic mice were measured biweekly starting at 12 weeks. *A,* starting at 12 weeks, EZC-JOCK (EZC-prostate × JOCK-1) mice were treated with dimerizer drug (CID, $n = 6$) or diluent (no CID, $n = 3$). *B,* starting at 12 weeks, EZC2-JOCK (EZC2-prostate × JOCK-1) mice ($n = 3$) were treated with CID or diluent. *Points,* means; *bars,* SD. *C,* prostates (+ seminal vesicles) of 60-week (50 weeks ± CID) EZC2-JOCK mice imaged *ex vivo*. Average ($n = 3$) photons/s/cm^2 ± SD. *, $P < 0.05$; **, $P < 0.005$.

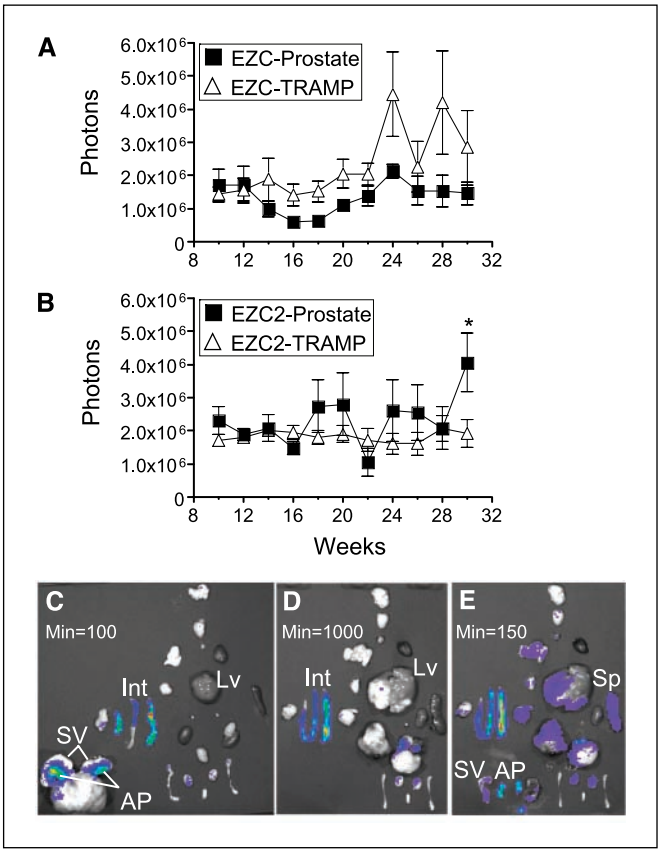

Figure 6. Imaging the prostates and metastasis of EZC-TRAMP mice. *A,* living imaging of equivalent regions of interest (covering lower abdomens) of EZC-prostate (FVB × BL/6) or EZC-TRAMP [EZC-prostate (FVB) × TRAMP (BL/6)] bigenic mice measured fortnightly starting at 10 weeks. *B,* starting at 10 weeks, EZC2-prostate or EZC2-TRAMP (EZC2-prostate × TRAMP) mice ($n = 3$) were imaged as above. *Points,* means; *bars,* SD. *, $P < 0.05$. *C, ex vivo* imaging of 30-week EZC-TRAMP mouse with undetectable metastasis. *D* and *E, ex vivo* imaging of 30-week EZC-TRAMP mouse with visible metastases imaged at high (*D*, minimum counts = 1,000) or low (*E*, minimum counts = 150) pseudocolor threshold. *Lv,* liver; *Sp,* spleen.

Because residual androgen-independent signaling in some tissues could, in principle, limit the total drop in reporter activity, we analyzed tissues *ex vivo* in intact and castrated mice (Fig. 8*D*). Surprisingly, the drop in reporter activity in prostates following castration was >1,000-fold, much larger than the measured change in intact mice when chemiluminescence over the entire lower abdomen was integrated. As described above, weak reporter activity was also detected in intestines, which was not subject to the effects of castration. Thus, narrowing the region-of-interest for measuring reporter activity during analysis to just over the prostate should further improve the sensitivity of the EZC2-prostate model for remote detection of AR activity.

In EZC3-prostate mice, castrate levels of total lower abdomen reporter activity in living mice were ~3% of intact levels (Fig. 9*A* and *B*), suggesting that this model may provide even greater AR sensitivity than EZ2 mice. Interestingly, the drop in reporter activity from prostate tissue following castration was not as great as in EZC2-prostate mice (~65-fold versus ~2,500-fold), but the near

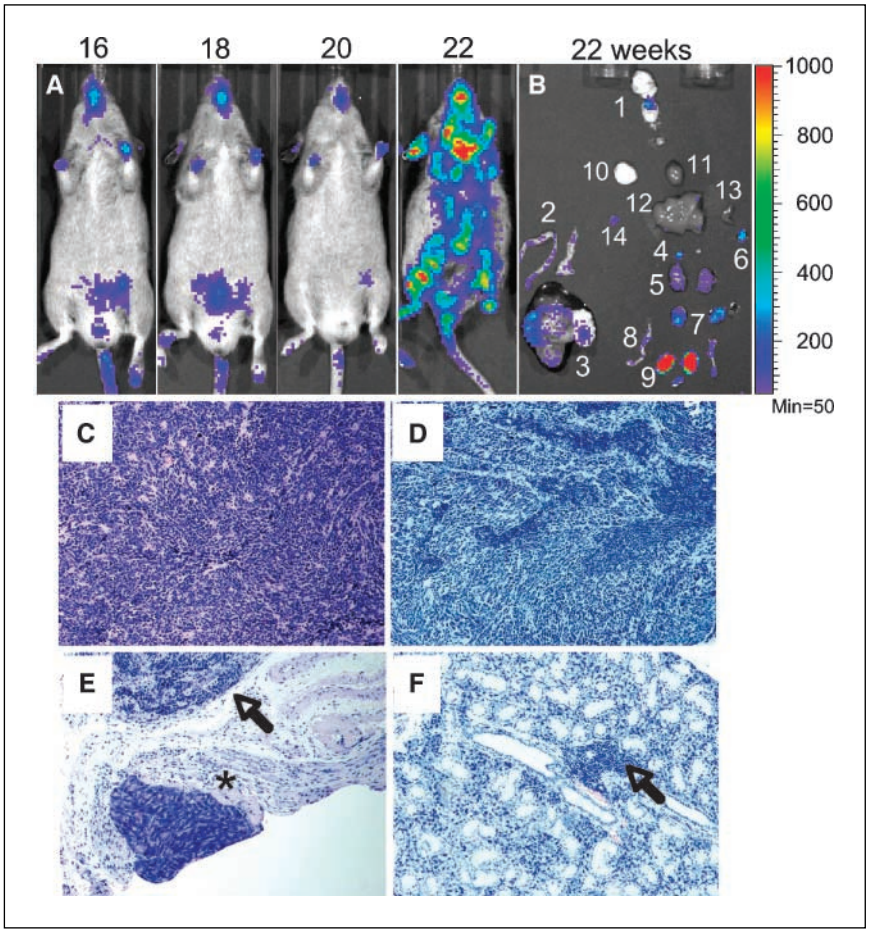

Figure 7. Detection of metastasis in living EZC3-TRAMP mice. *A,* mouse 2153 imaged from 16 to 22 weeks at equivalent conditions. *B,* mouse 2153 imaged *ex vivo* upon dissection at equivalent color scale. *1,* salivary gland; *2,* cecum and colon; *3,* urogenital tract; *4,* adrenal gland; *5,* kidney; *6,* mesenteric lymph node; *7,* para-aortic draining lymph node; *8,* epididymis; *9,* testes; *10,* lung; *11,* heart; *12,* liver; *13,* spleen; *14,* pancreas. *C* to *F,* H&E staining of draining para-aortic lymph node (*C*), mesenteric lymph node (*D*), pancreas (*E*), and salivary gland (*F*) imaged in (*B*). *Arrows,* tumor lesions. *, pancreatic tissue.

absence of intestinal reporter activity apparently more than compensates for residual prostate-localized signal (Fig. 9*C*). Peripheral signals in feet and jaw are well removed from prostate-derived signals. Thus, the EZC3-prostate model should be ideal for testing the efficacy of some classes of AR-targeted drugs.

Discussion

A number of traditional and novel imaging modalities have now been applied to small-animal studies (reviewed in ref. 28). Many of these applications are driven by technology improvements with miniaturization of probes and detectors appropriate for small animals. This sequence contrasts bioluminescent imaging, as its applications in animal research have preceded clinical applications in which the significant absorption and scattering of visible light by most vascularized tissues has limited applications to superficial lesions. Despite possible limited translational applications, BLI has proven quite practical for tumor, signaling, and other applications in small animals, particularly mice.

Other methodologies are also unlikely to have the throughput of optical imaging, as in micro-PET, micro–computed tomography, micro–single-photon emission computed tomography, micro–magnetic resonance imaging, and ultrasound, animals are scanned and imaged individually by skilled personnel and large computer files are required to reconstruct and quantify images in three dimensions; however, continuous improvements in computer power will obviate this concern. Similarly, however, it is likely that reengineering of optical imaging stations to accommodate multi-angle imaging can greatly improve linearity and dimensionality, coincident with engineering of luciferase and fluorescent reporters with favorable red-shifted emission profiles that better penetrate mammalian tissue. Therefore, despite the allure of optical imaging, the ultimate choice of imaging technologies is application and budget driven.

Although inevitable improvements in imaging will further expand the use of the EZC-prostate models described here, there are already several current applications of these prostate reporter mice. First, we were able to successfully compare three distinct (12–14), robust prostate-specific promoters in an unbiased *in vivo* setting. Due to the strength of all three AR-responsive composite promoters used in this study, we were able to easily image mice in 10 to 30 seconds. Weaker tissue-specific promoters can require additional manipulations, such as two-step transcriptional amplification (29), to amplify reporter activity to convenient levels for imaging; however, prostate-directed luciferase activity based on two-step transcriptional amplification technology seems to have much lower tissue specificity than the EZC-prostate models (30). In the composite promoters used for the EZC models, multimerization of AREs was largely responsible for magnifying the transcriptional rates while maintaining extremely high (>99%) tissue specificity; however, each line displayed unique characteristics. This comparison indicated that the composite PSA-E2/P and ARR_2PB promoters were probably somewhat (~2-fold) more potent and prostate specific than hK2-E3/P, whereas hK2-E3/P

seemed to be less susceptible to position-effect variegation (i.e., qualitatively similar expression patterns in six of six founders). All promoters were highly AR dependent with dramatic drops in prostate reporter expression up to 2 or 3 orders of magnitude in the EZC3-prostate (PSA) and EZC2-prostate (ARR_2PB) models, respectively. At the same time, low-level AR-independent expression in the intestines of EZC1-prostate (hK2) and EZC2-prostate mice make the EZC3-prostate model likely better for appraising AR activity. Although qualitatively similar data is likely to occur in gene therapy vectors (12, 27), adjacent promoter elements, such as those found in viral vectors, can modulate tissue specificity (31).

We were also able to detect relatively small metastasis in TRAMP mice when bred onto the EZC3-prostate background, facilitated by the extremely low background expression outside of the urogenital tract. Low-level signals from the intestines of EZC1- and EZC2-prostate mice make detection of distant metastasis more challenging in these models as stochastic movements of the gastrointestinal tract to surface proximal and distal positions can reduce signal-to-noise ratio. Although all three promoters may be useful for prostate epithelial-specific expression of most transgenes, the extreme sensitivity of BLI can cause confounding signals from even minute levels of luciferase that are orders of magnitude lower than in the prostate, especially if the nontargeted expression emanates from surface-proximal or relatively large tissues. Thus, the unusually high prostate specificity of the EZC3-prostate model makes it ideal for identifying early metastasis in genetically engineered mice predisposed to prostate cancer.

Background bioluminescence is much less of a factor when applying BLI to the tracking of adoptively transferred luciferase-transfected cells. In numerous reports, tumor cell growth and metastasis were accurately measured and identified with BLI, although *in vivo* imaging was less sensitive than *ex vivo* imaging as expected (32). Further, response of tumor cells to traditional therapies or immunotherapy has been accurately monitored *in vivo* as well as the tracking of leukocytes to neoplastic tissue (33). Despite the extra challenges of transgenic models, a number of reports indicate their broad use (reviewed in ref. 8).

Due to both the exquisite AR sensitivity of both the three composite promoters used in this study and the involution of the prostate that occurs following medical or chemical castration, the EZC-prostate models are also useful for monitoring AR activity in the prostate in living mice. As proof-of-principle, we were able to show a drop in reporter activity up to 2 orders of magnitude following castration in living EZC2- and EZC3-prostate mice. Similar results were achieved when GnRH antagonist, PPI-258, was added to EZC2-prostate mice. This model should permit comparisons of not only distinct reagents but also of dosing schedules and routes of injection. Of course, there are always concerns about the applicability of animal studies to humans, but due to high conservation of the AR axis, these mice should be appropriate for preclinical evaluation of other classes of AR-blocking compounds. The high magnitude of the inhibition following castration was somewhat surprising as adrenal-derived androgens comprise up to 5% of circulating testosterone and have been shown to activate the

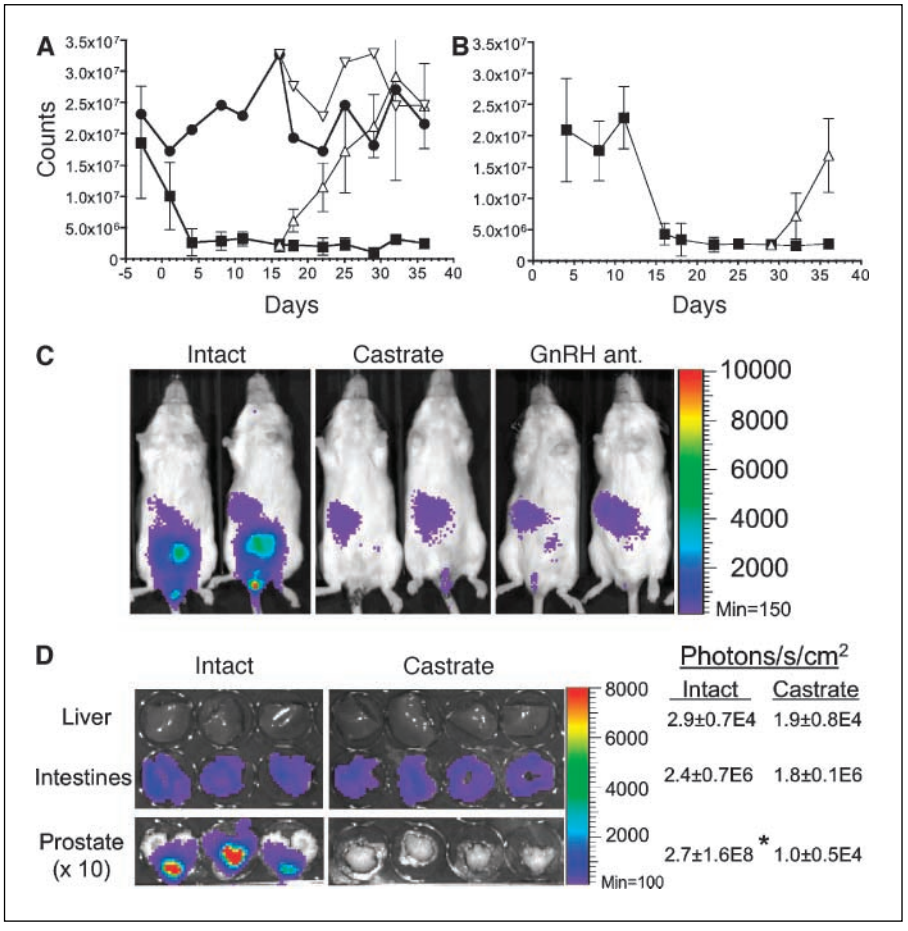

Figure 8. *In vivo* imaging of pharmacologic responses of AR activity. *A,* total luminescence from lower abdomens of intact (●) or castrate (day 0, ■) EZC2-prostate mice ($n = 10$) was measured biweekly. Testosterone (10 mg/21 days) tablets were administered s.c. at day 16 in intact (▽) or castrate (△) animals ($n = 5$). *Points,* mean; *bars,* SD. (Error bars were removed from intact mice for clarity). *B,* total luminescence of intact mice ($n = 10$) treated at day 11 with GnRH antagonist s.c. (■). Testosterone tablets were administered s.c. at day 29 (□, $n = 5$). *C, in vivo* imaging of luciferase activity in two representative intact, castrate (day 15 following castration) or GnRH antagonist-treated EZC2-prostate mice (day 11 of GnRH treatment). *D, ex vivo* imaging of liver, intestines (cecum and colon only), and prostates of intact and castrate [5 weeks (first two), 11 weeks (last two)] mice. Average ± SD of photon flux ($p/s/cm^2/sr$) is shown to the right. Note that prostate images were measured separately to avoid reflected light and are shown with a 10-fold increased pseudocolor scale. *, $P < 0.05$.

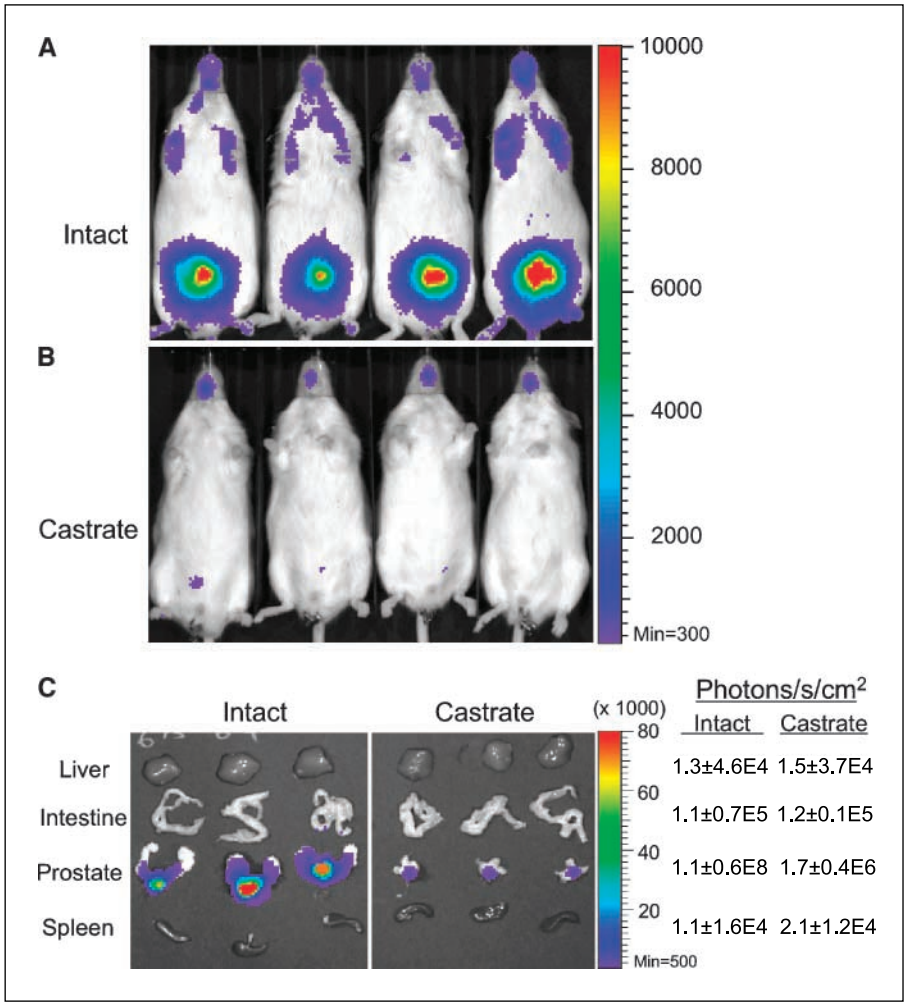

Figure 9. Effects of castration on EZC3-prostate mice. *A* and *B, in vivo* imaging of luciferase activity in representative intact (*A*) or castrate (*B*, 4 weeks following castration) EZC3-prostate mice. *C, ex vivo* imaging of liver, intestines (cecum and colon only), prostates, and spleen of intact and castrate (4 weeks) mice. The average ± SD of photon flux (p/s/cm^2/sr) is shown to the right. Note that prostates from intact mice were measured separately to avoid reflected light. *, $P < 0.05$.

AR (reviewed in ref. 25). Nevertheless, the combination of prostate involution and promoter inhibition following castration or GnRH antagonist administration almost completely inhibited prostate-derived luciferase in all three models. It will be interesting to evaluate other classes of drugs, such as 5α-reductase inhibitors, nonsteroidal antiandrogens, and selective AR modulators using these mice. Similarly, these models should be useful for elucidating the potential roles of numerous transcriptional coactivators associated with AR signaling in normal or prostate cancer tissue (33, 34).

The recent development of genetically engineered mouse modeling prostate cancer has stimulated our understanding of disease progression and has been a platform for treatment development. Further developments in imaging technologies will synergize with that work. These new EZC-prostate models should not only expand the use of transgenic prostate cancer mouse models, but will also be useful for drug and treatment development and a better understanding of the role(s) of the AR axis during prostate development and disease progression.

Acknowledgments

Received 11/3/2005; revised 3/13/2006; accepted 4/11/2006.

Grant support: Prostate Cancer Research Initiative (Scott Department of Urology, Baylor College of Medicine) and NIH grant U01-CA84296.

The costs of publication of this article were defrayed in part by the payment of page charges. This article must therefore be hereby marked *advertisement* in accordance with 18 U.S.C. Section 1734 solely to indicate this fact.

We thank K. Slawin (Baylor College of Medicine) for helpful discussions and W. Westlin (Praecis Pharma, Waltham, MA) for providing PPI-258-CMC.

References

1. Kasper S. Survey of genetically engineered mouse models for prostate cancer: analyzing the molecular basis of prostate cancer development, progression, and metastasis. J Cell Biochem 2005;94:279–97.
2. Roy-Burman P, Wu H, Powell WC, Hagenkord J, Cohen MB. Genetically defined mouse models that mimic natural aspects of human prostate cancer development. Endocr Relat Cancer 2004;11:225–54.
3. Kasper S, Smith JA, Jr. Genetically modified mice and their use in developing therapeutic strategies for prostate cancer. J Urol 2004;172:12–9.
4. Massoud TF, Gambhir SS. Molecular imaging in living subjects: seeing fundamental biological processes in a new light. Genes Dev 2003;17:545–80.
5. Wirtzfeld LA, Wu G, Bygrave M, et al. A new three-dimensional ultrasound microimaging technology for preclinical studies using a transgenic prostate cancer mouse model. Cancer Res 2005;65:6337–45.
6. McElroy WD, DeLuca MA. Firefly and bacterial luminescence: basic science and applications. J Appl Biochem 1983;5:197–209.
7. Contag CH, Contag PR, Mullins JI, Spilman SD, Stevenson DK, Benaron DA. Photonic detection of bacterial pathogens in living hosts. Mol Microbiol 1995;18:593–603.
8. Contag CH, Bachmann MH. Advances in *in vivo* bioluminescence imaging of gene expression. Annu Rev Biomed Eng 2002;4:235–60.

9. Weissleder R. Scaling down imaging: molecular mapping of cancer in mice. Nat Rev Cancer 2002;2:11–8.
10. Edinger M, Cao YA, Hornig YS, et al. Advancing animal models of neoplasia through *in vivo* bioluminescence imaging. Eur J Cancer 2002;38:2128–36.
11. Xie X, Luo Z, Slawin KM, Spencer DM. The EZC-prostate model: noninvasive prostate imaging in living mice. Mol Endocrinol 2004;18:722–32.
12. Xie X, Zhao X, Liu Y, et al. Robust prostate-specific expression for targeted gene therapy based on the human kallikrein 2 (hK2) promoter. Hum Gene Ther 2001;12:549–61.
13. Zhang J, Thomas TZ, Kasper S, Matusik RJ. A small composite probasin promoter confers high level of prostate-specific gene expression through regulation by androgens and glucocorticoids *in vitro* and *in vivo*. Endocrinology 2000;141:4698–710.
14. Latham JP, Searle PF, Mautner V, James ND. Prostate-specific antigen promoter/enhancer driven gene therapy for prostate cancer: construction and testing of a tissue-specific adenovirus vector. Cancer Res 2000;60:334–41.
15. Greenberg NM, DeMayo F, Finegold MJ, et al. Prostate cancer in a transgenic mouse. Proc Natl Acad Sci U S A 1995;92:3439–43.
16. Gingrich JR, Barrios RJ, Morton RA, et al. Metastatic prostate cancer in a transgenic mouse. Cancer Res 1996; 56:4096–102.
17. Linja MJ, Savinainen KJ, Saramaki OR, Tammela TL, Vessella RL, Visakorpi T. Amplification and overexpression of androgen receptor gene in hormone-refractory prostate cancer. Cancer Res 2001;61:3550–5.
18. Uchida K, Masumori N, Takahashi A, Itoh N, Tsukamoto T. Characterization of prostatic neuroendocrine cell line established from neuroendocrine carcinoma of transgenic mouse allograft model. Prostate 2005;62:40–8.
19. Vashchenko N, Abrahamsson PA. Neuroendocrine differentiation in prostate cancer: implications for new treatment modalities. Eur Urol 2005;47:147–55.
20. Kaplan-Lefko PJ, Chen TM, Ittmann MM, et al. Pathobiology of autochthonous prostate cancer in a pre-clinical transgenic mouse model. Prostate 2003;55: 219–37.
21. Evangelou AI, Winter SF, Huss WJ, Bok RA, Greenberg NM. Steroid hormones, polypeptide growth factors, hormone refractory prostate cancer, and the neuroendocrine phenotype. J Cell Biochem 2004;91: 671–83.
22. Freeman KW, Welm BE, Gangula RD, et al. Inducible prostate intraepithelial neoplasia with reversible hyperplasia in conditional FGFR1-expressing mice. Cancer Res 2003;63:8256–63.
23. Miyamoto H, Messing EM, Chang C. Androgen deprivation therapy for prostate cancer: current status and future prospects. Prostate 2004;61:332–53.
24. Zhu P, Baek SH, Bourk EM, et al. Macrophage/cancer cell interactions mediate hormone resistance by a nuclear receptor derepression pathway. Cell 2006;124: 615–29.
25. Tammela T. Endocrine treatment of prostate cancer. J Steroid Biochem Mol Biol 2004;92:287–95.
26. Linnoila RI, Zhao B, DeMayo JL, et al. Constitutive achaete-scute homologue-1 promotes airway dysplasia and lung neuroendocrine tumors in transgenic mice. Cancer Res 2000;60:4005–9.
27. Xie X, Zhao X, Liu Y, et al. Adenovirus-mediated tissue-targeted expression of a caspase-9-based artificial death switch for the treatment of prostate cancer. Cancer Res 2001;61:6795–804.
28. Iyer M, Wu L, Carey M, Wang Y, Smallwood A, Gambhir SS. Two-step transcriptional amplification as a method for imaging reporter gene expression using weak promoters. Proc Natl Acad Sci U S A 2001;98: 14595–600.
29. Iyer M, Salazar FB, Lewis X, et al. Non-invasive imaging of a transgenic mouse model using a prostate-specific two-step transcriptional amplification strategy. Transgenic Res 2005;14:47–55.
30. Adams JY, Johnson M, Sato M, et al. Visualization of advanced human prostate cancer lesions in living mice by a targeted gene transfer vector and optical imaging. Nat Med 2002;8:891–7.
31. Jenkins DE, Yu SF, Hornig YS, Purchio T, Contag PR. *In vivo* monitoring of tumor relapse and metastasis using bioluminescent PC-3M-luc-C6 cells in murine models of human prostate cancer. Clin Exp Metastasis 2003;20:745–56.
32. Edinger M, Cao YA, Verneris MR, Bachmann MH, Contag CH, Negrin RS. Revealing lymphoma growth and the efficacy of immune cell therapies using *in vivo* bioluminescence imaging. Blood 2003;101:640–8.
33. Culig Z, Comuzzi B, Steiner H, Bartsch G, Hobisch A. Expression and function of androgen receptor coactivators in prostate cancer. J Steroid Biochem Mol Biol 2004;92:265–71.
34. Ye X, Han SJ, Tsai SY, et al. Roles of steroid receptor coactivator (SRC)-1 and transcriptional intermediary factor (TIF) 2 in androgen receptor activity in mice. Proc Natl Acad Sci U S A 2005;102:9487–92.